Automating Experimentation in Miniaturized Reactors

Tajsoleiman, Tannaz

Publication date:
2018

Document Version
Publisher's PDF, also known as Version of record

Automating Experimentation in Miniaturized Reactors

Tannaz Tajsoleiman

PhD Thesis

October 2018

DTU Chemical Engineering
Department of Chemical and Biochemical Engineering

Automating Experimentation in Miniaturized Reactors

PhD thesis

Tannaz Tajsoleiman

Process and System Engineering (PROSYS)
Department of Chemical and Biochemical Engineering
Technical University of Denmark

October 2018

Address: Process and Systems Engineering Center (PROSYS)

Department of Chemical and Biochemical Engineering

Technical University of Denmark

Building 229

Dk-2800 Kgs. Lyngby

Denmark

Phone: +45 4525 2800

Web: www.kt.dtu.dk/forskning/prosys

Print: STEP

DTU Chemical Engineering
Department of Chemical and Biochemical Engineering

Preface

This thesis was written at the Process System Engineering Center (PROSYS), Department of Chemical and Biochemical Engineering, Technical University of Denmark (DTU). The work is done in the period from August 2015 to October 2018 under the supervision of Associate Professor Ulrich Krühne, Professor Krist V. Gernaey and Associate Professor Jakob Kjøbsted Huusom. This project has received funding from the European Union's Horizon 2020 research and innovation program under the Marie Skłodowska-Curie actions grant agreement No. 643056. The authors gratefully acknowledge this financial support.

I would like to thank my supervisors for this great experience with all its up and downs and the joy of solving new challenges under your supervision. Thanks to Ulrich for all your scientific and life lessons, all your encouragements and motivations and finally your trust during this four years from my master thesis to Ph.D.. Thanks to Krist for all your support from any new ideas and the big effort in making a great working environment. I also want to appreciate Jakob's scientific inputs during this project. Additionally, I want to thank Graham McCreath at FujiFilm Diosynth and Sjef Cornelissen and Lisa Mears both at Novozymes A/S for their valuable industrial inputs and the fruitful discussions. Working with them was definitely one the best experiences during my education. And, I would like to thank Jarka Glassey for providing this great opportunity to work in such an amazing project which gave me the chance of visiting so many places, meeting great peoples and finding wonderful friends.

A big thank goes to all my colleagues in DTU. Thanks to Mafalda for being such a great friend and an officemate, thanks to Carolina and Tiago for all your pure friendships, thanks to Robert for all your support and great memories, thanks to Francesco for being like my brother, thanks to Christian for being such a nice friend with incredible patience to help, thanks to Gisela for being such a dream teammate and an amazing friend, thanks to Dasha for all the memorable moments. Thank you very much Gitte and Eva for all your kindly supports. I also want to thank Mahshid, Mohsen, Sara, Arash, Zari and Mohammad for all the crazy memories, laughs and joys.

Finally, I would like to thank my family. My mom and dad, I cannot imagine myself at this point without all your support in every single day of my life. My brothers, your love and supports are always with me. My family in law, I cannot even explain how lucky I am to have you in my life. And, Soheil, who thought me how is a life full of passion and dignity.

Tannaz Tajsoleiman
Kongens Lyngby, October 2018

Abstract

Operation of informative experiments has always been the necessity of an efficient process characterization at different stages of research and development. However, running experiments and collection of data is usually considered as a resource-demanding task. Hence, it is critically important to make educated designs for minimizing the number of required experiments. An unappropriated design of experiments (DoE) can easily end up with a waste of materials and resources for a small given information.

Application of different modeling techniques for DoE is to guarantee a high-level of information from every single one and move more towards the optimum experiments. This capability can be considered in different aspects of design of experiment for studying the effect of process variables, to design of the experimental operating condition which provides a similar process environment as the real-scale system in the lab-scale.

Model-based DoE is a category of DoE methods that is based on the integration of modelling techniques with statistical analysis. A Model-based DoE method benefits from the potential of mathematical modelling to predict the process behavior under various conditions. As the result, the proposed experiments are more focused on a set of target objectives. These objectives could be the identification of the key process variables, studying the process response to the change of environment, characterization of the interactions or even discrimination between some theories.

On the other hand, application of modelling approaches have been established for designing representative scale-down models for operation of the experiments. An ideal scale-down model has to provide a comparable process condition as the corresponding full-scale reactor to guarantee similar process behavior to the designed process variables. However, reaching such a design is usually a challenging task with respect to the limitations of different scales.

Considering the importance of presenting more robust and efficient DoE approaches, this thesis provides a comprehensive study on the application of model-based methods for design of optimum experiments. The studied topics cover different angles of the experimental design in miniaturized reactors including a framework to choose the values for the process variables and a method for design of a scale-down model for operation of the experiments.

Resumé

Udførelsen af informative eksperimenter har altid været en nødvendighed for effektivt at kunne karakterisere forskellige processer i forskellige udviklingsstadier. Imidlertidig, er det at udføre og indsamle data fra eksperimenter at betragte som et yderst ressourcekrævende foretagende. Derfor er et indsigtsfuldt design af afgørende betydning for at minimere antallet af eksperimenter. Et uhensigtsmæssigt eksperimentelt design (DoE) kan let medføre store materiale- og ressourceomkostninger for meget begrænset indsigt.

Anvendelsen af forskellige modelleringstekniker til DoE kan garantere et højt niveau af indsigt, kombineret med et lavt antal eksperimenter. Denne egenskab kan tages i betragtning i forskellige stadier af det eksperimentelle design når effekten af forskellige proces variable skal evalueres, eksempelvis til design af identiske vilkår i små og storskala systemer.

Modelbaseret DoE høre under en kategori af DoE Metoder der integrerer kendte modelleringsteknikker med statistisk analyse. Et modelbaseret DoE drager fordele af matematisk modellerings egenskab til at forudse procesadfærd under et utal af vilkår. Resultatet deraf er at de anviste eksperimenter i højere grad kan skræddersyes til at klarlægge kendte problemstillinger. Disse problemstillinger kunne være; identifikation af proces nøgleparametre, procesadfærd ved skift i procesforhold, samt karakterisering og endda validering af forskellige teorier.

Matematisk modellering er, derudover, en etableret metode til design af repræsentative nedskalerings eksperimenter. En ideel nedskalerings model er i stand til biddrage med samme forhold i lille skala som observeres i stor, og dermed garanteres samme effekt af proces nøgleparametre. Forskellen i størrelsesforhold, gør dog opgaven til en kompliceret af slagsen.

Med behovet for robuste og effektive DoE metoder i mente, præsenteres der i denne afhandling, et omfattende stude i anvendelsen af matematisk modellering til bestemmelse af ideelle eksperimenter. Emner der behandles i afhandlingen inkluderer forskellige aspekter af eksperimentelt design i miniature reaktorer inklusiv en fremgangsmåde til at værdisætte nøglevariable og en metodologi til design af nedskalerings modeller til brug i udførelsen af eksperimenter.

List of contents

Preface ..... **i**
Abstract ..... **ii**
Resumé ..... **iii**
List of contents **5**
Chapter 1 ..... **1**
1.1. Background *1*
1.2. Scope *3*
1.3. Thesis structure *4*
References *6*
Chapter 2 ..... **9**
2.1. Model-based Design of Experiments *11*
2.1.1. Framework and Methodology 14
2.1.2. Case study, Chemical reaction 20
Summary *22*
Glossary *23*
References *24*
Chapter 3 ..... **27**
3.1. Miniaturized reactors *28*
3.2. Characterization of the Ambr®250 bioreactors *32*
3.2.1. Ambr®250 for mammalian cell culture 32
3.2.2. Ambr®250 for microbial cell culture 47
Summary *60*
Glossary *61*
References *62*
Chapter 4 ..... **67**
4.1. Scale-down, a trade-off between the selection of key parameters *68*
4.2. Scale characteristics and the challenges of scaling down *71*
Summary *79*
Glossary *79*
References *80*
Chapter 5 ..... **85**
5.1. Compartment based scale-down *85*
5.2. An automated approach towards a representative scale-down model *86*

5.2.1. CFD based compartment modeling 87
5.2.2. The principle of the compartment modelling and the scale-down design 105
Summary *115*
Glossary *117*
References *118*
Chapter 6 ..... **121**
References *126*
Acknowledgments **129**
List of publications **131**
Articles *131*
Under review *131*

Chapter 1
Introduction

1.1. Background

During the last decades, the application of industrial-scale bio-based production processes has seen a significant growth. Hence, competitive forces drive companies to design more efficient and economic bio-based production processes in order to reach high-quality products within the shortest possible operating time. The focus on cost control applies not only to manufacturing but also in the early stages of research and development (R&D). In the majority of cases, the R&D stage is the most resource demanding part of a development procedure, which requests efficient and fast scientific strategies.

A detailed system characterization is a key to success in process development. In order to design, establish, or improve a process, it is essential to understand the system, identify the effective parameters, and investigate the interactions between the key factors. At the same time, a system cannot be well defined without understanding its potentials, weaknesses and limitations. The depth of this understanding strongly depends on the outcome of analytical analyses over an adequate quantity of experimental data. Experimental evaluation of as many conditions as possible is favorable to study the response of the process to the change of the key 'process variables'. For instance, in the operation of a cell culture fermentation, the effect of various nutrient concentrations or the pH level (as two example for process variables) needs to be studied in detail for characterization of the cell metabolism (Spann et al. 2018). However, it should be considered that increasing the number of experiments results in an increase of the experimental costs, which can easily make a research project economically unfeasible. Therefore, there is a substantial need to use systematic approaches for

designing the set of experiments which deliver the maximum level of information with the minimum number of trials (Dejaegher & Vander Heyden 2011; Lee & Gilmore 2006; Wang & Wan 2009).

Maximizing the level of information or minimizing the number of experiments are not the only challenges encountered when building knowledge from experimental data. Execution of numerous experiments according to the designed plan, as necessary for characterizing complex bioprocesses, brings along new challenges. Since experimentation at the manufacturing scale is not economically and practically feasible, there is an inevitable need to use representative scale-down models, which resemble the corresponding full-scale process conditions in smaller volumes (Li et al. 2006). Reducing the scale not only addresses the difficulty of operating experiments in the large reactors, but also provides the possibility of running consistent experiments with significantly less consumption of materials and resources (Kistler et al. 2016; Bareither & Pollard 2011; Ladner et al. 2017; Noorman 2011; Tsang et al. 2014). The important point in using a scale-down model is that the achieved results and the conclusions can only guarantee similar outcomes or responses in the full-scale reactor if the provided operating conditions are identical or at least similar to the full-scale environment. An ideal scale-down model has to provide comparable gradients, distribution of materials, fluid dynamic conditions and other 'process operating conditions' as the large production-scale tank, but in a smaller reactor. Therefore, the design of a representative scale-down model is also a crucially important step before the execution of experiments in the lab.

Scale-down experimentation has seen a great improvement in various aspects of technology, from monitoring platforms to advanced bioreactors. Recently, research towards the development of new miniaturized bioreactors (MBR) for the operation of scale-down models has become a hot topic among biotech related companies (Bareither & Pollard 2011; Gernaey et al. 2012; Hegab et al. 2013). The application of MBRs made it possible to reduce the size of experimental set-ups even more than with traditional pilot or bench scales, which was not an option for about 10-15 years ago.

Due to the long time required to execute a single experiment, usually, running a complex Design of Experiments (DoE) is only practical when combined with parallelization of experiments. By presenting high throughput principles, the application of MBRs has moved further towards the design of automated platforms with the possibility of parallelizing series of experiments at lab scale (Kensy et al. 2009; Maharbiz et al. 2004; Bhambure et al. 2011; Rameez et al. 2014). In recent years, the application of high throughput platforms in areas of medium development, strain screening, and bioprocess design has undergone significant improvements (Ladner et al. 2017). A large number of automated high throughput platforms has been commercialized, which are equipped with various types of bioreactors, sensors for monitoring and sampling setups (Vallejos et al. 2006). The side effect

of developing such high throughput platforms is the generation of large amounts of data in a relatively short period of time, which demands advanced data management systems for analyzing the results fast.

1.2. Scope

Despite all the achievements in developing different DoE methods and providing the appropriate experimental platforms for high-throughput experimentation such as MBRs, there is nevertheless a lack of a systematic study – from design to implementation – that substantially narrows down the experimental demand of a process development study. The here presented study has the intention to provide a comprehensive look at the different aspects of an optimized DoE from the initial stage of choosing the experimental process variables to the design of a representative scale-down model for the operation of the experiments in a miniaturized scale. This work contributes therewith considerably to extending the application of model-based methods for improving the traditional approaches in experimental design.

The thesis covers three main topics: 1. development of a systematic model-based DoE approach with focus on the selection of the most informative settings for the process characterization; 2. the model-based characterization of miniaturized setups which can be used for the operation of the designed experiments at lab-scale; and 3. development of a new model-based scale-down method for the design of the operating conditions that can deliver a comparable process environment as the full-scale reactor. Figure 1.1 shows the tree chart of the subjects discussed in this work. Each of the mentioned topics is studied individually within a chapter including an introduction, a short discussion of the challenges and the bottlenecks, presenting the developed methods, discussing the results and finally summarizing the main highlights of the work.

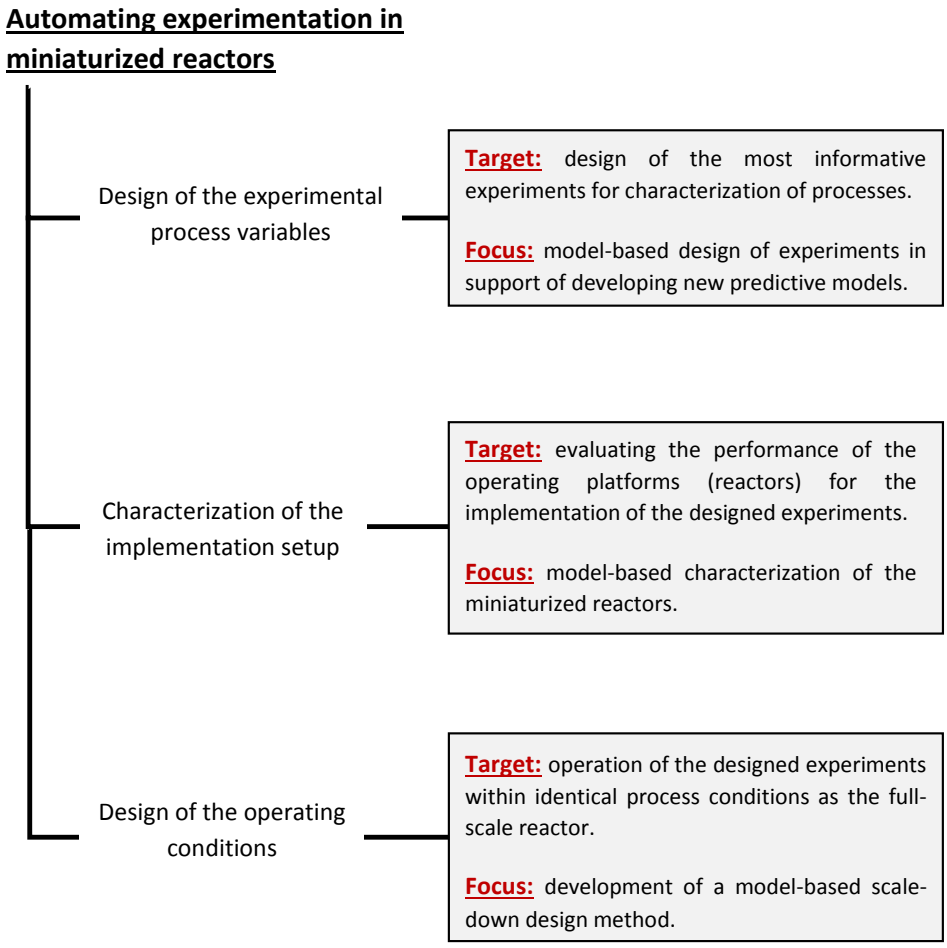

Figure 1.1. The tree chart of the discussed subjects in the thesis.

1.3. Thesis structure

The thesis is structured into six chapters:

Chapter 1. This chapter gives a brief overview of the overall idea behind this Ph.D. work.

Chapter 2. The aim of this chapter is to use the potential of some well-established DoE methods for the development of a new integrated Model-based DoE (M-DoE) framework in the form of a dynamic platform. The main target of this platform is to effectively support the development of a predictive model that is made based on the most informative experimental data. The developed approach helps to minimize the number of required experiments for process characterization.

The achieved designs have to be operated in the lab or in pilot scale setups (scale-down model) to study the process behavior under various conditions. The outcome can potentially be used for further process development, possible improvements and ideally optimization of the process at full scale.

Chapter 3. Operation of the designed experiments requires appropriate lab-scale setups. This chapter has a contribution to the evaluation of some well-known miniaturized reactors for the implementation of the experiments in the lab. In the scope of this part of the thesis, the advantages and disadvantages of using different MBRs and high throughput setups will be studied. As an example, the performance of a miniaturized stirred bioreactor (Sartorius Ambr 250) for both mammalian and microbial cell cultures will be investigated with different experimental tests and using computational fluid dynamics (CFD).

Chapter 4. It is important to operate the designed experiments in comparable process conditions as the full-scale reactor to guarantee similar process responses to specific disturbances across scales. Hence, it is crucial to apply an efficient scale-down strategy within the selected MBR. This chapter introduces some established scale-down approaches available in the scientific literature, and the weaknesses and strengths of each approach will be studied in detail.

Subsequently, the chapter has a critical look at the limitations, challenges and difficulties of scaling down a process into miniaturized reactors. Unfortunately, the scope and the nature of these limitations and challenges are not often addressed sufficiently in the literature. This part of the thesis aims to contribute to a more balanced discussion about the potentials and limitations of MBRs for providing a representative scale-down model of a larger scale process.

The achieved results and discussions in chapter 3 and 4 substantially help creating a good overview about the considerations and the difficulties for providing a representative scale-down model for the operation of the designed experiments (chapter 1).

Chapter 5. In this chapter, a new automated method for the design of a compartment-based scale-down model will be introduced. The focus of this chapter is mostly on reproducing the heterogeneity and gradients in a large-scale tank with a network of connected smaller reactors. In the development of this approach, a new CFD-based compartmentalization technique will be presented to identify the semi-homogeneous volumes within the full-scale reactor. Based on the achieved results, the network of scale-down reactors is designed and characterized. This method is critically evaluated in two different industrial case studies of a 700 L lactic acid bacteria fermentation and a 100 m^3 fermentation with *Saccharomyces cerevisiae*, respectively.

Chapter 6. Finally, the conclusions and potential future work are presented in this chapter.

References

Bareither, R. & Pollard, D., 2011. A review of advanced small-scale parallel bioreactor technology for accelerated process development: Current state and future need. *Biotechnology Progress*, 27(1), pp.2–14.

Bhambure, R., Kumar, K. & Rathore, A.S., 2011. High-throughput process development for biopharmaceutical drug substances. *Trends in Biotechnology*, 29(3), pp.127–135.

Dejaegher, B. & Vander Heyden, Y., 2011. Experimental designs and their recent advances in set-up, data interpretation, and analytical applications. *Journal of Pharmaceutical and Biomedical Analysis*, 56(2), pp.141–158.

Gernaey, K. V. et al., 2012. Monitoring and control of microbioreactors: An expert opinion on development needs. *Biotechnology Journal*, 7(10), pp.1308–1314.

Hegab, H.M., ElMekawy, A. & Stakenborg, T., 2013. Review of microfluidic microbioreactor technology for high-throughput submerged microbiological cultivation. *Biomicrofluidics*, 7(2), p.21502.

Kensy, F. et al., 2009. Validation of a high-throughput fermentation system based on online monitoring of biomass and fluorescence in continuously shaken microtiter plates. *Microbial Cell Factories*, 8(1), p.31.

Kistler, C. et al., 2016. High-Throughput Bioprocess Development. *Genetic Engineering & Biotechnology News*, 36(7), pp.30–31.

Ladner, T. et al., 2017. Application of Mini- and Micro-Bioreactors for Microbial Bioprocesses. In *Current Developments in Biotechnology and Bioengineering*. Elsevier, pp. 433–461.

Lee, K.-M. & Gilmore, D.F., 2006. Statistical Experimental Design for Bioprocess Modeling and Optimization Analysis: Repeated-Measures Method for Dynamic Biotechnology Process. *Applied Biochemistry and Biotechnology*, 135(2), pp.101–116.

Li, F. et al., 2006. A Systematic Approach for Scale-Down Model Development and Characterization of Commercial Cell Culture Processes. *Biotechnology Progress*, 22(3), pp.696–703.

Maharbiz, M.M. et al., 2004. Microbioreactor arrays with parametric control for high-throughput experimentation. *Biotechnology and Bioengineering*, 85(4), pp.376–381.

Noorman, H., 2011. An industrial perspective on bioreactor scale-down: What we can learn from combined large-scale bioprocess and model fluid studies. *Biotechnology Journal*, 6(8), pp.934–943.

Rameez, S. et al., 2014. High-throughput miniaturized bioreactors for cell culture process development: Reproducibility, scalability, and control. *Biotechnology Progress*, 30(3), pp.718–727.

Spann, R. et al., 2018. Model-based process development for a continuous lactic acid bacteria fermentation. *Computer Aided Chemical Engineering*, 43, pp.1601–1606.

Tsang, V.L. et al., 2014. Development of a scale down cell culture model using multivariate analysis as a qualification tool. *Biotechnology Progress*, 30(1), pp.152–160.

Vallejos, J.R. et al., 2006. Optical analysis of liquid mixing in a minibioreactor. *Biotechnology and Bioengineering*, 93(5), pp.906–911.

Wang, J. & Wan, W., 2009. Experimental design methods for fermentative hydrogen production: A

review. *International Journal of Hydrogen Energy*, 34(1), pp.235–244.

Chapter 2

Optimum design of experiments

The collection of experimental data is usually a demanding procedure in terms of required human effort and the consumption of materials. Poorly designed experiments can easily lead to a waste of resources for obtaining a given and relatively small piece of required information. An appropriate design of experiments (DoE) helps to manage these efforts in an efficient way (Fedorov & Hackl 1997). In complex processes, usually the response of the process is dependent on several factors. DoE is a systematic approach to design informative experiments which can deliver valuable information about the effect of changes in the operating conditions on the process behavior. Hence, the application of DoE is mostly useful for three main purposes: 1. screening and identification of the key factors (variables), 2. specifying the correlations and the interactions between key factors and process variables, and finally 3. formulating the responses with mathematical models (Franceschini & Macchietto 2007; Kumar et al. 2014). The results provide the essential inputs for design or improvement of the process, tuning the operating conditions, controlling the settings or in general, optimizing the system.

Using proper DoE strategies plays a critical role in the development of more precise models, and is both concerned with the model structure selection and the model parameter estimation. The capability of a model to predict the process behavior highly depends on the available input information, from the early stage of development until the last validation steps. Building a model is also highly supported by some prior knowledge, such as fundamental equations, and conservation laws applied to chemical/biochemical systems (Galvanin et al. 2016). Nevertheless, the major source of information for model development normally comes from the experimental data during the development stage. Since collecting data is a resource demanding procedure, it is necessary to only

operate the experiments, which can deliver a high level of information. Operation of informative experiments substantially reduces the need for large experimental campaigns and subsequently, excessive analyses.

Different DoE methods have been presented in the scientific literature. Fisher performed the preliminary studies on the basic principles of choosing the optimum patterns in the experimental settings for efficient characterization of process responses (Fisher 1935). He introduced a new group of DoE approaches called black-box designs, which was based on finding general correlations between the inputs (factors) and outputs (responses). Throughout the years, many scientific efforts were invested in that field by different research groups (Box & Behnken 1960; Atkinson & Donev 1992; Box & Wilson 1992; Chen & Wang 2004; Baş & Boyacı 2007). The full factorial design is an established black-box method particularly for screening purposes (Plackett & Burman 1946; Box & Meyer 1986; Box et al. 2005; Montgomery 2008). This approach is one of the most common statistical designs which is wildly used in the biological area for measuring the process responses to the change of a number of input parameters (Franceschini & Macchietto 2007). For most of the cases, the application of full factorial designs serves as a preliminary study of the interactions between different process parameters. The biggest advantage of this method is the simplicity of the implementation. However, in the case of involving a high number of key parameters, the application of a full factorial design may not be economically feasible. The development of the fractional factorial design was done to partly reduce the load of experiments that is resulting from a full factorial design (Box & Draper 1987). However, this method is not suitable if there are some constraints on the outputs. Moreover, none of the factorial designs has been developed for handling dynamic experiments, where both input factors and the corresponding responses reach multiple values as a function of time.

In contrast with the black-box methods, the Model-based DoE (M-DoE) approaches were introduced to design the experiments based on some specific inputs from the models that are under development. In such an approach, the mathematical models are explicitly used to predict the information content of the experiments that can potentially be conducted within the feasible operating range. Accordingly, the optimum settings are selected corresponding to that combination of input settings which has the highest probability to deliver the most informative experimental data. Various M-DoE methods have been presented with the focus on different aspects of developing a model (Box & Lucas 1959; Box & Hunter 1965; Hunter & Reiner 1965; Box 1968; Hill et al. 1968a). Most of these works targeted only one modelling objective in terms of identifying the model structure, discriminating between rival model candidates or estimating the parameters in a mathematical model. However, the lack of having a comprehensive approach, which targets all the stages of the modelling process at the same time, has until now remained a big issue.

This chapter focuses on building a new integrated M-DoE framework to provide an informative experimental support for the development of more precise models from the early model development stages to the final validation. This framework proposes a dynamic platform for adjusting the focus of the experimental design based on the level of progress in developing a model. The outcome is a significant reduction in the load of physical and computational experiments, required at the early stage of system characterization and design. The framework was established in MATLAB R2016b.

2.1. Model-based Design of Experiments

The general procedure in model-based designs (Figure 2.1) is to start by proposing one or more candidate models, which have the possibility to serve as the right model candidate. The identifiability of the models with respect to their parameters has to be initially checked. In the case that none of the models passes that test, a new group of candidate models has to be suggested.

The next steps are to design sets of experiments, which support the task of discriminating between the rival model candidates and estimate the corresponding parameters to reach the final model. Eventually, the model has to be critically validated by confronting it with a new independent set of data. If the predictions are not satisfactory, the procedure has to be repeated for a group of new model candidates. For each individual stage of the development, model discrimination, parameter estimation and model validation, different DoE approaches were presented in the literature (Box & Hill 1967a; Atkinson & Hunter 1968; Agarwal & Brisk 1985; Bruwer & MacGregor 2006).

Following this general approach and with the help of some established DoE methods, a new integrated M-DoE strategy is introduced in the next part. The main novelty of this work is in presenting a dynamic platform that can take the maximum advantage from some well-established DoE criteria. Figure 2 gives an overview of the developed algorithm (Tajsoleiman et al. 2017).

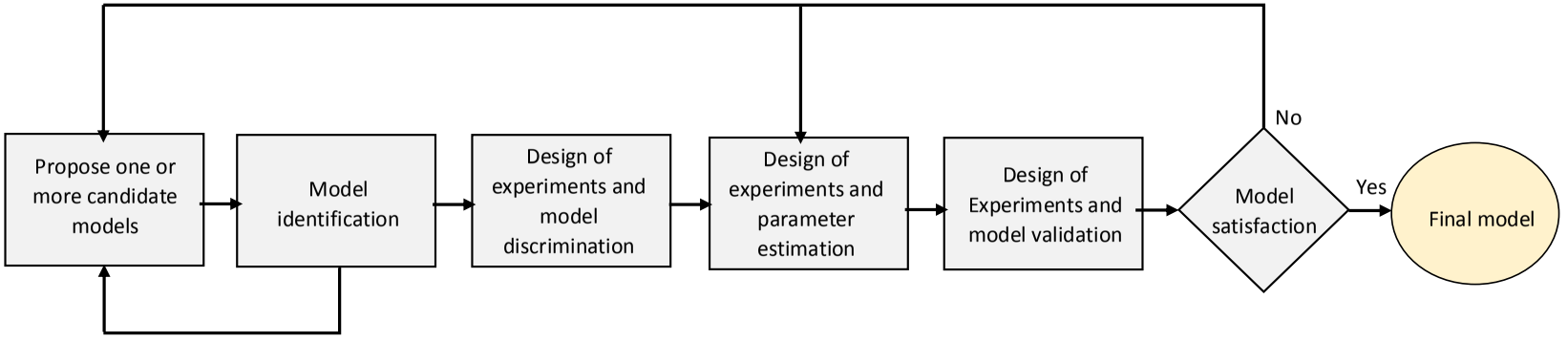

Figure 2.1. The generic scheme of a model-based design of experiments.

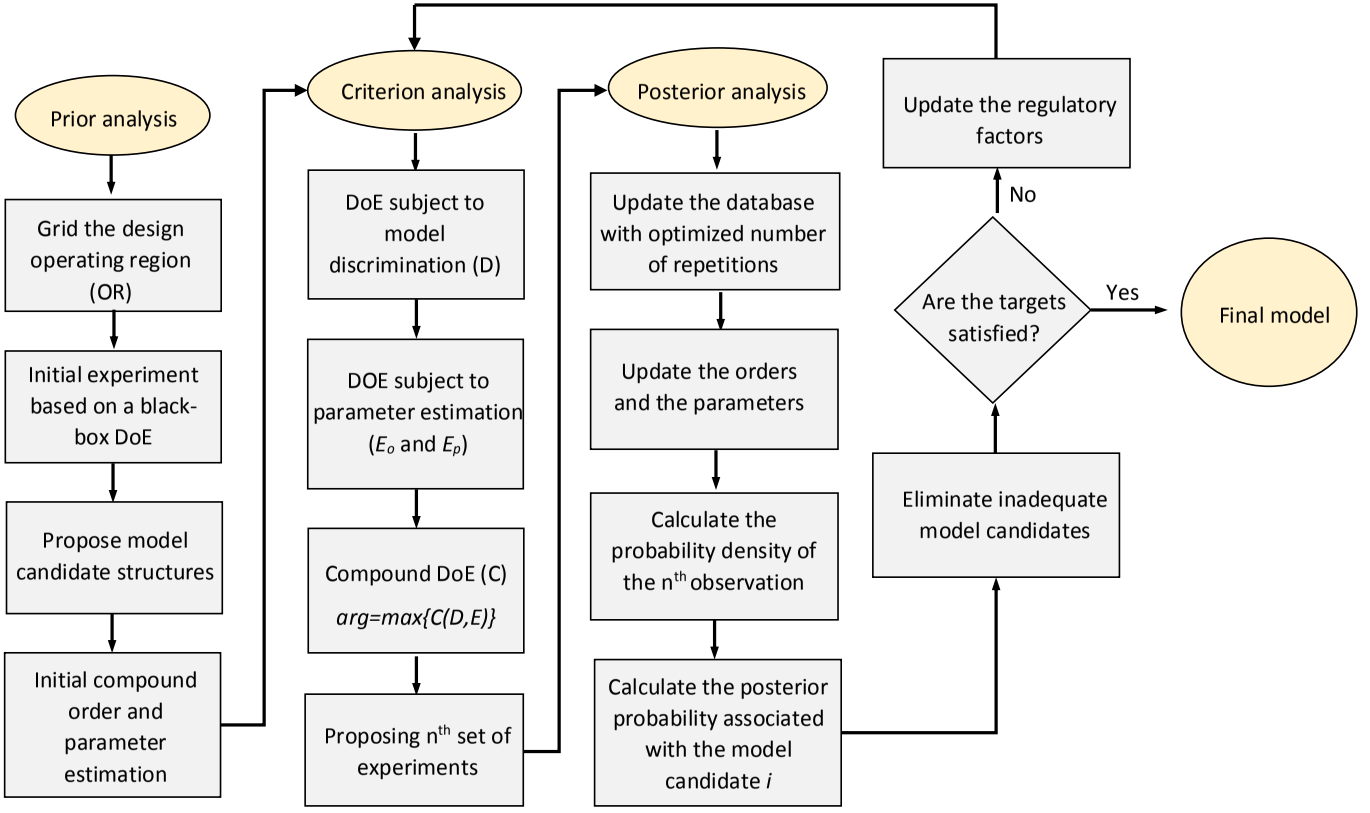

Figure 2.2. The integrated M-DoE framework for development of mechanistic models.

2.1.1. Framework and Methodology

In order to discuss the presented framework in Figure 2.2, it is assumed that an unknown process is going to be described with the function H (Eq. 2.1):

$$\begin{cases} f(\dot{x}(batch), x(batch), \mathrm{t}, \theta, \lambda, \xi) = 0 \\ \hat{y}(t) = H(x(batch)) \end{cases} \tag{2.1}$$

The state of the process 'x' as a function of time 't' is dependent on 'n_{op}' operating factors $\xi = \{\xi_1, \dots, \xi_{\mathrm{n}_{op.}}\}$ such as temperature, pressure or the composition of materials and a set of parameters $\{\theta, \lambda\}$. Each factor varies within a specified operating region OR. The state of the process refers to the specific value of '$\mathrm{n}_{rep.}$' responses $y(t)$ which are going to be predicted as $\hat{y}(t)$. The routine initiates by proposing 'm' candidate structures $H = \{h_1, \dots, h_i, \dots, h_m\}$ as functions of 'x'. In this approach, the parameters are divided into two groups, the model orders 'λ' and the rest of the parameters 'θ'. Below, an example of distinguishing between λ and θ is shown as Eq. 2.2.

$$h_1 = \theta_1 . {x_1}^{\lambda_1} + \theta_2 . \exp(x_2)^{\lambda_2} \tag{2.2}$$

The M-DoE framework is based on three major blocks: 1. Prior analysis; 2. Criterion analysis; and 3. Posterior analysis. Each block is described individually as follows:

Prior analysis: This step has the purpose to provide an initial perspective of the design's restrictions and the potential model structure candidates. This block consists of four main steps, which starts by limiting the possible experimental settings into a few values. This can be done by dividing the OR in all dimensions based on $\{\xi_1, \dots, \xi_{\mathrm{n}_{op.}}\}$. Figure 2.3 shows the discretization of a two-dimensional OR based on two operating factors ξ_1 and ξ_2. In this figure, each black point represents one experimental setting. At each iteration step of the design, the optimum experimental setting has to be selected from the specified points.

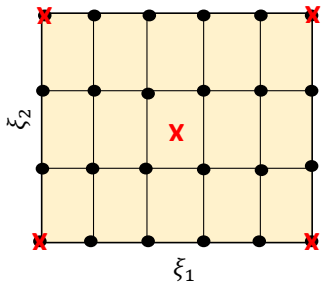

Figure 2.3. Discretization of the operating region for two operating factors ξ_1 and ξ_2 with constant intervals.

In the case that no historical data are available, the initial data can be extracted according to a black-box method such as a factorial design with one center point (the red crosses in Figure 3). Based on the extracted data, the candidate structures have to be introduced for further analysis. Usually, the development of a model is preliminarily supported by some established laws, which are helpful when proposing the candidate model structures for the description of the process. For instance, the Monod kinetics model structure is frequently used for modelling the kinetics of biological phenomena (Postma et al. 1989; Muthuvelayudham & Viruthagiri 2002; Arutchelvan et al. 2006; Moser 2012). It is important that the proposed models cover different possible scenarios. At this stage of the design, the corresponding parameters are roughly estimated based on the few available input data.

- **Criterion analysis:** The purpose this analysis is to find the optimum settings Φ (ξ, t^{samp}) for the n^{th} experiment according to $(n-1)$ data points, estimation of the models and the sensitivity of the candidate structures. t^{samp} represents the sampling time in a dynamic process.

  The focus of the designed Φ has to vary dynamically based on the requirement of the model at the different stages of the model development. For instance, the type of required data for discriminating between the candidate models is completely different from the essential information that is required for estimating the parameters. In this routine, a combination of different DoE criteria is used to provide a compound design criterion with a flexible orientation. The well-established *D-criterion* (Kullback 1959; Box & Hill 1967a) and the *E-criterion* (Box & Lucas 1959) are the two main applied criteria in this routine:

  a) **<u>Design criterion D:</u>** This criterion was established to identify the experimental settings, where the extracted information from the data potentially helps to discriminate between the candidate models. Box *et al.* used a similar concept as the definition of entropy to define a criterion which can deliver the maximum discrimination power (Box & Hill 1967a). This criterion is based on statistical analysis of $(n-1)$ data points and sensitivity analysis of the candidate models to identify the n^{th} experimental point. Eq. 2.3 shows the corresponding equation for the calculation of the *D-criterion* (Kullback 1959; Box & Hill 1967a).

$$D = 1/2 \times \sum_{i=1}^{m} \sum_{j=i+1}^{m} \Pi_i^{n-1} \Pi_j^{n-1} \left\{ \frac{\left(\sigma_i^2 - \sigma_j^2\right)^2}{\left(\sigma^2 + \sigma_i^2\right)\left(\sigma^2 + \sigma_j^2\right)} + \left(\widehat{y_n}^{(i)} - \widehat{y_n}^{(j)}\right)^2 \left(\frac{1}{\sigma^2 + \sigma_i^2} + \frac{1}{\sigma^2 + \sigma_j^2} \right) \right\} \tag{2.3}$$

Box *et al.* assumed that the observations are normally distributed with a known variance σ^2. The variance σ_i^2 in the estimated result $\widehat{y_{rep}}_n^{(i)}$ by the candidate model 'i' is calculated according to Eq.2.4-2.7.

$$\sigma_i^2 = x_n^i . (X_i' X_i^i)^{-1} x_n^{i'} \sigma^2 \tag{2.4}$$

Where,

$$x_n^i = [x_{1,n}^i, x_{2,n}^i, \dots, x_{p,n}^i] \tag{2.5}$$

$$x_{l,n}^i = \left[\frac{\partial h_i(\theta_i, \xi_n)}{\partial \theta_{il}} \right]_{\theta_i = \widehat{\theta_i}} \tag{2.6}$$

$$X_i = \begin{bmatrix} x_{1,1}^i & \cdots & x_{p,1}^i \\ \vdots & \ddots & \vdots \\ x_{1,n-1}^i & \cdots & x_{p,n-1}^i \end{bmatrix} \tag{2.7}$$

In Eq. 2.3, Π_i^{n-1} is the prior probability of model 'i' to be the right model structure based on $(n-1)$ experimental data points (Eq. 2.8-2.10).

$$\Pi_{i,n-1} = \frac{\Pi_{i,n-2}\, p_i}{q(y_{n-1})} \tag{2.8}$$

$$q(y_{n-1}) = \sum_{i=1}^{m} \Pi_{i,n-2} p_i \tag{2.9}$$

$$p_i = \frac{1}{\sqrt{2\pi\left(\sigma^2 + \sigma_i^2\right)}} \exp\left\{ -\frac{1}{2\left(\sigma^2 + \sigma_i^2\right)} \left(y_n - \tilde{y}_n^{(i)}\right)^2 \right\} \tag{2.10}$$

p_i is the probability density of the nth observation based on the prediction of the i^{th} model. The initial prior probability of the candidates for an unknown process can be assumed the same and equal to $\Pi_i{}^1 = 1/m$.

The operating conditions which maximize the *D-criterion* result in data that delivers the highest discrimination power. Hence, the *D-criterion* needs to be calculated for each specified experimental setting. The points are ranked based on their information content

for discriminating between the candidate models. The maximum information corresponds to an operating condition, where the predictions of the models show the maximum deviation from each other. Hence, evaluating the models in terms of their level of accuracy in predicting the nth experimental point becomes relatively easier.

b) **Design criterion E:** The other implemented criterion focuses more on the level of information for evaluating the orders 'λ' of the model and for the estimation of the other parameters 'θ' for each candidate model. Box and Lucas introduced the *E-criterion* to specify the experiments which provide the required information for precise estimation of the overall parameters (Box & Lucas 1959). The design criterion for the nth experimental point is based on maximizing the determinant of the information matrix $M(\xi, \theta^{\circ}, \lambda^{\circ})$. θ° and λ° are the estimated parameters based on $(n-1)$ available data points. The information matrix can be simplified to Eq. 2.11 (Box & Lucas 1959; Hill et al. 1968; Atkinson & Bogacka 2002).

$$M(\xi, \theta^{\circ}, \lambda^{\circ}) = X'X \tag{2.11}$$

At the early stage of building a model, the evaluation of the orders has higher priority, while when getting more close to the final model, the estimation of θ needs to be the main focus of the experimental design. In order to adjust the design between the evaluation of 'λ' and 'θ ', Atkinson and Bogacka introduced the application of a subset criterion where the interest is only on part of the parameters (Atkinson & Bogacka 2002). The optimal design M_1 with focus on $\psi_1 \in \{\psi_1, \psi_2\}$ is calculated according to Eq. 2.12.

$$\mathrm{M}_1 = \max\left\{\left|\frac{\mathrm{M}(\xi, \psi)}{\mathrm{M}_2(\xi, \psi)}\right|\right\} \tag{2.12}$$

Similarly, two design criteria are introduced based on providing the supportive information for estimation of the orders E_λ and the other parameters E_θ, separately. The corresponding information matrix to E_θ is M_1, and for E_λ it is called M_2. Accordingly, the *E-criterion* is updated to a linear combination of E_λ and E_θ (Eq. 2.13) (Atkinson & Bogacka 2002).

$$E(\xi, \psi, \lambda) = (1-\alpha)\, E_\theta + \alpha\, E_\lambda = (1-2\alpha) \log\left|M_1(\xi, \theta^{\circ}, \lambda^{\circ})\right| + \alpha \log\left|M(\xi, \theta^{\circ}, \lambda^{\circ})\right| \tag{2.13}$$

α is a weight factor to adjust the focus of the design between only the evaluation of the orders ($\alpha = 1$) or only the estimation of the other parameters ($\alpha = 0$). This approach was

already established and demonstrated for different case studies (Cook & Wong 1994; Atkinson & Bogacka 1997).

The discussed criteria are used when the aim of the design is either discrimination between the candidate models or estimation of their parameters. During the development of a model, both steps are necessarily required. The common approach is to first discriminate between the model candidates, and then to focus on the estimation of the parameters for the selected model structure. However, proper integration of the discussed criteria into a compound design is an efficient solution to decrease the number of required experiments. The compound criterion *'C'* can be calculated according to Eq.2.14 and Eq.2.15.

$$\mathrm{C} = w_1 \times D/D_{max}|_{\theta^\circ,\lambda^\circ} + w_2 \times \sum_{i=1}^{m} \Pi_{i,n-1} E/E_{max}\big|_{\theta^\circ,\lambda^\circ} \tag{2.14}$$

$$w_1 = \left\{\frac{m\left(1-\Pi_{b,n-1}\right)}{m-1}\right\}^{\beta}, \qquad w_2 = 1 - w_1 \tag{2.15}$$

Where, $\Pi_{b,n-1}$ is the highest prior probability between the candidate model based on $(n-1)$ observations, that corresponds to the probability of the most precise candidate model in providing a satisfactory description of the system that is studied. By letting $\Pi_{b,n-1}$ approach a value of one, and thus getting close to discrimination of the ultimate model structure from rival candidates, the power of the design moves toward parameter estimation. β is another dynamic regulatory factor to keep the emphasis mostly on the estimation of $\{\theta, \lambda\}$ ($\beta \gg 1$) or on discrimination between the models ($\beta \ll 1$). A similar criterion was introduced by Hill *et al.* when estimation of only θ was considered in the definition of the *E-criterion* while the orders were known (Hill et al. 1968).

The specified experimental settings are ranked based on their calculated *C-criterion* values. The optimum design is identified based on the experimental setting that can maximize the compound criterion *'C'* among the other experimental points. Through a dynamic platform, the focus of the new experiments is adjusted with respect to the state of the development procedure. The emphasis of the integrated design can vary between three main targets: discrimination between the rival candidates, evaluation of the orders and estimation of the other parameters. The main advantage of the introduced criterion is the extension of the design's focus particularly in the evaluation of the model orders while the prior designs were only limited to the discrimination between the candidates and estimation of θ (Hill et al. 1968; Galvanin et al. 2016; Quaglio et al. 2018).

- **Posterior analysis:** The purpose is to provide the required statistical analysis for the next iteration. This block starts with updating the data set with an optimized number of repetitions: High variance in the experimental data can potentially decrease the accuracy of the final model, for example by increasing the variance on the estimated parameters. Part of this problem can be addressed by repeating an experimental setting combined with complex data preprocessing techniques to treat the data and eliminate the outliers. Although increasing the number of repetitions (S) may improve the quality of the average data, the disadvantage is that it also demands higher efforts and consumption of materials. The default number of repetitions (S>2) for each experimental design is updated according to the variance of the measurements for the nth design compared to the estimated value σ_i^2. In the case of high variance ($> \sigma_i^2$), extra repetitions are recommended to eliminate the effect of disturbances on the accuracy of the models. The average value of the extracted data will be added to the rest of the data points.

  According to the updated dataset, the matrices containing the model orders 'λ' and the parameters 'θ' are re-estimated. Moreover, the probability densities of p_i and the posterior probabilities $\Pi_{i,n}$ of each model candidate are recalculated. The posterior probability associated with the i^{th} model shows the possibility of candidate 'i' to be the right model. Based on that, the candidate model with a probability that is less than a specified threshold has to be eliminated. The possibility of experiencing erroneous rejection of a correct model structure is significantly decreased by searching for the best fitting structure for different model orders before making any model discrimination attempt.

  In the last step, the focus of the next design has to be adjusted by updating the specified regulatory factors α and β. Figure 2.4 shows the scheme of this moving of the emphasis of the design during the procedure.

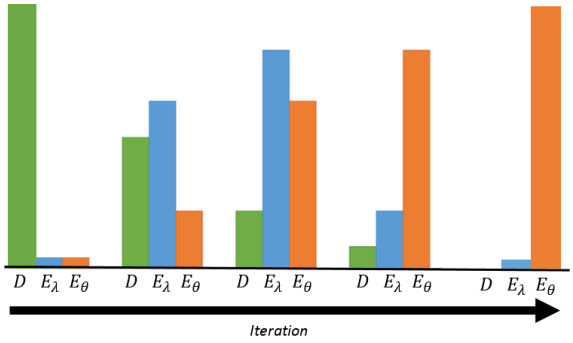

Figure 2.4. Adaptation of the design emphasis between the model discrimination D, order evaluation E_λ and parameter estimation E_θ with development of the model.

The regulatory factor α gradually decreases at each iteration to change the focus of the design from the orders to the other parameters. Meanwhile, β is constant until at least two candidates are potentially recognized as similar. In the case of reaching a situation with two nearly identical posterior probabilities, the models are initially marked as similar candidates. To increase the discrimination power, β needs to be updated with a constant factor $\beta = \beta \times \gamma$, $0 < \gamma < 1$ for the next iteration. If at least for two iterations in a row the models are marked as similar then, the similarity of the models is established and one of the models has to be randomly eliminated.

This methodology was tested in a case study, which will be described in more detail below.

2.1.2. Case study, Chemical reaction

The developed M-DoE strategy is demonstrated by means of a hypothetical chemical reaction A→B with an unknown kinetic model as a function of time 't' and temperature 'T''. It was assumed that each experiment takes 150 minutes at a temperature between 450-600 K. Hill *et al.* used a similar compound criterion as Eq. 2.14 for development of the kinetic model for this reaction with focus only on discrimination between the candidate models and estimation of θ (Hill et al. 1968). In their study, the orders of the candidate models were known. However, in the present study, the orders are assumed to be unknown.

In this study, the experimental data were computationally generated based on the Eq. 2.16 as the reference equation and the input standard deviation $\sigma = 0.05$.

$$[A] = \left[1 + t \times \exp\left\{-3.53 - 5000\left(\frac{1}{T} - \frac{1}{525}\right)\right\}\right]^{-1} \tag{2.16}$$

In this example, the sampling time and the temperature are considered as the two operating factors for the design of experiments. 36 (6×6) experimental points were specified for further analysis within the operating region. The initial set of data was generated based on a full factorial design plus one center point (Table 2.1). Since the sampling time is one of the operating factors, two of the experimental points became similar to two of the initial conditions (0 min, 450 K) and (0 min, 600 K). Therefore, the considered range for the sampling time was updated to [25-150] min for the factorial design.

Table 2.1. Full factorial design plus one center point.

Design number	Sampling time [min]	Temperature [K]
1	25	450
2	150	450
3	25	600
4	150	600
5	87.5	525

Accordingly, three candidate model structures were proposed (Eq. 2.17 to 2.19).

$$M_I: \quad [A]^{(1)} = \exp\left[-t \times \exp\left\{\theta_1^{(1)} - \theta_2^{(1)}\left(\frac{1}{T} - \frac{1}{525}\right)\right\}\right]^{\lambda^{(1)}} \tag{2.17}$$

$$M_{II}: \quad [A]^{(2)} = \left[1 + t \times \exp\left\{\theta_1^{(2)} - \theta_2^{(2)}\left(\frac{1}{T} - \frac{1}{525}\right)\right\}\right]^{\lambda^{(2)}} \tag{2.18}$$

$$M_{III}: \quad [A]^{(3)} = \left[1 + 2t \times \exp\left\{\theta_1^{(3)} - \theta_2^{(3)}\left(\frac{1}{T} - \frac{1}{525}\right)\right\}\right]^{\lambda^{(3)}} \tag{2.19}$$

The initial prior probability Π_i^0 associated with each candidate model was assumed to be 1/3, meaning that each model has equal probability of representing the data properly.

For the first iteration, the regulatory factors were set as $w_1 = 1, w_2 = 0$ and $\beta = 1$ which concentrates the emphasis of the design on discrimination between the model candidates. The outcome was a distinct distribution of the posterior probabilities as Π = [0.0144, 0.4928, 0.4928] corresponding to the candidate models= $[M_I, M_{II}, M_{III}]$. Accordingly, the candidate I was recognized as an unqualified model structure and was removed from the matrix of model candidates at the elimination step. Rapid elimination of the unsatisfactory candidates in order to decrease the size of the analysis is one of the main concerns to optimize the computational demands. The resulting distribution of probabilities also indicates the likelihood of presenting two similar structures, and therefore M_{II} and $M_{III}$are marked as similar. Accordingly, the regulatory factors were updated to α=0.9, $\beta = 0.5$, $w_1 = 0.8722$ and $w_2 = 0.1278$ for the next iteration

At the second iteration, the input regulatory factors gradually shift the focus of the design from only model discrimination to partly parameter estimation. Meanwhile, the emphasis is still on the discrimination power since two candidate structures (M_{II}, M_{III}) were marked as similar in the last iteration. On the other hand, the setting α=0.9 keeps the focus of the *E-criterion* mostly on the orders rather than the other parameters. Accordingly, the second experimental point was extracted and the posterior probabilities were updated to Π = [0.5000 0.5000]. The calculated probabilities show the high possibility of having two similar or dependent structures. Thereby, one structure was randomly

eliminated. It was assumed that the candidate III was selected for elimination. By limiting the candidate model structures to only one, the regulatory factors w_1 and w_2 are updated accordingly to 0 and 1, respectively. This adjustment moves the focus of the next iterations completely towards the parameter estimation. Meanwhile, the gradual decrease of α at each iteration step changes the focus of the *E-criterion* from mostly evaluation of orders to estimation of other parameters.

After 30 iterations, the following model (Eq. 2.20) was achieved with more than 95% significance.

$$[A] = \exp\left[1 + t\exp\left\{-3.33 - 5159\,(\frac{1}{T} - \frac{1}{525})\right\}\right]^{-0.8476} \tag{2.20}$$

Comparison between the matrix of real parameters [θ^{real}, λ^{real}]=[-3.53, 5000, -1] and the estimated one[θ, λ]=[-3.33, 5159, -0.8476] shows a slight deviation. It should be considered that the model is developed based on the generated data with input variance of 0.25. The achieved model is able to predict the generated data with 83% less deviation compared to the reference model, which indicates the potential of the strategy to capture the implemented noise. The possibility of evaluating the orders provides an additional degree of freedom for the model to achieve a more precise estimation from the data and the potential noise. This capability is of the great importance for setting model-based control strategies, which are able to consider the environmental noises.

It should be mentioned that for this case study, at each iteration, only one design is extracted. However, in the case of having the sampling time as an operative factor, this approach might not be practically efficient. Ideally, the sampling time has to be specified in advance before running a new experiment. This work can be potentially done through this framework. Since the designs are based on ranking the experimental settings with their probable information content, at each iteration more than one data point can be selected. This approach would correspond to specifying e.g. more than one sampling time for each temperature setting.

Summary

The growing competition to generate new compounds forces industries to accelerate their process development. One of the essential elements towards a successful industrial process is to use efficient and rapid strategies at the early stages of research and process development.

To achieve a well-designed bioprocess, understanding the ongoing phenomena and the involved reaction kinetics is crucial. By development of advanced miniaturized reactors, a promising opportunity arises for parallel screening of multiple processes in reduced volumes within high throughput platforms. However, the collection of data that is required for building the model and validating it can still be a resource intensive task, which requires efficient and informative

experimental designs. Increasing the information content of the experiments is one of the main challenges, particularly for complex bio-systems.

This work introduces a generic Model-based Design of Experiments (M-DoE) framework with the focus on model development and system characterization. The aim is to make an interactive connection between the experimental design and the modelling to reduce the load of physical and computational experiments at the stage of system characterization and design. Within this framework, a set of informative experiments are specified to effectively support the development of predictive models for unknown processes. In the last part, the method was demonstrated on a hypothetical case study.

Glossary

m	Number of candidate models
n	Number of experiments
T	Temperature [K]
t	Time [s]
x	State of the process
ξ	Operating factors
y	Process response
λ	Model order
θ	Model parameter
σ^2	Variance
β, α and γ	Regulatory factors

References

Agarwal, A.K. & Brisk, M.L., 1985. Sequential experimental design for precise parameter estimation. *1197. Sole, K. Collect. Czech. Chem. Commun*, 24(2), p.1742.

Arutchelvan, V. et al., 2006. Kinetics of high strength phenol degradation using Bacillus brevis. *Journal of Hazardous Materials*, 129(1–3), pp.216–222.

Atkinson, A. & Donev, A., 1992. Optimum Experimental Designs, volume 8 of Oxford Statistical Science Series. *Oxford University Press*.

Atkinson, A.C. & Bogacka, B., 2002. Compound and other optimum designs for systems of nonlinear differential equations arising in chemical kinetics. , 61, pp.17–33.

Atkinson, A.C. & Bogacka, B., 1997. Compound D - and D S -Optimum Designs for Determining the Order of a Chemical Reaction. *Technometrics*, 39(4), pp.347–356.

Atkinson, A.C. & Hunter, W.G., 1968. The Design of Experiments for Parameter Estimation. *Technometrics*, 10(2), pp.271–289.

Baş, D. & Boyacı, İ.H., 2007. Modeling and optimization I: Usability of response surface methodology. *Journal of Food Engineering*, 78(3), pp.836–845.

Box, G. & Draper, N., 1987. *Empirical model-building and response surfaces.*,

Box, G.E.P. & Behnken, D.W., 1960. Some New Three Level Designs for the Study of Quantitative Variables. *Technometrics*, 2(4), pp.455–475.

Box, G.E.P. & Hill, W.J., 1967. Discrimination Among Mechanistic Models. *Technometrics*, 9(1), pp.57–71.

Box, G.E.P., Hunter, J.S. & Hunter, W.G., 2005. Statistics for experimenters: design, innovation and discovery. *Wiley*, 13.

Box, G.E.P. & Hunter, W.G., 1965. The Experimental Study of Physical Mechanisms. *Technometrics*, 7(1), pp.23–42.

Box, G.E.P. & Lucas, H.L., 1959. Design of Experiments in Non-Linear Situations. *Biometrika*, 46(1/2), p.77.

Box, G.E.P. & Meyer, R.D., 1986. An Analysis for Unreplicated Fractional Factorials. *Technometrics*, 28(1), pp.11–18.

Box, G.E.P. & Wilson, K.B., 1992. On the Experimental Attainment of Optimum Conditions. In Springer, New York, NY, pp. 270–310.

Box, M.J., 1968. The Occurrence of Replications in Optimal Designs of Experiments to Estimate Parameters in Non-Linear Models. *Journal of the Royal Statistical Society. Series B (Methodological)*, 30, pp.290–302.

Bruwer, M.-J. & MacGregor, J.F., 2006. Robust multi-variable identification: Optimal experimental design with constraints. *Journal of Process Control*, 16(6), pp.581–600.

Chen, J. & Wang, K.-P., 2004. Sequential Experimental Design Strategy for Optimal Batch Profiles Using Hybrid Function Approximations.

Cook, R.D. & Wong, W.K., 1994. On the Equivalence of Constrained and Compound Optimal Designs. *Journal of the American Statistical Association*, 89(426), pp.687–692.

Fedorov, V. V. & Hackl, P., 1997. *Model-Oriented Design of Experiments* 41st ed., Springer.

Fisher, R., 1935. *The design of experiments.*, Oxford, England: Oliver & Boyd.

Franceschini, G. & Macchietto, S., 2007. Model-based design of experiments for parameter precision : State of the art. , 63, pp.4846–4872.

Galvanin, F. et al., 2016. A joint model-based experimental design approach for the identification of kinetic models in continuous flow laboratory reactors. *Computers & Chemical Engineering*, 95, pp.202–215.

Hill, W.J., Hunter, W.G. & Wichern, D.W., 1968. A Joint Design Criterion for the Dual Problem of Model Discrimination and Parameter Estimation. *Technometrics*, 10(1), pp.145–160.

Hunter, W.G. & Reiner, A.M., 1965. Designs for Discriminating Between Two Rival Models. *Technometrics*, 7(3), pp.307–323.

Kullback, S., 1959. *Information theory and statistics*, John Wiley & Sons, Inc.

Kumar, V., Bhalla, A. & Rathore, A.S., 2014. Design of experiments applications in bioprocessing: Concepts and approach. *Biotechnology Progress*, 30(1), pp.86–99.

Montgomery, D.C., 2008. *Design and analysis of experiments*,

Moser, A., 2012. *Bioprocess technology: kinetics and reactors*,

Muthuvelayudham, R. & Viruthagiri, T., 2002. *African journal of biotechnology.*, Academic Journals.

Plackett, R.L. & Burman, J.P., 1946. The Design of Optimum Multifactorial Experiments. *Biometrika*, 33(4), p.305.

Postma, E., Alexander Scheffers, W. & Van Dijken, J.P., 1989. Kinetics of growth and glucose transport in glucose-limited chemostat cultures ofSaccharomyces cerevisiae CBS 8066. *Yeast*, 5(3), pp.159–165.

Quaglio, M., Fraga, E.S. & Galvanin, F., 2018. Model-based design of experiments in the presence of structural model uncertainty: an extended information matrix approach. *Chemical Engineering Research and Design*, 136, pp.129–143.

Tajsoleiman, T. et al., 2017. An Efficient Experimental Design Strategy for Modelling and Characterization of Processes. *Computer Aided Chemical Engineering*, 40, pp.2827–2832..

Chapter 3

Scale-down and miniaturized reactors

The growing market for biotech products is constantly looking for inexpensive solutions for establishing efficient, robust, and sustainable bioprocesses. The knowledge of predicting the target strain behavior under the influence of the individual process characteristics plays a crucial role in the success of a bioprocess design and development study. Hence, bioprocess characterization is an essential step at early stages of process development to investigate the system, analyze the process and extract the potential and the challenges of the specific process towards an optimized bioprocess design.

Due to the high level of complexity in most of the bio-based processes, the investigation of numerous key parameters is required for a comprehensive process characterization. This task can for instance only be done through the execution of efficient DoE strategies on sets of well-controlled experimental environments (Tai et al. 2015; Łącki 2014). Different DoE techniques were discussed and a new integrated model-based DoE approach was presented in Chapter 2.

Despite the potential of DoE techniques to optimize the experiments, both in terms of number of experiments to be conducted and the amount of information that can be extracted from such experiments, it should be considered that the operation of the designed experiments still can become a critical issue from the economic perspective. On the other hand, characterization of an extended group of factors requires well-controlled environments and consistent performance to minimize the operational sources of variation. Therefore, researchers have always been looking for approaches capable of minimizing the cost of operating experiments and simultaneously, improving the controllability of the operating conditions.

Since experimentation in the manufacturing scale is not economically possible and not practically feasible, for example due to potential loss of production time, there is an essential need to initially study processes in smaller volumes. Reducing the scale not only makes the experiments economically

reasonable but also provides the possibility of developing well-controlled environments for more consistent experimentation. In the context of industrial-scale process design, using scaled-down models aims at efficiently generating data in a small scale to screen the process performance under various operating conditions (Noorman 2011; Tsang et al. 2014). Scale-down experimentation has seen a great improvement in various aspects of technology from monitoring platforms to advanced bioreactors. For instance, the application of miniaturized bioreactors (MBR) made it possible to reduce the size of experimentations even more than traditional pilot/lab scales, which was not an option 10-15 years ago. Recently, research in the development of new MBRs for more representative scale-down models has become a hot topic for both biotech related companies and academia.

By introduction of high throughput principles, the application of MBRs has moved further towards design of automated platforms with the possibility of parallelizing series of experiments at lab scale. Frequently, running a complex design of experiments (DoE) is only practical with parallelization of experiments. The consequence of developing such a parallelized experimental platform is the generation of large amounts of data in a relatively short time period, which demands advanced data management systems to analyze the results. In recent years, the application of high throughput platforms in areas of medium development, strain screening, and bioprocess design has undergone significant improvements (Ladner et al. 2017). A large number of automated high throughput platforms has been commercialized, which are equipped with various types of bioreactors in the range of microliter to milliliter working volume (Vallejos et al. 2006; Long et al. 2014).

This chapter focuses on new high throughput platforms for the operation of complex DoEs. In the following section, the performance of different miniaturized bioreactors (MBR) is investigated and an example of a well-designed stirred MBR (Ambr 250) will be studied in detail.

3.1. Miniaturized reactors

The growing application of MBRs is intended to support the implementation of scale-down models within high throughput platforms for accelerated bioprocess development (Neubauer et al. 2013; Bareither et al. 2013; Long et al. 2014). In recent years, the development of capable high throughput reactors has seen enormous progress in the aspects of the operation, monitoring, and control. 96 well plates, shake flasks, microchannels, microtiter plates, miniaturized bubble columns, spin tubes and different small-scale stirred tank reactors are some of the established examples with different qualifications (Ladner et al. 2017; Łącki 2014; Bareither et al. 2013). Long *et al.* provided a comparison between a number of state of the art commercialized high throughput platforms and their application in bioprocess development (Long et al. 2014). Figure 3.1 indicates a qualitative comparison between

different types of bioreactors concerning the performance of the MBR to mimic an industrial stirred tank operating condition and its robustness in terms of screening and controllability (Neubauer et al. 2013).

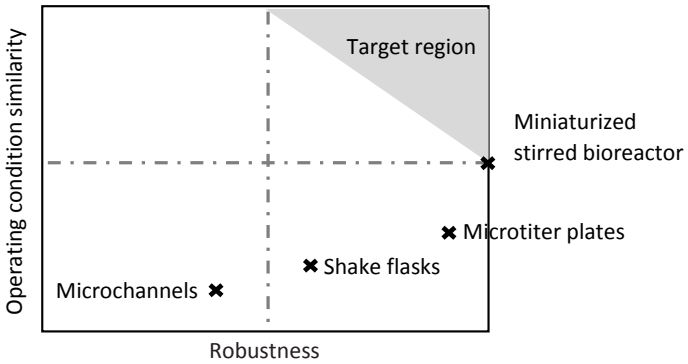

Figure 3.1. Capability of various types of miniaturized bioreactor.

Shake flasks are one of the most frequently cited small scale reactor systems which have been widely used for strain selection, growing inoculums and screening raw materials (Li et al. 2006; Bareither & Pollard 2011), with working volumes spanning from milliliters to liters (Ladner et al. 2017). Gas transfer in shake flasks is mainly limited to surface aeration. The orbital movement of the reactor dominates the level of gas transfer rate during operation. Low gas transfer rates and subsequently low levels of dissolved oxygen are the main reported issues of using shake flasks particularly for fast-growing organisms such as *E. coli* or *S. cerevisiae*. In addition, the operation of shake flasks usually suffers from the difficulty of maintaining a steady feed stream, poor controllability and lack of geometrical similarities to common large-scale bioreactors (Ladner et al. 2017).

The microtiter plate has been introduced as an alternative design to shake flasks to improve the gas transfer rate and the controllability of the reactor. This type of reactor is easy to operate with low running costs. The centrifugal movement of the reactor stimulates the surface aeration and the gas transfer rate into the liquid. The induced rotation provides a satisfactory level of oxygen transfer rate compare to shake flasks despite its poor mixing performance within the bulk of the liquid (Bareither & Pollard 2011). Regardless of all the achieved progress in the design of microtiter plate reactors, still, our knowledge of cell culture condition inside such reactors is rather limited due to the disability of online process monitoring inside the reactor (Long et al. 2014; Vallejos et al. 2006). Table.3.1 shows a list of some well-described MBRs and their applications, advantages and weaknesses.

It has been observed that some microbial cells behave differently in various bioreactors due to the intrinsic geometric differences and the corresponding fluctuating environments (Ladner et al. 2017). To minimize the design related deviations, it is crucial to have comparable geometrical configurations between scales. Miniaturized stirred bioreactors are the best alternative for the shake flasks and microtiter plates to mimic the geometrical configurations of traditional stirred tanks (Klein et al. 2013; Soley et al. 2012; Puskeiler et al. 2005; Hortsch & Weuster-Botz 2010). Controllability, mixing efficiency and higher gas transfer rates are the main improved criteria in operation of stirred high throughput bioreactors, compared to shake flasks and microtiter plates.

Over the last decade, different miniaturized stirred bioreactors were designed and developed. Hortsch and Weuster-Botz provided an interesting overview on different stirred bioreactors, used for various cell cultures in the range of 100 µl to 100 ml (Hortsch & Weuster-Botz 2010). The Ambr®250 system has recently attracted the attention of the biotech industry as a new generation of high throughput stirred bioreactors, which mimics the functionality and geometry of a typical stirred tank bioreactor. Application of this reactor has been successfully established for screening targets, process characterization and optimization (Xu et al. 2017) and the reproducibility of cultivations with this reactor was also evaluated (Kistler et al. 2016; Xu et al. 2017; Bareither et al. 2013). The design of the Ambr system was a significant move towards simulating large-scale stirred bioreactor conditions within an ideal high throughput platform. Despite its wide range of applications from animal cell culture to microbial fermentations, still, the present knowledge about this reactor is limited. Hence, the performance of an Ambr, as a well-established MBR, is critically evaluated in this chapter.

Table 3.1. Advantages and weakness of some MBR systems

MBR	Application	Advantages	Weaknesses
Shake flask (Mandenius 2016, Büchs 2001)	- Media screening - Batch and fed-batch cultures - Clone selection	- Simple - Average high throughput application - Easy to operate - Cheap - Wide range of working volumes - Easy to control the temperature	- Low controllability - Low gas transfer rate and $k_l a$ - Difficulty of feeding - Intense shaking - Lack of similarity to the industrial stirred tank
Microtiter plates (Formenti et al. 2014, Mandenius 2016)	- Media screening - Batch cultures - Clone selection	- High throughput applications - Automated robotic platform - Low labor demands	- Expensive - Limited sampling due to its low working volume - Low controllability - Difficulty of feeding - Low gas transfer rate and $k_l a$ - Evaporation - Lack of similarity to the industrial stirred tank
Micro-bioreactors (Mandenius 2016, Bareither & Pollard 2011)	- Media screening - Clone selection - Batch and fed batch culture - QbD studies - Process characterization	- Low cost - High throughput application - Application of modular concept - High controllability - Low labor demands - Possibility of different feeding and operating strategies - Possibility of integrating various measurement platforms	- Difficulty of fabrication - Small volume and limited sampling - Limitation in achieving high cell densities (Long et al. 2014) - Evaporation (Formenti et al. 2014) - Difficulty of establishing the connections to the surroundings (e.g. sensors) - Lack of similarity to the industrial stirred tank - Different flow regime
Milliliter-stirred bioreactors (Formenti et al. 2014)	- Media screening - Clone selection - Batch and fed-batch culture - QbD studies - Process characterization - Process verifications	- Geometrical similarity to industrial stirred tank - High controllability - Possibility of different feeding and operating strategies - High throughput application - Good sampling possibility - Almost similar flow regime	- Expensive - Complex

3.2. Characterization of the Ambr®250 bioreactors

The Ambr®250 system is a new generation of miniaturized stirred bioreactors (designed and commercialized by TAP Biosystems, Sartorius Biotech). 24–48 single-use pre-calibrated bioreactors can be simultaneously operated within an automated robotic workstation. The reactor and the working station are shown in Figure 3.2. Each reactor has a 250 ml working volume as the maximum capacity, with four baffles on the sides. This working volume provides enough material for sufficient sampling during an experiment. Four separate displacement pumps are used for addition of feed, base, acid, or antifoam. 24hr sampling protocols can be programmed and operated by the integrated sampling arm of the working station. The automated sampling platform guarantees the quality of screening while minimizing the involved human errors (Bareither et al. 2013; Rameez et al. 2014).

Figure 3.2. Ambr®250 by TAP Biosystems.

The Ambr®250 system is equipped with either two Rushton impellers for microbial cultures, or two elephant ear impellers for shear sensitive cell cultures. A fixed fluorescence (PreSens) sensor at the bottom of the reactor and a fixed pH gel electrode, respectively measure the dissolved oxygen level and pH during the operating process.

The performance of this reactor for animal cell cultures and bacterial bioprocesses is investigated individually in sections 3.2.1 and 3.2.2.

3.2.1. Ambr®250 for mammalian cell culture

Large-scale mammalian cell cultures have become one of the most interesting kinds of bioprocesses for the production of recombinant proteins for biotherapeutic drug products (Farid 2007; Slingsby & Dewar 2015). The market for recombinant proteins has seen a great development until 2008, a point where 120 related drugs were available on the market and more than 600 drug candidates were going through the submission process for clinical trials (Clincke et al. 2011).

Despite all the efforts to fully characterize different mammalian cell lines, still, some important metabolic kinetics have remained poorly understood (Nolan & Lee 2011). This is particularly true with respect to the influence of environmental changes, such as temperature, nutrient concentrations and inhibitor concentrations or fluid dynamics properties like shear stress or turbulence intensity on the metabolic pathways (Chalmers 2015). Using mathematical modelling and simulation tools can provide a good overview of the physical environment, which the cells are exposed to during a cell culture. The results help to better understand the consequence of changing an operating parameter with respect to the behavior of the system.

The focus of this part of the thesis is to study the influence of the fluid induced stresses on mammalian cell cultures (section 3.2.1.1). Accordingly, the performance of an Ambr bioreactor to provide an appropriate cell culture environment is evaluated (section 3.2.1.2).

3.2.1.1. Hydrodynamic limitations for mammalian cell culture

Mammalian cells are mostly known as fragile with respect to the hydrodynamic stresses due to their unique specifications such as big average cell size and the lack of a rigid cell wall (Schneider et al. 1996; Xing et al. 2009; Marks 2003; Chalmers 2015; Tajsoleiman et al. 2018). Hence, cultivating these cell cultures has always been a challenging task, which requires a deep understanding of the effective parameters, the inhibition factors, the limitations and the flexibilities. In this section, some of the most important hydrodynamic parameters in a mammalian cell culture are highlighted.

3.2.1.1.1. Eddy-cell interaction

Turbulent flow regimes are mostly characterized by a series of rotating flow units (eddies) with different size and energy (Bird et al. 2015). Mass, energy and momentum are transferred by movement of the eddies in three-dimensional space and by interactions between eddies. According to the Kolmogorov theory, the flow's kinetic energy is absorbed by the liquid in the form of heat. This phenomenon happens by passing the energy from a large primary eddy to a chain of smaller ones (Joshi et al. 1996).

A moving eddy can have an effective interaction with a suspended particle in the liquid, e.g. a cell. The type of this interaction is a function of the size of the interacting eddies compared to the size of the particle. The small particles are most likely engulfed and entrained by relatively bigger eddies (Figure 3.3.a) while smaller eddies mainly act on the surface of the particles (Figure 3.3.b). The action of a small eddy on the surface of a big particle may cause strong oscillations on the particle's wall and eventually breakage of the surface. In the case of animal cell culture, lack of a rigid cell wall increases the possibility of cell damage 'with increasing turbulence'.

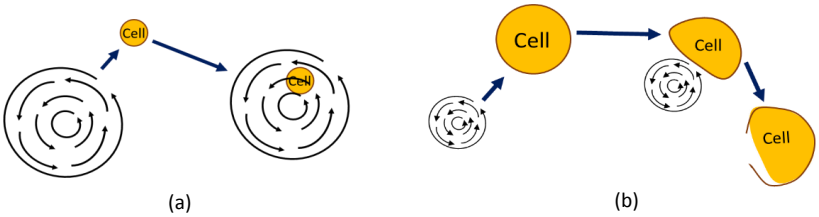

Figure 3.3. Eddy-cell interactions. a) an entrained cell by a larger eddy, b) a damaged cell by a small eddy.

The size of an eddy is estimated by the 'Kolmogorov length scale' of turbulence 'λ_k' according to Eq. 3.1 (Joshi et al. 1996). In which, 'ν' represents the medium kinematic viscosity.

$$\lambda_k = \left(\frac{\nu^3}{\varepsilon}\right)^{\frac{1}{4}} \tag{3.1}$$

The energy dissipation rate ε is the absorbance rate of turbulence kinetic energy by the liquid. According to Eq. 3.2 and Eq. 3.3 the mean specific energy dissipation rate in an aerated stirred tank is a function of the agitation speed 'N_i' and the superficial gas velocity v_s (Paul et al. 2004).

$$(\bar{\varepsilon})_{total} = \bar{\varepsilon}_{agitation} + v_s g \tag{3.2}$$

$$\bar{\varepsilon}_{agitation} = \frac{P_0 \, {N_i}^3 D^5}{V} \tag{3.3}$$

Where, P_0 is the power number as a function of impeller type and Re number, D is the impeller swept diameter and V is the volume (Nienow 2015). According to the mentioned equations, the average size of eddies decreases by increasing the agitation speed which leads to a higher risk of experiencing damaging eddy-cell interactions.

Croughan *et al.* designed a wide range of experiments to study the possibility of turbulent damages in animal cell cultures (Croughan et al. 1989). Figure 3.4 qualitatively illustrates their experimental results. According to these results, eddies smaller than the cell size can exponentially decrease the cell specific growth rate. McQueen *et al*. also found a similar correlation between the size of eddies and the death rate of suspended cells in a turbulent flow (McQueen et al. 1987).

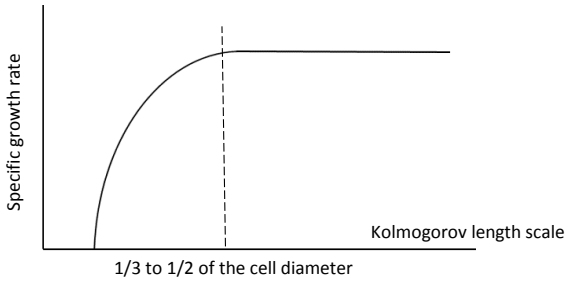

Figure 3.4. Relative specific cell growth rate versus Kolmogorov eddy length (Croughan et al. 1989).

According to Eq. 3.1, the average size of eddies in a turbulent flow increases with their fluid kinematic viscosity. Thereby, lower cell-eddy damages are expected in a more viscous medium. The supportive effect of increasing viscosity becomes more significant at higher agitation speeds. Figure 3.5 qualitatively illustrates the influence of adding a small amount of viscous additive (20 g/l dextran) in a mammalian cell culture (human diploid fibroblast) (Croughan et al. 1989). While increasing the viscosity in a mildly agitated environment doesn't show a significant effect on the cell culture, addition of the viscous compound helps to partially limit the damaging effect of small eddies in an intensive agitation condition.

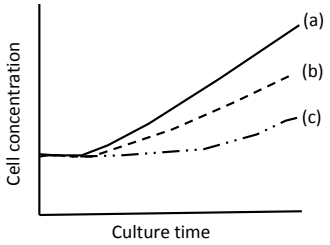

Figure 3.5. Effect of viscosity on controlling eddy-cell damaging interactions on animal cell culture: a) Low agitation speed with no viscous additive and low agitation speed with low amount of viscous additive, b) High agitation speed with low amount of viscous additive, and c) High agitation speed with no viscous additive (Croughan et al. 1989).

With similar operating conditions and only the addition of more of the viscous agent, a different aspect of using the viscous additive was studied (Croughan et al. 1989). As the qualitative Figure 3.6 illustrates, an addition of high concentrations of viscous agent can create a mildly toxic environment for the cells, which is reflected by the differences in the level of cell concentration achieved at low agitation speed with and without the viscous additive. However, at higher agitation speeds, an addition of the viscous agent can still be beneficial and protect the cells from the destructive eddy-cell interaction.

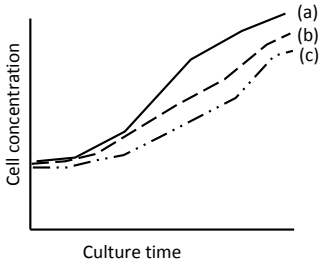

Figure 3.6. Effect of viscosity on controlling eddy-cell damaging interactions on animal cell culture: a) Low agitation with no viscous additive, b) Low agitation with high amount of viscous additive and, high agitation with high amount of viscous additive, c) High agitation with no viscous additive (Croughan et al. 1989).

3.2.1.1.2. Shear stress

The damaging effect of the flow shear stress on animal cell cultures is frequently cited in the scientific literature. Strong hydrodynamic forces caused by high shear stress may potentially trigger cell lysis and eventually cell death (Joshi et al. 1996).

Vickroy *et al.* modeled the effect of shear stress on a suspended Chinese hamster cell line by performing a set of single pass capillary experiments (Vickroy et al. 2007). Two sample solutions with moderate (87%) and low (67%) cell viability were exposed to maximum shear stress of 50 to 300 Pa. By increasing the capillary flow rate and subsequently, the level of shear stress, the cell viability showed a considerable drop. This decrease was less dramatic in the solution with higher viability. Like the previous section, the corresponding damaging effect is a function of fluid properties. By increasing the fluid dynamic viscosity, similar agitation speed creates a more intense shear stress condition. Croughan *et al.* designed a new set of experiments to study the damaging effect of shear stress on a mammalian cell culture (Croughan et al. 1989). Figure 3.7 qualitatively shows the experimental results.

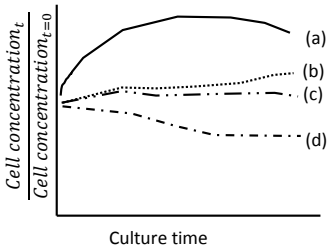

Figure 3.7. Effect of viscosity on controlling shear stress damaging interaction in an animal cell culture, a) low agitation with no viscous additive, b) high agitation with low viscous additive, c) high agitation with high viscous additive and, d) high agitation, no viscous additive (Croughan et al. 1989).

The experimental data showed that increasing the viscosity caused two opposite effects on the cell culture. With high agitation, a low concentration of the viscous additive could improve the cell culture condition (b). However, the higher additive concentration, still within the cells toxicity tolerance range, showed less improvement in the cell growth rate compare to the previous case (c). The main effect of increasing the viscosity is an increase in the flow shear stress which was expressed as an inhibiting factor for the cell culture.

In summary, for most of the animal cell cultures, a reasonable increase in medium viscosity minimizes the fluid induced cell damages mostly in high agitation speed conditions (Croughan et al. 1989). This is a true statement as long as the cells do not experience an excessive environmental stresses, such as a high shear stress or a drop in the oxygen and nutrient concentrations. It is worth to mention that the operating conditions such as mixing intensity and the gas transfer rate change in viscous media. The medium composition has to be carefully selected, not only from the material distribution point of view but also from the physical properties perspective. A balanced medium has to be able to protect the cell from the environmental stresses during a cell culture.

3.2.1.1.3. Bubble-cell interaction

Some studies of animal cell cultures reported a dramatic drop of the cell viability after starting continuous aeration (Velez-Suberbie et al. 2013; Nienow 2015; Nienow 2006). Kioukia *et al.* did an intensive investigation on the effect of aeration on mouse hybridoma cells (Kioukia et al. 1992). The experimental results showed a significant drop in the cell number and the antibody production by changing the aeration strategy from headspace aeration to a continuous sparging. This result was more significant at higher agitation speeds.

Chisti formulated the effect of aeration on the cell viability as a function of cell loss, $\frac{dC}{dt}$ in Eq. 3.4 (Chisti 2000):

$$\frac{dC}{dt} = -k_b C \tag{3.4}$$

$$k_b = \frac{24\ QV_k}{\pi^2 d_b^3 d_T^2 h_l} \tag{3.5}$$

Where, h_l is the liquid height, d_T is the vessel diameter and V_k is a hypothetical killing volume around a bubble with average diameter d_b, which can affect a trapped suspended cell. And, Q is gas flow rate.

The raising bubbles in the liquid and bursting the bubbles at the liquid surface are the main sources of bubble-cell interactions in an aerated liquid, which are individually discussed below:

- **Bursting bubbles and the suspended cell**

The released energy by rupturing bubbles at the liquid surface has always been cited as one of the main sources of cell damages in aerated animal cell cultures (Nienow 2006). A suspended cell moves towards the liquid surface by attaching to the surface of a rising bubble or getting entrapped in the wake behind it (Figure 3.8).

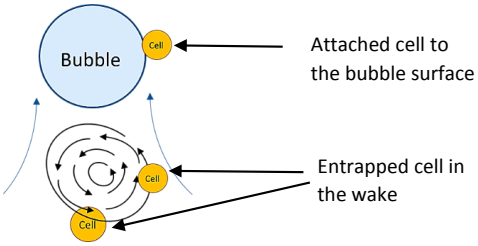

Figure 3.8. Illustration of entrained cells by a rising bubble.

The surface of a bubble thins during its rising to the liquid surface and eventually, a hole develops at the liquid film around the bubble (Figure 3.9). The bubble ruptures by expanding the surrounding ring and liquid starts flowing into the bubble space volume. Consequently, an intense turbulent area is created around the bursting bubble due to the sudden change in the liquid/gas interface and the excessive flow gradient (Chisti 2000).

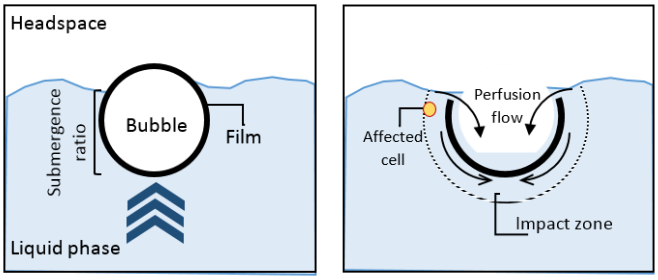

Figure 3.9. A bursting bubble at the liquid/gas interface.

Chisti did a comprehensive study to characterize the bursting energy as a function of the bubble size (Chisti 2000). Accordingly, for a bubble size in the range of 0.1-0.6 cm, smaller bubbles are corresponding to the most intensive energy releases.

The released energy and the consequent turbulent eddies may directly influence the surface of the cells present around the bursting area (impact zone). The bursting impact zone is a function of the released energy and the submergence level of the bubble in the liquid. The degree of submergence is generally bigger for smaller bubbles. Hence, bursting smaller bubbles at the liquid surface generally creates a bigger impact zone due to their higher submergence level and the higher released energy. It means that the presence of smaller bubbles in the liquid potentially increases the risk of experiencing cell damages, while bubbles larger than approximately 6 mm do not show a significant effect on the cells (Chisti 2000).

- **Influence of rising bubbles on suspended cells**

Turbulent circulation behind a rising bubble causes the secondary interaction between a bubble and a suspended cell. This interaction usually is not considered as a big issue, however, it is important to be aware of that interaction especially for the design of sensitive cell cultures in bioreactors with more than 1 m height (Chisti 2000). For bubble size less than 1 cm, the energy-dissipation rate of the wake behind a rising bubble is higher for smaller bubbles. The created eddies actively interact with the cells present at the wake impact zone (equivalent to V_k in Eq. 3.5). Even though the wake impact zone increases with the bubble diameter, the total ratio of $V_k/{d_b}^3$ in Eq. 3.5 is generally smaller for large bubbles.

3.2.1.2. CFD simulation of the fluid dynamics in an Ambr 250 system for mammalian cell cultures

In this section, the performance of an Ambr 250 bioreactor in an animal cell culture is evaluated by using CFD simulation. The results help to better understand the cell behavior under different operating conditions and flow regimes. This understanding provides crucial information for the design of optimum experiments with respect to the operating conditions.

A Chinese Hamster Ovary (CHO) cell culture is selected as a case study for this part of the thesis. In recent years, CHO cell lines were frequently considered as a potential animal cell host for producing various recombinant proteins (Jayapal et al. 2007; Clincke et al. 2011).

- **Geometrical configuration and the simulation settings**

The studied bioreactor is equipped with two elephant ear impellers connecting to a central rotating shaft and 4 stationary baffles at the reactor wall (Figure 3.10). Application of elephant ear impellers aims at minimizing the agitation shear rate for the cells (Bustamante et al. 2013). The inlet air is injected at the bottom of the reactor, below the first impeller.

The fluid dynamics inside the reactor is studied by solving an Eulerian-Eulerian two-phase model in ANSYS CFX 17.1. Two different computational domains, rotating and stationary, were assigned to the surrounding area around the impeller and the rest of the working volume, respectively (Ochieng & Onyango n.d.). The rotating and the stationary domains are shown in Figure 3.10.

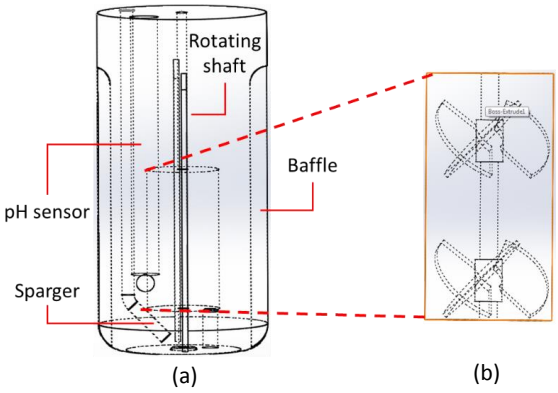

Figure 3.10. The applied geometry in the CFD simulation: a) stationary domain, b) rotating domain.

In this case study, the practical agitation varies in the range of 200-730 rpm. According to Eq. 3.6, this agitation range is corresponding to a Reynolds number (Re) of 2.5×10^3 – 9.22×10^3 in a liquid with characteristics similar to water.

$$Re = \frac{\rho N D^2}{\mu} \tag{3.6}$$

It is worth to note that the applied Reynold equation does not include the type and the number of impellers, and the reactor geometrical configurations. However, still, it's good enough to give an approximate overview of the flow regime in the reactor. There is no consensus on the range of Re for accepting a turbulent flow regime, but a significant group of literature references seem to agree with considering $Re > 10^4$ as the limit for having a turbulent flow (Stocks 2013; Paul et al. 2004). Accordingly, the estimated Reynold numbers indicate the persistence of a transitional flow regime within the specified operating range.

Simulation of a transition regime has always been a challenging task due to the high complexity of the flow and the lack of descriptive models (Larsson et al. 2015). According to the ANSYS CFX solver theory guide, the shear stress transport (SST) model is the recommended turbulence model for predicting transitional flows, which was also considered in this simulation. This model behaves like a normal k-ω based model close to the walls while it changes to a k-ε model in the free stream far from the walls (Larsson et al. 2015). This adjustment represents a transition between a low Reynold flow next to the walls, to turbulent motion in the rest of the volume. To solve a SST model, two extra equations (compared to either fully turbulent or fully laminar models) have to be solved to estimate the fluid dynamics based on the relative percentage of k-ω and k-ε. These additional calculations significantly increase the computational costs. A rough estimation for the same grid shows 18% increase in the CPU time for solving a SST model compared to a k-ε model (ANSYS CFX theory guide).

By choosing the SST model, the wall function will be automatically set to the 'automatic wall treatment'. This setting adjusts the ratio of the laminar to turbulent models at the wall based on the implemented mesh nodes close to the wall. The quality of the applied mesh particularly close to the walls plays a crucial role in the performance of a SST model. According to the 'ANSYS CFX theory guide', the dimensionless distance y^+ indicates the quality of the mesh close to the walls as a function of the distance between the wall and the first node (Eq. 3.7). Note that the physical location of the first node in ANSYS is always at the wall. However, the first node is treated as if it was Δn away from the wall. Δn is the distance between the actual first and the second node.

$$y^+ = \frac{\sqrt{\tau_\omega/\rho}.\,\Delta n}{v} \tag{3.7}$$

In Equation 3.7, τ_ω is the wall shear stress and ν is the kinematic viscosity. The comparison between the calculated y^+ and the thickness of the flow's boundary layer at the walls indicates the performance of the SST model. Figure 3.11 shows the traditional diagram of a flow profile at a fixed wall (Rao 2010). In a transitional flow regime, the boundary layer consists of a linear viscous and a logarithmic layer while in a developed turbulent flow the linear sublayer is negligible. By setting the y^+ in the linear viscous sublayer (<2), the automatic wall treatment function adjusts the SST model to solve the k-ω based equations at the wall while y^+ >30 updates the model to solve the standard wall functions for ε based models. For y^+ in between 2 and 30, the wall treatment function applies a blending factor to smooth the transition from the linear profile to the logarithmic flow profile. To take the maximum advantage of this setting, implementation of at least 10 nodes at the boundary layer is recommended. It should be considered that y^+>11.06 automatically changes the SST model to work similarly as the k-ε model.

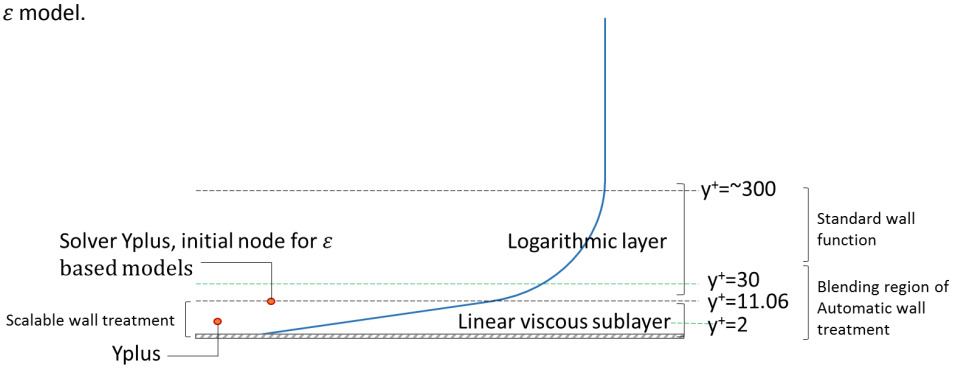

Figure 3.11. Flow boundary layers over a stationary wall in the CFD model.

Accordingly, the mesh was generated with maximum y^+=3, an expansion factor of 1.05 at the walls and a maximum aspect ratio of 1.5 for the rest of the volume. Due to the geometrical complexity, the unstructured tetrahedron elements were selected as part of the meshing strategy. 51817 elements for the impeller domain and 312972 elements for the rest of the reactor were generated in ICEM CFD 15.0.

The simulation was developed by indicating the defining as a continuous phase while the gas is modelled as disperse phase. The bubble size was set constant and equal to the calculated size for the bubble at the sparger (Eq. 3.8) (Wutz et al. 2016). The influence of agitation on breaking the bubbles was not considered in this case study.

$$d_b = \left[\left(\frac{d_o\sigma}{\rho_l}\right)^{\frac{4}{3}} + \left(\frac{81\,\mu_l Q}{\rho_l\,\pi\,g}\right) + \left(\frac{135\,Q^2}{4\,\pi^2\,g}\right)^{\frac{4}{5}}\right]^{\frac{1}{4}} \quad (3.8)$$

Where, Q is the gas flow rate, d_o is the orifice diameter and σ is the surface tension in the liquid.

A no slip boundary condition at the walls and degassing settings at the headspace interface are the main applied assumptions in the simulation. Furthermore, the interfaces between the reactor and the impeller domain were set as 'frozen rotor' with 'automatic' pitch change.

To predict the distribution of gas in the liquid, the 'Buoyant' option was activated for the gas phase. The liquid/gas interface was simulated by using 'Particle Model' with the surface tension coefficient of 0.073 N/m and the drag coefficient equas to 0.44. The Oxygen Transfer Rate (OTR) to the liquid phase is calculated according to Eq. 3.9.

$$OTR = k_l a\ (C_i^* - C_i) \quad (3.9)$$

$C_i^*$and C_l represents saturated and local oxygen concentration in the liquid, respectively. k_l stands for the liquid mass transfer coefficient and 'a' shows the liquid-gas specific interface area, calculated from Eq. 3.10.

$$a = \sum \frac{A_{p,n}}{V_l} \quad (3.10)$$

Where, $A_{p,n}$ is the bubble surface area and V_l is the liquid volume. The mass transfer coefficient k_l was estimated according to Eq. 3.11 (Wutz et al. 2016):

$$k_l = 0.7\sqrt{D_{O_2}}\left(\frac{\varepsilon\,\rho_l}{\mu_l}\right)^{\frac{1}{4}} \quad (3.11)$$

$D_{O_2}$is the diffusion coefficient of oxygen in the liquid at the operating temperature (2.81×10^{-9} m^2/s in water at a temperature of 35°C).

The solubility of gas in the liquid can be estimated by Henry's law (Eq. 3.12) (Nienow 2015), where H is Henry's constant and P_g is for instance the oxygen partial pressure in the gas phase.

$$C_i^* = \frac{P_g}{H} \quad (3.12)$$

The liquid temperature has a direct influence on the solubility of a gas by changing the Henry's constant according to Eq. 3.13. The Henry's constant for oxygen in 20°C water is 770 $\frac{L.atm}{mol}$, which was calculated to decrease up to 560 $\frac{L.atm}{mol}$ at 37 °C.

$$H(T) = H^0 \times \exp\left[\frac{-\Delta_{sol}H}{R}\left(\frac{1}{T} - \frac{1}{T^0}\right)\right] \quad (3.13)$$

Where $\Delta_{sol}H$ is the enthalpy of dissolution. Steady-state CFD simulations were operated by setting the timescale control to 'Auto Timescale' with the length scale option as 'Conservative' with time scale factor equal to 0.01. The convergence criterion was set as RMS equals to 10^{-4} conditional to reach a steady gas holdup over the liquid volume.

- **Results and discussions**

Figure 3.12.a shows the simulation result of the fluid flow in the ambr reactor containing 250 ml water with 200 rpm agitation and 40 mL/min gas flow rate. The mean bubble diameter at the sparger was calculated to be 3 mm. The gas distribution profile within the liquid phase is shown in Figure 3.12.b.

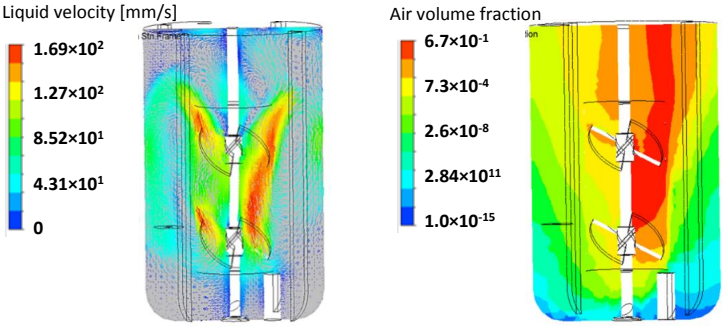

Figure 3.12. CFD simulation of gas distribution in water in Ambr 250 with two elephant ear impellers, 200 rpm agitation and 40 ml/min gas flow rate. a) liquid velocity profile and b) gas distribution profile.

The result predicts a high heterogeneity in the distribution of the gas in the liquid phase. This gradient is mainly caused by using a low power input below the critical effective agitation range. Paul *et al*. showed that for Froude (Fr) numbers below 0.04, the impeller cannot have a discernible action on the sparged gas (Paul et al. 2004), where Fr was calculated to be 0.029 in this simulated case. The applied poor mixing condition causes the formation of uncompleted flow circulating patterns, particularly below the bottom impeller, which subsequently creates some stagnant zones with low gas volume fractions. For Rushton turbines, Nienow *et al.* introduced a critical agitation speed to effectively

circulate a given gas flow rate (Nienow et al. 1977). According to Eq. 3.14 and 3.15, a minimum agitation speed of ~460 rpm is required to efficiently disperse 40 ml/min gas in the simulated Ambr reactor.

$$Fl_G < 13\, Fr^2\, (D/T)^{5.0} \tag{3.14}$$

$$Fl_G = Q_G/ND^3 \tag{3.15}$$

Where, Q_G is the sparged gas flow rate, D is the impeller diameter and T is the reactor diameter.

The gas transfer rate in a cell culture is always a key parameter. As discussed before, this parameter is mainly controlled by $k_l a$ as a function of the energy dissipation rate. Figure 3.13 shows the distribution of the energy dissipation rate and the consequent $k_l a$ distribution.

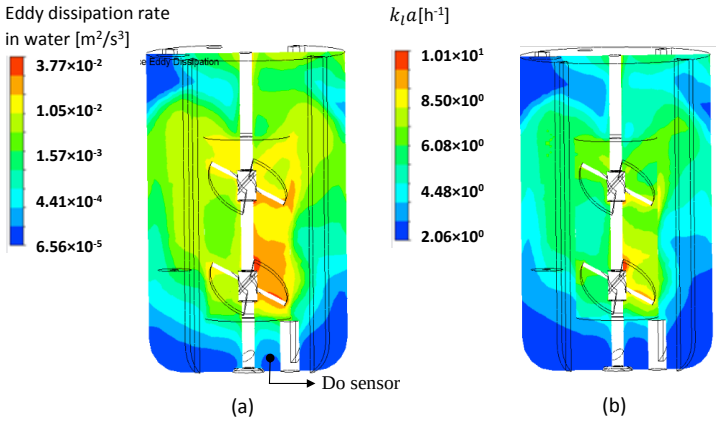

Figure 3.13. Distribution of a) eddy dissipation rate and b) $k_l a$ water in Ambr 250 with two elephant ear impellers, 200 rpm agitation and 40 mL/min gas flow rate.

The experimental measurements and the estimated $k_l a$ values for 200 rpm agitation and different air flow rates are shown in Figure 3.14. It should be considered that the measurements only provide the value for one point in the reactor. Hence, validation of the results is only based on single point measurements.

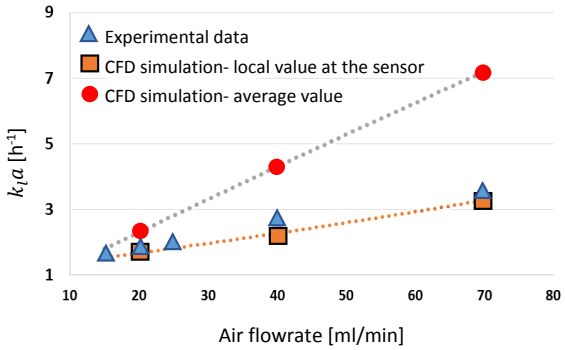

Figure 3.14. $K_l a$ values for 200 rpm agitation and different air flow rates.

The predicted $k_l a$ at the location of the DO sensor is estimated to be 2.27 h^{-1}, which is comparable with the experimental measurements (2.63 h^{-1} in 200 ml water). Part of the underestimated error is corresponding to the implementation of a higher power input in the experiment due to the difference in the volumes (250 ml for the simulations and 200 ml for the experiments). In Figure 3.13, the presence of strong turbulent zones at the impeller areas is notable while the energy dissipation rate substantially drops at the bottom of the reactor where the DO sensor is located. This result is comparable with the extracted $k_l a$ profile. The $k_l a$ distribution shows significantly higher values around the impellers compared to the rest of the reactor. On the other hand, the location of the DO sensor is at the contour volume with the lowest range of the $k_l a$. Thereby, the estimated average $k_l a$ value over the liquid volume (4.3 h^{-1}) was estimated to be much higher than the local value at the sensor point (2.27 h^{-1}). This result indicates a potential risk of having measurements, which do not represent the overall cell culture condition. It is critically important to be aware of that issue before designing the new experiments or changing the operating strategies.

The deviation between the local and the average $k_l a$ value increases for higher air flow rates where the applied agitation strategy becomes increasingly incapable of dispersing the gas in the liquid. By increasing the gas volume fraction in an inefficiently stirred environment, the risk of forming gas cavities behind the blades increases which additionally reduces the impeller power input to the liquid. Therefore, the applied mixing strategy becomes even more incapable of providing a well-mixed condition in the reactor.

By increasing the agitation speed over the critical value for similar gas flow rate (40 mL/min), the deviation between the estimated local $k_l a$ at the DO sensor point and the average value over the liquid volume decreases significantly. For 730 rpm the local $k_l a$ was estimated to reach 3.25 h^{-1} while the average value is 3.84 h^{-1}.

As discussed before, eddy-cell interaction is a critical parameter in mammalian cell cultures, which needs to be considered in the design of experiments. Regardless of being aware of having a

transitional flow regime in the liquid volume, calculation of the Kolmogorov scale of turbulence can provide useful information of the possible tension between the liquid and the cells. Figure 3.15 shows the estimated eddy size distribution at various operating conditions in the Ambr 250 reactor. As shown in Figure 3.15.a and 3.15.b, by increasing the gas flow rate and exciting the flow fluctuations, the primary eddies break into smaller units. Increasing the agitation speed has a similar but stronger influence on the size of eddies. Even though the used air flow rate in Figure 3.15.c is smaller than in Figure 3.15.a, a considerably smaller eddy size distribution was predicted under the influence of the higher agitation speed.

As discussed before, the eddy-cell interaction is characterized based on the size of the eddies and the cells. Formation of the smallest eddies around the impeller and subsequently presence of the most fluctuating part of the liquid in that region shows the most critical zones regarding the cell-eddy interactions. In the case of a CHO cell culture, the average cell diameter is more than 14 μm (Pan et al. 2017) while the predicted smallest eddy at the impeller area is 26 μm for 730 rpm agitation. Although the predicted range indicates a safe flow condition concerning the eddy induced tensions, the potential risk of cell damages for a slightly higher agitation speed is considerable. Unfortunately, no experimental results were available for the higher agitation speeds.

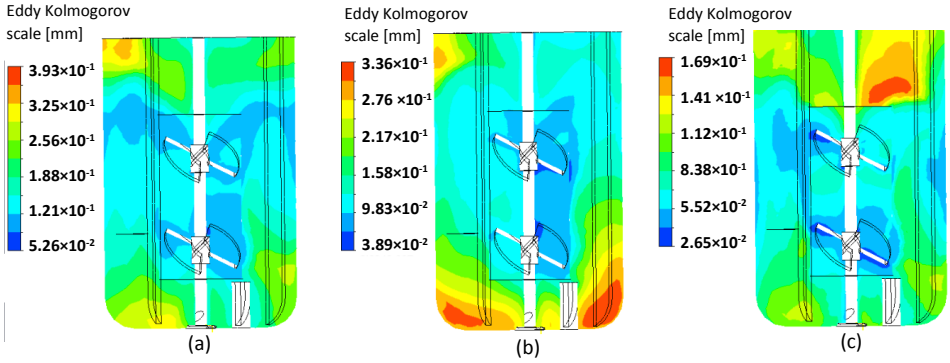

Figure 3.15. Eddy size distribution, a) with 200 rpm agitation and 20 mL/min aeration, b) with 200 rpm agitation and 70 mL/min aeration and c) with 730 rpm agitation and 15 mL/min aeration.

3.2.2. Ambr®250 for microbial cell culture

In the last half century, the application of different microbial cell cultures for the production of valuable enzymes, proteins and other bioproducts have seen tremendous growth and significant improvements. A variety of host microorganisms such as *Escherichia coli*, *Saccharomyces cerevisiae, and Bacillus subtilis* have been employed to produce different biological compounds (Geciova et al. 2002). However, the design of an efficient microbial bioprocess has always been connected with a

range of difficulties and challenges, which requires a deep understanding of the process characteristics. For instance, having a viscous broth and high oxygen demand are the common characteristics of aerobic microbial fermentations (Hortsch & Weuster-Botz 2010). The bioreactor operating conditions have to be designed in such a way that the bioreactor is capable of delivering sufficient oxygen and nutrients to the microorganisms regardless of the difficulty associated with mixing a viscous liquid.

According to the general characteristics of a microbial fermentation process, the performance of an Ambr bioreactor is evaluated in this part. The studied bioreactor is equipped with two sets of Rushton turbines to provide an appropriate level of gas transfer while delivering an efficient mixing performance in a viscous broth.

3.2.2.1. Flow regime analysis

One of the most important factors in scaling processes is to keep the flow regime constant across the scales. Turbulent flow is the most established flow regime in large-scale stirred tank bioreactors and an ideal scale-down reactor needs to provide almost similar flow properties. However, extensive reduction in the size of a reactor potentially limits the range of operating flows (Stocks 2013). Achieving a turbulent flow within the operating range of a miniaturized bioreactor might become completely infeasible, particularly in the case of having viscous media, which is common for microbial cell cultures.

In the previous case study, it was shown that the implementation of elephant ear impellers with low agitation speeds risks the flow regime to hit into the transitional range. In this part, the implemented low shear impeller was replaced with a set of Rushton turbines and the range of agitation speeds is extended to more than 2000 rpm. On the other hand, the range of operating medium viscosity conditions is usually much higher in microbial fermentations than in mammalian cell cultures. Most of the microbial fermentation broths have viscosities of more than 5 mPa.s (Latifian et al. 2007). Figure 3.16 shows the estimated minimum agitation speeds that are required to create a turbulent flow at different liquid viscosities. The threshold Reynolds number for the turbulent flow was reported between 1000-10000 (Latifian et al. 2007). Hence, the estimated agitation conditions were shown for both sides of the reported range. A Reynolds number of 10000 is the most often cited value for turbulent flow in stirred tanks, which will be also considered for this case study (Stocks 2013). The results indicate that the Ambr system is able to provide a fully turbulent regime in viscous liquids with a viscosity higher than 5 mPa.s, and with agitation speeds that are more than 3300rpm. This means that an Ambr reactor can provide a turbulent flow if it operates with quite intensive agitation speed.

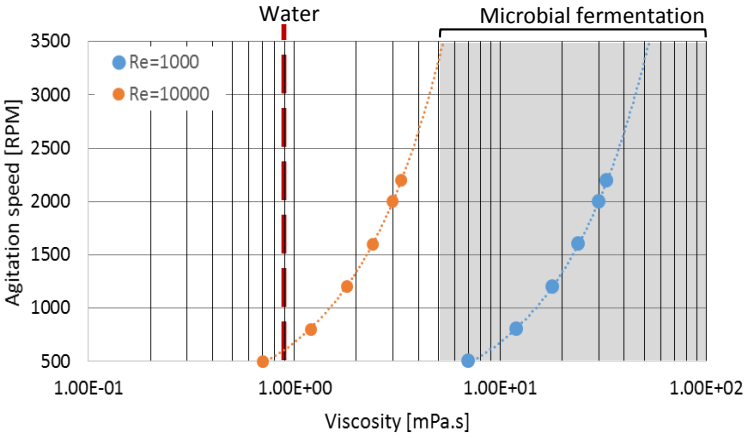

Figure 3.16. Minimum agitation speed for a turbulent flow condition in the Ambr 250 reactor.

3.2.2.2. $k_l a$ measurements

Similar to all other aerobic bioprocesses, the operation of a microbial fermentation requires a sufficient high level of the oxygen transfer rate. According to Eq. 3.9, the gas transfer rate is a function of $k_l a$. A dynamic method was used to measure the $k_l a$ values corresponding to different agitation speeds (Latifian et al. 2007). The applied method is based on the change in the level of dissolved oxygen (DO) as a function of time during a dynamic gasification step. The $k_l a$ value is measured as follows: Initially, the level of DO is reduced to zero by sparging nitrogen in the agitating liquid. After reaching a DO value of zero (or close to it), the input nitrogen flow is stopped while the liquid is kept agitated for a couple of minutes with the headspace saturated with nitrogen. This step is to eliminate the nitrogen bubbles around the DO sensor spot. The input air is then opened and the gas phase is distributed by the designed agitation condition. The increasing DO is monitored and data are saved. Finally, $k_l a$ is calculated according to Eq. 3.16 (Paul et al. 2004). X is the percentage of the dissolved oxygen concentration compared to the oxygen saturation. In this case study, X_0 is assumed as 20% oxygen saturation and X as 80% oxygen saturation.

$$k_l a(t - t_0) = \ln\left(\frac{100 - X_0}{100 - X}\right) \tag{3.16}$$

Accordingly, fifteen experiments were designed (Table 3.2) to study the influence of agitation speed and air flow rate on $k_l a$ values.

Table 3.2. Experimental design for measuring $k_l a$ values for 250 mL water at 25 C

Experiment	Agitation speed [rpm]	Air flow rate [ml/min]
1	500	100
2	500	160
3	500	225
4	800	100
5	800	225
6	1200	100
7	1200	160
8	1200	225
9	1600	100
10	1600	225
11	2000	100
12	2000	225
13	2200	100
14	2200	160
15	2200	225

The experimental measurements for a gas flow rate of 100 ml/min are shown in Figure 3.17. The data are shown with 30 s interval between each time step. As expected, the oxygen transfer rate increases with the agitation speed (Figure 3.17.a). However, after 1200 rpm an additional increase in the agitation speed showed an opposite effect on the gas transfer rate (Figure 3.17.b).

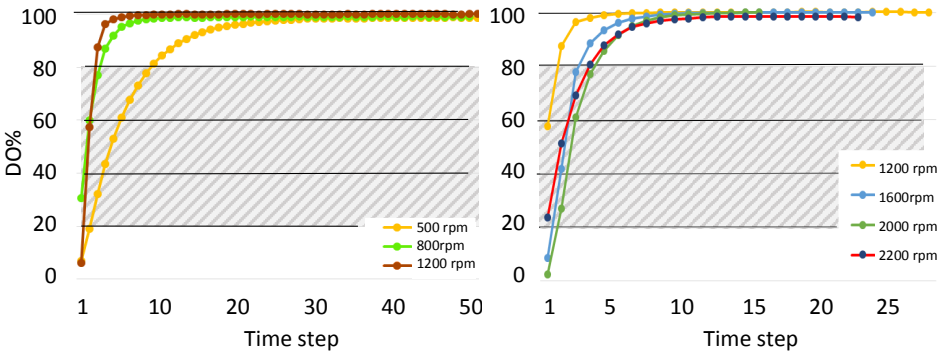

Figure 3.17. DO measurements in 250 ml water with 100 ml/min aeration in the microbial Ambr 250 with Rushton impellers.

Figure 3.18 shows the calculated $k_l a$ values for an air flow rate of 100 ml/min and 225 ml/min, respectively, in different agitation conditions. For both aeration conditions, the $k_l a$ value increased with the agitation speed until it reaches a critical rotational speed, where a further increase in the agitation shows an opposite effect on the $k_l a$ values. This behavior is explained in detail in section 3.2.2.3. The second identical thing that can be observed from the calculated results is the influence of air flow rate on increasing the $k_l a$ value and changing the critical agitation speed to a higher value.

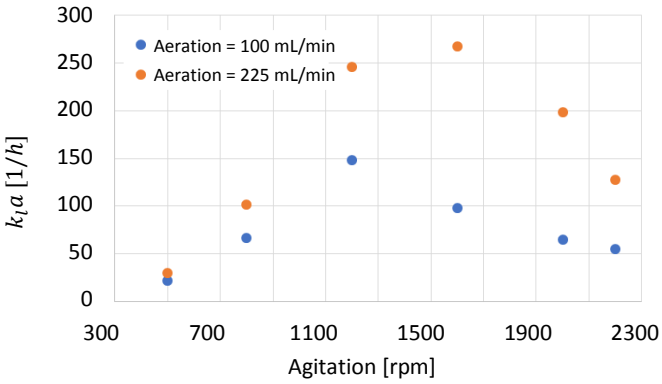

Figure 3.18. $k_l a$ measurements in 250 ml water in the microbial Ambr system.

The operated liquid property is not in the common range of viscosity values for fermentation broths. 0.125% and 0.25% Xanthan solutions can provide a better representation of microbial cell culture properties (Bach et al. 2017). The prepared liquid is a non-Newtonian shear thinning solution in which the viscosity varies with the shear strain rate. Similar $k_l a$ experiments as the previous part were executed according to the designed operating conditions in Table 3.3.

Table 3.3. Experimental design for measuring $k_l a$ values for 200 mL liquid volume with 100 mL/min aeration at 25 C.

Agitation speed(rpm)	
0.125% Xanthan solution	0.25% Xanthan solution
500	500
800	800
1200	1200
1600	1600
2000	2000
2200	2200

Based on the measured DO values, the $k_l a$ values were calculated for both prepared solutions, and the results are shown in Figure 3.19. Similar to the previous case study, the differences in the influence of the agitation speed on the $k_l a$ value, below and above a critical impeller speed, is noticeable. The most important point in this experiment is the effect of viscosity on changing the critical agitation speed. The critical agitation speed shows a higher value in the viscous solution. The influence of viscosity on the critical agitation speed is studied by means of CFD simulations in section 3.2.2.3.

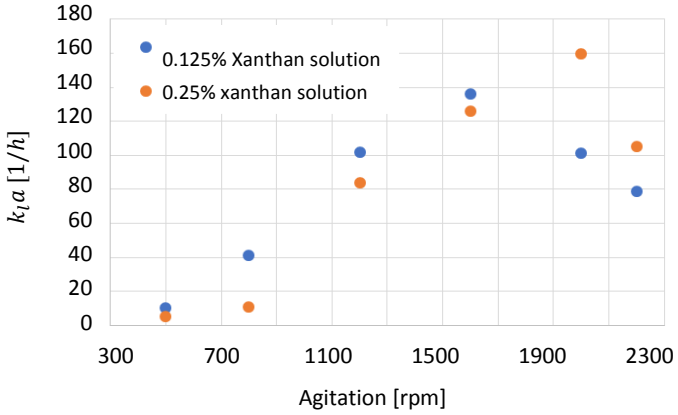

Figure 3.19. $k_l a$ measurements in 200 ml Xanthan solution in the microbial Ambr system.

Experimental results indicate the enhancing influence of the aeration speed on the gas transfer rate. Figure 3.20 shows the rate of increase of the DO concentration as a function of time under different aeration conditions in low and highly intense agitated water.

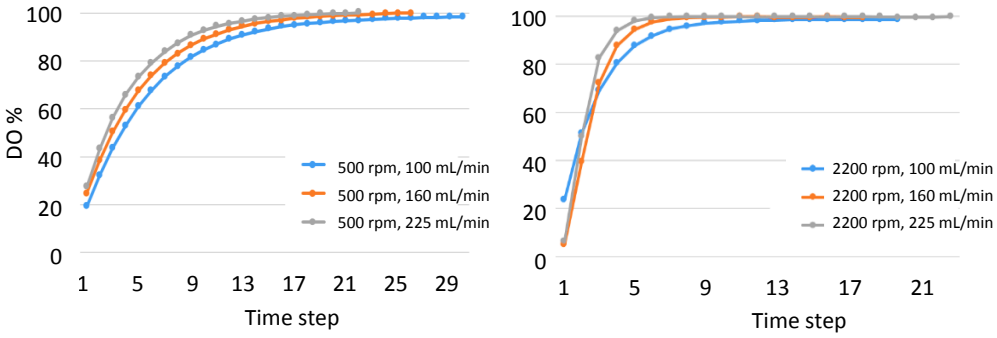

Figure 3.20. The effect of aeration on the gas transfer rate in 25 0ml water in the microbial Ambr

In both cases, the gas transfer rate is increased by the increase of the air flow rate. However, the influence of aeration on the gas transfer rate compared to the agitation speed is not significant. Experimental results indicate that 60 % increase in the agitation speed from 500 rpm to 800 rpm shows a higher effect on the $k_l a$ value than a 125 % increase in the air flow rate (Figure 3.21).

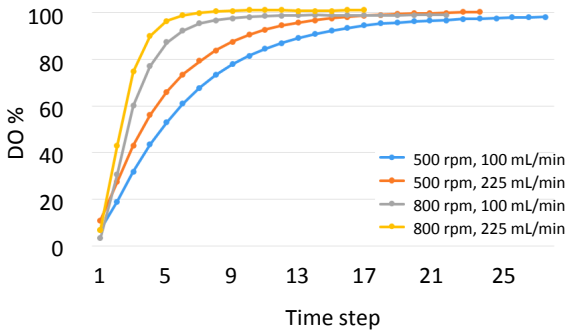

Figure 3.21. The effect of aeration compared to the agitation on the gas transfer rate in 250 ml water in the Ambr with Rushton turbines.

The extracted experimental data in this part are analyzed more in the next section, and are put in perspective in comparison with the CFD results.

3.2.2.3. CFD simulation of the fluid dynamics in Ambr 250

In this section, the performance of an Ambr bioreactor for microbial cell culture is evaluated in the case of 'cellulases' fermentation with Trichoderma reesei (Bach et al. 2017). *Trichoderma reesei* fermentation yields one of the most complex rheologies. The broth is a non_Newtonian shear thinning liquid. The average medium viscosity increases by growing the cells during the fermentation (Scargiali et al. 2013). Hence, mixing performance and the mass transfer rate inside the reactor change substantially during a cultivation.

- **Geometrical configurations and the simulation settings**

The studied bioreactor is equipped with two sets of Rushton turbines connecting to a central rotating shaft and 4 stationary baffles at the reactor wall. Similar to the previous CFD case study, two rotating and stationary domains were assigned to the surrounding area around the impeller and the rest of the working volume, respectively. These domains are illustrated in Figure 3.22. In total, 9444 elements/ml for the impeller domain and 2091 elements/ml for the rest of the reactor were generated in ICEM CFD 15.0.

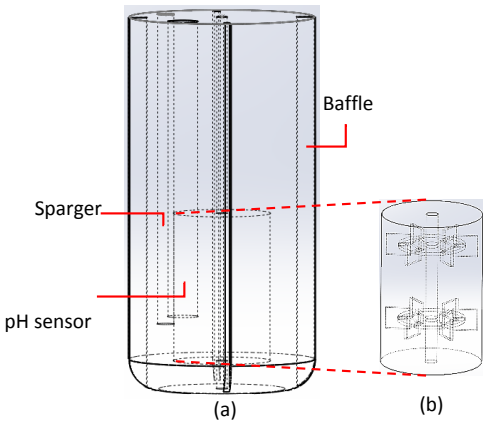

Figure 3.22. The applied geometry in the CFD simulation: a) stationary domain, b) rotating domain.

Transient CFD simulation of a two-phase system was performed by using the 'Second Order Backward Euler' transient scheme in ANSYS CFX 17.1. Up to 40 s real time experiment were simulated with 0.001 s initial time step, which was changed during the simulation to a maximum of 0.05 s. The gas/liquid interface was specified by indicating both liquid and gas as continuous phases with Buoyant reference density of 1.185 kg/m^3. The interface between the liquid and the headspace is simulated by using the standard 'Free surface model' with the surface tension coefficient of 0.073 N/m. Despite the possibility of operating the reactor in the transitional regime, the k-ε turbulent model with 'scalable wall function' was selected for simulating the fluid dynamics. According to the 'ANSYS CFX theory guide', by choosing the scalable wall function, the closest nodes to the walls with $y^+ < 11.06$ are treated as they are placed at $y^+=11.06$. Therefore, reducing the size of elements at the walls more than the critical $y^+=11.06$ does not bring any extra precision.

The simulation is initialized by setting the liquid /headspace interface with 0 Pa relative pressure at the headspace. A no-slip boundary condition at the walls and an open boundary at the reactor's cap are the main applied assumptions in the simulation. Furthermore, the top and the bottom interfaces between the reactor and the impeller domain were set as 'frozen rotor' while the cylindrical interface was defined as 'Transient Rotor stator' with 'automatic' pitch changes. In this simulation, the convergence criterion was set to RMS equals to 10^{-4} with maximum 50 coefficient loops.

- **Results and discussions**

Despite the fact that the CFD simulation of a transient regime may not deliver accurate predictions, the results can give valuable information about the fluid dynamics and its influence on the process

properties, and then specifically on the $k_l a$ value. The outcome of the simulation part is mostly used for interpretation of the experimental results.

From the experimental part, it was seen that the $k_l a$ value decreases with increasing agitation speed after a critical agitation setting has been exceeded. The source of this behavior can be investigated by looking at the situation of the liquid/headspace interface at different agitation speeds. Figure 3.23 shows the transient simulation of 250 ml water with 800 rpm agitation speed. The results are shown at the simulation time of 0 s and 36 s, respectively.

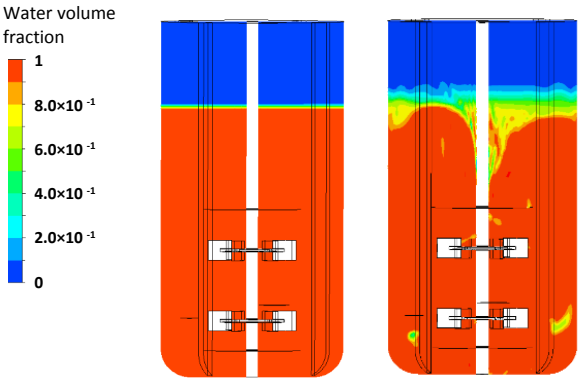

Figure 3.23. Transient CFD simulation of the liquid/gas interface for 800 rpm agitation and no aeration.

The results indicate the possibility of forming a significant central vortex at the liquid/gas interface due to the high implemented power input (P/V) and the corresponding strong tangential velocities (Nagata 1975). Formation of a vortex in miniaturized bioreactors was already discussed in the scientific literature, however, it did not receive the adequate attention so far (Larsson et al. 2015)(Assirelli et al. 2008)(Haque et al. 2006).

Assirelli *et al.* modeled the formation of a vortex in an agitated tank. The height of the vortex was shown to vary as a function of the agitation speed to the power of two (Assirelli et al. 2008). Figure 3.24 illustrates the different stages of vortex formation in a stirred reactor. The critical agitation speed is the operating condition, which the vortex reaches to the impeller plane (Figure 3.24.b). An excessive agitation speed, more than the identified critical value. can extend the height of the vortex beyond the impeller plane. In that situation, the blades are completely or partially placed in the headspace volume. Rotation of blades outside the liquid phase is equivalent to the complete loss of their effect and the partial submergence of the blades means that the effect of only a portion of implemented power input is transferred to the liquid phase, corresponding to the surfaces of the impeller that are

below the water. Rotation of partially submerged blades pushes the headspace gas directly into the liquid (Figure 3.24.c). In transparent liquids, this phenomenon can be observed by appearance of relatively large bubbles around the affected impeller. Accumulation of bubbles around the blades and subsequently, the formation of big cavities can dramatically reduce the influence of the applied agitation power input on the liquid.

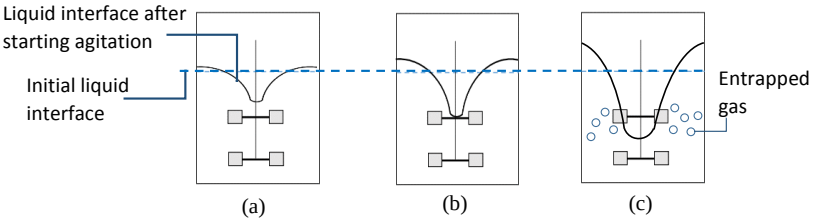

Figure 3.24. Development of a vortex by increasing the agitation. a) formation of a vortex, b) development of the vortex up to the impeller plane, c) extended vortex behind the blades and trapping the headspace gas into the liquid.

Hence, running the experiment above the critical agitation speed is equivalent to the loss of a portion of the agitation power input and consequently a reduction of the $k_l a$ value. Figure 3.25 shows CFD simulations of 800 rpm and 1600 rpm agitation speeds after 36 s real time. The simulations show that the generated vortex with 800 rpm agitation speed does not reach the top blades while with 1600 rpm the depth of the vortex extended to the impeller surface. Consequently, the gas holdup is estimated to increase by partial rotation of the top impellers in the headspace gas volume.

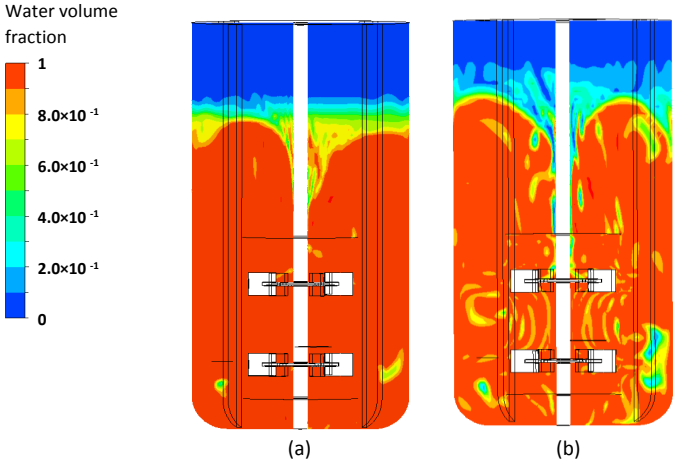

Figure 3.25. CFD simulation of the vortex at 36 s simulation time in 250 ml water with a) 800 rpm and b) 1600 rpm agitation.

Figure 3.26 shows the measured $k_l a$ values as a function of agitation speeds versus the estimated vortex height in 250 ml water. The results indicate that by reaching the vortex to the top impeller at the critical agitation speed, a further increase in the rotational speed costs a drop in the oxygen transfer coefficient.

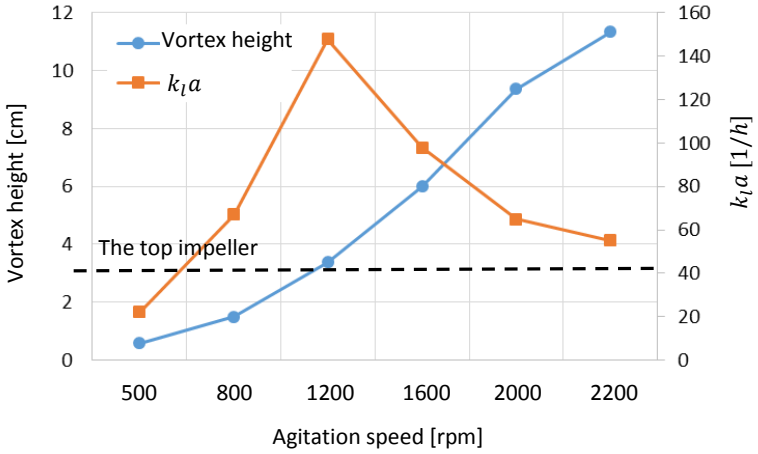

Figure 3.26. The critical agitation speed in 250 ml water in the microbial Ambr.

Similarly, in the 0.125% and 0.25% xanthan experiments the measured $k_l a$ decreased by increasing the agitation speeds more than 1600 rpm and 2000 rpm, respectively (the extracted values are with 100 ml/min aeration). The estimated critical agitation speeds for liquid viscosities equal to 0.01 Pa.s and 0.02 Pa.s with no aeration are estimated as 1600 and 2700 rpm, respectively. The applied viscosities are within the expected range for the prepared solutions (Bach et al. 2017).

It should be considered that the value of the critical agitation speed is also a function of the distance between the stationary liquid surface and the impeller plan. Figure 3.27 shows the estimated vortex in 150 ml and 250 ml water with 800 rpm agitation. For 250 ml liquid the selected mixing condition is below the critical agitation speed while in the smaller volume, the vortex is predicted to have passed the critical value and reaches the impeller zone.

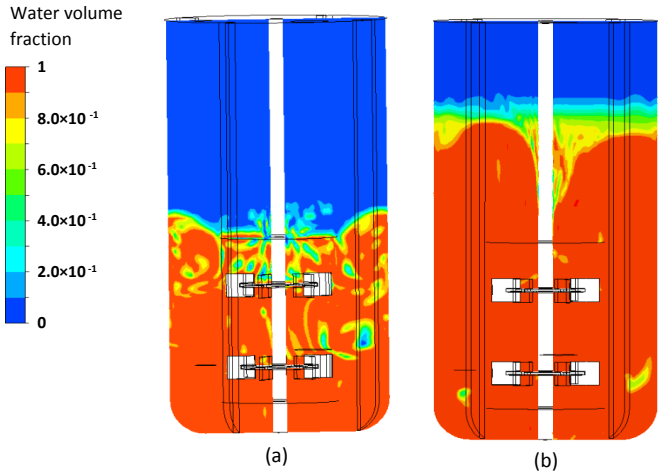

Figure 3.27. CFD simulation of the vortex at 25s simulation time in a) 150 ml water and b) 250 ml water with 800 rpm agitation.

Figure 3.28 shows the estimated critical agitation speeds in the Ambr 250 reactor with different working volumes and viscosities. It is shown that the critical agitation speed increases with the liquid viscosity and the working volume.

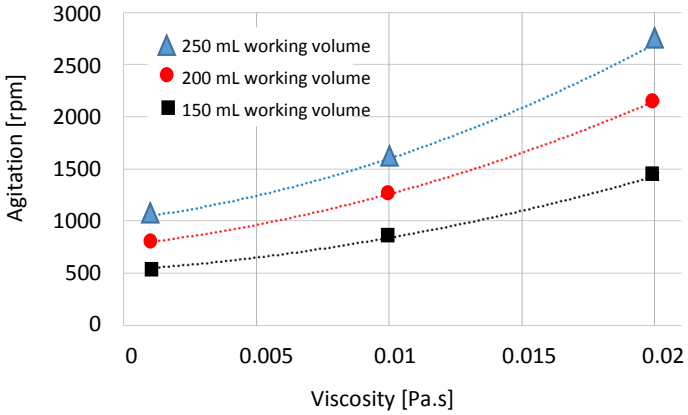

Figure 3.28. Critical agitation speeds as a function of liquid viscosity for different filling volumes of the reactor.

According to Assirelli *et al.*, the height of a vortex is a strong function of the liquid viscosity (Assirelli et al. 2008). Hence, the risk of appearance of a significant vortex is less in viscous media e.g. the last part of a fermentation process. Figure 3.29 shows the predicted vortexes for 1600 rpm agitation speed in liquids with a viscosity of 0.001 Pa.s and 0.5 Pa.s, respectively. The results shown correspond to time equal to 25 s.

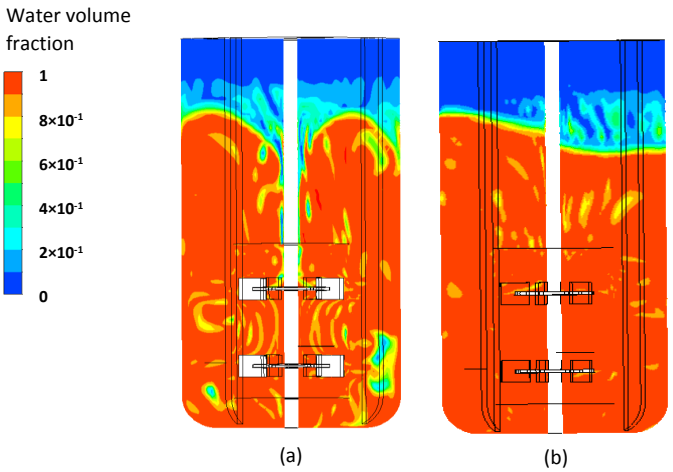

Figure 3.29. CFD simulation of the vortex at 25 s simulation time in 250 ml liquids with viscosities a) 0.001 Pa.s and b) 0.5 Pa.s and 1600 rpm agitation speed.

Finally, it should be considered that the critical agitation speed is also affected by the air flow rate. The liquid height changes by starting the aeration of the liquid phase. By increasing the gas hold up, the liquid is slightly lifted and the distance between the liquid/headspace interface and the impeller plane increases. Therefore, the critical agitation speed is always higher in an aerated stirred tank compared to a non-aeration condition. Figure 3.30 compares the DO measurements for various agitation speeds and two different aeration conditions in water. For an air flow rate of 100 ml/min, the measured gas transfer rate for 2200 rpm is even smaller than for 800 rpm due to the influence of the vortex while by increasing the aeration and lifting the liquid phase the gas transfer rate for 2200 rpm becomes higher than for 800 rpm. A similar behavior was observed in the Xanthan experiments.

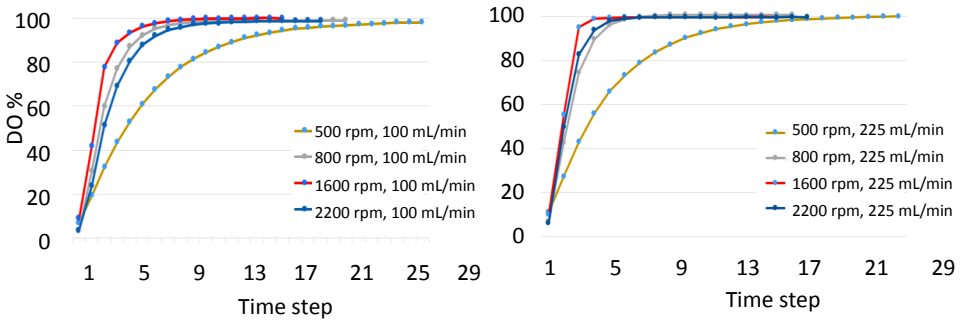

Figure 3.30. The effect of aeration on the liquid height and the critical agitation speed.

Summary

The scale-down theory is a potential approach for mimicking large-scale processes in lab scale units in order to operate complex DoE strategies within economic and well-controlled environments. Development of various high throughput reactors provides a capable physical platform for the operation of the designed experiments in lab-scale volumes.

Reducing the scale is only useful when the scaled model can represent similar conditions as the large-scale process. Moving across scales never becomes successful without a deep understanding of the ultimate scale and the performance of the full-scale bioreactor. It is critically important to be aware of the flexibilities and the limitations of the selected reactors before the design of a scaled-down model. The combination of the experimental results with mathematical modeling and simulation provides the possibility of improving our knowledge of the determining phenomena, e.g. fluid dynamics, mass transfer efficiency, in different systems. The results substantially help to evaluate the performance of the reactor under different operating conditions.

This chapter contributes to extending the present knowledge on MBRs for cell cultures and microbial fermentations by combining experimental data and simulation results. In this perspective, the potential of using a MBR was discussed by introducing several well-established MBRs and specifically, studying an example lab-scale bioreactor (Ambr 250) in detail. The capability of an Ambr bioreactor was critically evaluated with experimental data and the CFD simulations. In this study, different challenges of operating this reactor, such as the difficulty of developing a turbulent flow, the problem of creating a high shear condition around the impeller blades and the risk of forming a vortex in the liquid were identified and discussed in detail.

Glossary

$A_{p,n}$	Bubble surface area [m^2]
a	Liquid-gas specific interface area [m^{-1}]
C	Cell density [cell m^{-3}]
C_i^*	Gas solubility in the liquid [mol m^{-3}]
D	Impeller swept diameter [m]
D_{O_2}	Oxygen diffusion coefficient [m^2 s^{-1}]
d_b	Bubble diameter [m]
d_o	Orifice diameter [m]
d_T	Vessel diameter [m]
g	Gravity acceleration [m s^{-2}]
H	Henry's constant [mol m^{-3} Pa^{-1}]
h_l	Liquid height [m]
k_l	Liquid mass transfer coefficient [m h^{-1}]
N	Agitation speed [s^{-1}]
P_g	Gas partial pressure [atm]
P_0	Power number
Q	Gas flow rate [m^3 s^{-1}]
R	Gas constant [J mol^{-1} K^{-1}]
T	Temperature [K]
t	Time [s]
V	Volume [m^3]
V_k	Hypothetical killing volume [m^3]
X	Gas saturation level [%]
λ_k	Kolmogorov length scale [m]
ν	Kinematic viscosity [m^2 s^{-1}]
ν_s	Superficial gas velocity [m s^{-1}]
ε	Energy dissipation rate [m^2 s^{-3}]
ρ	Density [kg m^{-3}]
μ	Dynamic viscosity [Pa s]
τ_ω	Wall shear stress [N m^{-2}]
Δn	Distance between the first node and the wall [m]
σ	Liquid surface tension [N m^{-1}]

References

ANSYS® Academic Research, 2013, Release 15.0, Help System, Fluent: Theory Guide, ANSYS, Inc.

Assirelli, M. et al., 2008. Macro-and micromixing studies in an unbaffled vessel agitated by a Rushton turbine. *Chemical Engineering Science*, 63, pp.35–46.

Bach, C. et al., 2017. Evaluation of mixing and mass transfer in a stirred pilot scale bioreactor utilizing CFD. *Chemical Engineering Science*, 171, pp.19–26.

Bareither, R. et al., 2013. Automated disposable small scale reactor for high throughput bioprocess development: A proof of concept study. *Biotechnology and Bioengineering*, 110(12), pp.3126–3138.

Bareither, R. & Pollard, D., 2011. A review of advanced small-scale parallel bioreactor technology for accelerated process development: Current state and future need. *Biotechnology Progress*, 27(1), pp.2–14.

Bird, R., Stewart, W. & Lightfoot, E., 2015. *Introductory transport phenomena*,

Bustamante, M.C.C., Cerri, M.O. & Badino, A.C., 2013. Comparison between average shear rates in conventional bioreactor with Rushton and Elephant ear impellers. *Chemical Engineering Science*, 90, pp.92–100.

Büchs, J., 2001. Introduction to advantages and problems of shaken cultures. *Biochemical Engineering Journal*, 7(2), pp.91–98.

Chalmers, J.J., 2015. Mixing, aeration and cell damage, 30+ years later: what we learned, how it affected the cell culture industry and what we would like to know more about. *Current Opinion in Chemical Engineering*, 10, pp.94–102.

Chisti, Y., 2000. Animal-cell damage in sparged bioreactors. *Trends in Biotechnology*, 18(10), pp.420–432.

Clincke, M.-F. et al., 2011. Effect of surfactant pluronic F-68 on CHO cell growth, metabolism, production, and glycosylation of human recombinant IFN-γ in mild operating conditions. *Biotechnology Progress*, 27(1), pp.181–190.

Croughan, M.S., Sayre, E.S. & Wang, D.I.C., 1989. Viscous reduction of turbulent damage in animal cell culture. *Biotechnology and Bioengineering*, 33(7), pp.862–872.

Farid, S.S., 2007. Process economics of industrial monoclonal antibody manufacture. *Journal of Chromatography B*, 848(1), pp.8–18.

Formenti, L.R. et al., 2014. Challenges in industrial fermentation technology research. *Biotechnology Journal*, 9(6), pp.727–738.

Geciova, J., Bury, D. & Jelen, P., 2002. Methods for disruption of microbial cells for potential use in the dairy industry—a review. *International Dairy Journal*, 12(6), pp.541–553.

Haque, J.N. et al., 2006. Modeling Turbulent Flows with Free-Surface in Unbaffled Agitated Vessels. *Industrial & Engineering Chemistry Research*, 45(8), pp.2881–2891.

Hortsch, R. & Weuster-Botz, D., 2010. Milliliter-Scale Stirred Tank Reactors for the Cultivation of Microorganisms. *Advances in Applied Microbiology*, 73, pp.61–82.

Jayapal, K. et al., 2007. Recombinant protein therapeutics from CHO cells-20 years and counting. *Chemical Engineering*.

Joshi, J.B., Elias, C.B. & Patole, M.S., 1996. Role of hydrodynamic shear in the cultivation of animal, plant and microbial cells. *The Chemical Engineering Journal and the Biochemical Engineering Journal*, 62(2), pp.121–141.

Kioukia, N. et al., 1992. The impact of fluid dynamics on the biological performance of free suspension animal culture, Further studies. *Food bioprod Proc*, 70, pp.143–148.

Kistler, C. et al., 2016. High-Throughput Bioprocess Development. *Genetic Engineering & Biotechnology News*, 36(7), pp.30–31.

Klein, T., Schneider, K. & Heinzle, E., 2013. A system of miniaturized stirred bioreactors for parallel continuous cultivation of yeast with online measurement of dissolved oxygen and off-gas. *Biotechnology and Bioengineering*, 110(2), pp.535–542.

Łącki, K.M., 2014. High throughput process development in biomanufacturing. *Current Opinion in Chemical Engineering*, 6, pp.25–32.

Ladner, T. et al., 2017. Application of Mini- and Micro-Bioreactors for Microbial Bioprocesses. In *Current Developments in Biotechnology and Bioengineering*. Elsevier, pp. 433–461.

Larsson, H.K. et al., 2015. Modelling of Mass Transfer Phenomena in Chemical and Biochemical Reactor Systems using Computational Fluid Dynamics.

Latifian, M., Hamidi-Esfahani, Z. & Barzegar, M., 2007. Evaluation of culture conditions for cellulase production by two Trichoderma reesei mutants under solid-state fermentation conditions. *Bioresource Technology*, 98(18), pp.3634–3637.

Li, F. et al., 2006. A Systematic Approach for Scale-Down Model Development and Characterization of Commercial Cell Culture Processes. *Biotechnology Progress*, 22(3), pp.696–703.

Long, Q. et al., 2014. The development and application of high throughput cultivation technology in bioprocess development. *Journal of Biotechnology*, 192, pp.323–338.

Mandenius, C.-F., 2016. *Bioreactors : Design, Operation and Novel Applications.*, Wiley.

Marks, D.M., 2003. Equipment design considerations for large scale cell culture. *Cytotechnology*, 42(1), pp.21–33.

McQueen, A., Meilhoc, E. & Bailey, J.E., 1987. Flow effects on the viability and lysis of suspended mammalian cells. *Biotechnology Letters*, 9(12), pp.831–836.

Nagata, S., 1975. *Mixing : principles and applications*, Kodansha.

Neubauer, P. et al., 2013. Consistent development of bioprocesses from microliter cultures to the industrial scale. *Engineering in Life Sciences*, 13(3), pp.224–238.

Nienow, A.W., 2015. Mass Transfer and Mixing Across the Scales in Animal Cell Culture. In Springer International Publishing, pp. 137–167.

Nienow, A.W., 2006. Reactor Engineering in Large Scale Animal Cell Culture. *Cytotechnology*, 50(1–3), pp.9–33.

Nienow, A.W., Wisdom, D.. & Middleton, J.C., 1977. The Effect of Scale and Geometry on Flooding, Recirculation, and Power in Gassed Stirred Vessels. *Proc. 2nd Eur. Conf. on Mixing*, 1, pp.17–34.

Nolan, R.P. & Lee, K., 2011. Dynamic model of CHO cell metabolism. *Metabolic Engineering*, 13(1), pp.108–124.

Noorman, H., 2011. An industrial perspective on bioreactor scale-down: What we can learn from

combined large-scale bioprocess and model fluid studies. *Biotechnology Journal*, 6(8), pp.934–943.

Ochieng, A. & Onyango, M.S., CFD simulation of the hydrodynamics and mixing time in a stirred tank. *Chemical Industry and Chemical Engineering Quarterly / CICEQ*, 16(4), pp.379–386.

Pan, X. et al., 2017. Metabolic characterization of a CHO cell size increase phase in fed-batch cultures. *Applied microbiology and biotechnology*, 101(22), pp.8101–8113.

Paul, E.L., Atiemo-Obeng, V.A. & Kresta, S.M., 2004. *Handbook of industrial mixing : science and practice*, Wiley-Interscience.

Puskeiler, R., Kaufmann, K. & Weuster-Botz, D., 2005. Development, parallelization, and automation of a gas-inducing milliliter-scale bioreactor for high-throughput bioprocess design (HTBD). *Biotechnology and Bioengineering*, 89(5), pp.512–523.

Rameez, S. et al., 2014. High-throughput miniaturized bioreactors for cell culture process development: Reproducibility, scalability, and control. *Biotechnology Progress*, 30(3), pp.718–727.

Rao, S., 2010. Modeling of Turbulent Flows and Boundary Layer. In *Computational Fluid Dynamics*. InTech.

Scargiali, F. et al., 2013. Power Consumption in Uncovered Unbaffled Stirred Tanks: Influence of the Viscosity and Flow Regime. *Industrial & Engineering Chemistry Research*, 52(42), pp.14998–15005.

Schneider, M., Marison, I.W. & von Stockar, U., 1996. The importance of ammonia in mammalian cell culture. *Journal of Biotechnology*, 46(3), pp.161–185.

Slingsby, F. & Dewar, S., 2015. Use of the ambr®250 in combination with high-throughput design and analysis tools for rapid, scalable USP development.

Soley, A. et al., 2012. Development of a simple disposable six minibioreactor system for suspension mammalian cell culture. *Process Biochemistry*, 47(4), pp.597–605.

Stocks, S.M., 2013. Industrial enzyme production for the food and beverage industries: process scale up and scale down. In *Microbial Production of Food Ingredients, Enzymes and Nutraceuticals*. Elsevier, pp. 144–172.

Tai, M. et al., 2015. Efficient high-throughput biological process characterization: Definitive screening design with the Ambr250 bioreactor system. *Biotechnology Progress*, 31(5), pp.1388–1395.

Tajsoleiman, T. et al., 2018. Efficient computational design of a scaffold for cartilage cell Regeneration. *Bioengineering*, 5(2), p.33.

Tsang, V.L. et al., 2014. Development of a scale down cell culture model using multivariate analysis as a qualification tool. *Biotechnology Progress*, 30(1), pp.152–160.

Vallejos, J.R. et al., 2006. Optical analysis of liquid mixing in a minibioreactor. *Biotechnology and Bioengineering*, 93(5), pp.906–911.

Velez-Suberbie, M.L. et al., 2013. Impact of aeration strategy on CHO cell performance during antibody production. *Biotechnology Progress*, 29(1), pp.116–126.

Vickroy, B., Lorenz, K. & Kelly, W., 2007. Modeling Shear Damage to Suspended CHO Cells during Cross-Flow Filtration. *Biotechnology Progress*, 23(1), pp.194–199.

Wutz, J. et al., 2016. Predictability of $k_L a$ in stirred tank reactors under multiple operating conditions

using an Euler-Lagrange approach. *Engineering in Life Sciences*, 16(7), pp.633–642.

Xing, Z. et al., 2009. Scale-up analysis for a CHO cell culture process in large-scale bioreactors. *Biotechnology and Bioengineering*, 103(4), pp.733–746.

Xu, P. et al., 2017. Characterization of TAP Ambr 250 disposable bioreactors, as a reliable scale-down model for biologics process development. *Biotechnology Progress*, 33(2), pp.478–489.

Chapter 4

Scale-down, difficulties and challenges

Many works have discussed the advantages of scaling down bioprocesses, thereby providing economically attractive platforms for the efficient execution of various design of experiments (DoE), but there are not many studies on the limitations of such approaches (Stocks 2013). Regardless of the current trend in scaling industrial processes into miniaturized reactors, for example for screening purposes, it is crucially important to be aware of the potential challenges of using high throughput platforms for mimicking a large-scale operating condition. Design of a representative scaled-down model requires a deep understanding of the process, as well as the process flexibilities and the limitations in both large and small scales.

Usually, microorganisms are genetically manipulated and then tested in the lab before being transferred to the production scale. The problem arises when the conditions of the tests at small scale are so far from the real conditions, which might cause the organism to react differently at large scale. Therefore, the ideal scale down experiment should provide an exactly similar environment as the large scale. This equivalency needs to consider different aspects such as fluid dynamic properties, material distributions, and gradient profiles to guarantee similar process behavior in both scales.

However, in real life, the design of a scaled-down model usually experiences the limitation that not all the process parameters may be scaled or matched simultaneously. Practically, scaling processes is a task that requires certain compromises between some consistent parameters across the scales and some unselected ones to achieve the most representative process condition. Many books and articles have been written about the selection of various parameters for different systems, but so far, there is no consensus on one generic approach, which is applicable to all kinds of processes. It should be considered that targeting one or a group of scale-down parameters never guarantees the equivalency of the unchosen parameters and subsequently, the process responses from the two scales. For

instance, having a similar mixing time for both scales does not mean that the cells experience similar shear stress condition within both reactors. Hence, it is important to specify the differences between an ideal scaled-down model and the actual one and be aware of the influence of this deviation on the process behavior.

This chapter is an opinion/literature review section which aims to have a fresh look at the potential difficulties of scaling processes into miniaturized bioreactors (MBR). This work makes a significant contribution by providing a more balanced discussion between the opportunities and challenges of designing a scaled-down model for studying different processes. The focus of the chapter is on opening a new topic about the influence of the key parameters, which are rarely considered or being matched during a scale-down design, on the process performance. The provided discussions give a valuable understanding of different scaling considerations that is required for the design of a representative scaled-down model (Chapter 5).

4.1. Scale-down, a trade-off between the selection of key parameters

The design of a representative scaled-down model requires a deep understanding of the processes and the characteristics of the scales. The first step in the design of a scale-down model is to choose the size of the scaled-down model that is capable of providing comparable operating conditions as the corresponding large-scale system. There is no rule to specify the range of suitable reactor sizes for different case studies. However, a general factor in scaling processes is to not expose the cells to the environmental stresses beyond their tolerance range while trying to keep the consistency across the scales. Extreme process conditions can potentially influence the cell metabolic pathways or its viability (Tajsoleiman et al. 2018). The size of the smallest representative volume highly depends on the characteristics of the reactors and the processes. A reactor may not be suitable for a process if it cannot provide an identical operating condition to the large-scale system within the cell's tolerance range. Hence, an educated choice based on a comprehensive knowledge about the process and the reactor is needed before moving across the scales. In the case of choosing a system out of the suitable scaling range, the validity of the achieved results needs to be critically evaluated in pilot scale before making any decision for the ultimate large-scale process.

After choosing the target small scale reactor, the operational condition of the scaled-down model needs to be specified. For scaling a system, the identification of the key process parameters is crucial. Process parameters are traditionally categorized into two groups of volume-related parameters (for example the power input per unit volume (P/V) in stirred tanks and the volumetric flow rate per volume of the liquid (vvm), and the gas transfer coefficient ($k_l a$) in aerated reactors) and volume-

independent parameters (like pH, dissolved oxygen (DO) and temperature) (Xu et al. 2017). A general approach is to scale the volume-related parameters with a constant ratio while the volume-independent parameters stay constant across the scales. This approach should theoretically give an ideal scaled-down model. However, in reality, it is usually not very practical due to the scale related differences that are going to be discussed below:

In reality, it is quite rare to have similar geometries for both scales with respect to the design and the reactor configurations (Stocks 2013). The geometrical differences can affect some key process parameters. For instance, the ratio of the liquid surface-to-volume typically increases by reducing the size of the reactor. An increase in the surface-to-volume ratio contributes to increasing the influence of the headspace properties on the concentration of dissolved gases in the liquid (Li et al. 2006). On the other hand, for reactors with reduced height, the average residence time for the rising bubbles is less compared to full scale. Therefore, less gas transfer happens at the gas/liquid interface per bubble in small bioreactors. The geometrical differences are also observed in the design of the impellers, which cause different agitation impact and subsequently different mixing performance in the reactors. Usually, additional adjustments in the operating parameters such as the agitation speed or the air flow rate are required to compensate for these issues (Li et al. 2006).

The challenges related to scaling processes are not limited to some geometrical issues only. It should be considered that, in practice, usually a few of the key parameters can 'simultaneously' be matched between scales. Therefore, an important choice must be made between the candidate parameters to establish a scaled-down model. The selection of the scaling parameters has to be done based on the process properties and the outcome of analytical studies (Łącki 2014). Power input per volume (P/V), impeller tip speed, energy dissipation rate, Kolmogorov eddy length, gas transfer coefficient $k_l a$, oxygen transfer rate (OTR) and mixing time are the most frequently applied scaling parameters (scale-down criteria) in the scientific literature (Venkat & Chalmers 1996; Marks 2003; Nienow 2015). A list of different scale-down criteria is provided in Table 4.1.

The level of OTR and the $k_l a$ value are the most often selected scale-down criteria for aerobic bioprocesses such as microbial cell cultures (Hemmerich et al. 2018). The selection of these two parameters has the intention to guarantee an adequate amount of oxygen for metabolic activities during a cultivation. It is important to state that OTR and $k_l a$ are two distinct parameters, which are frequently misused or wrongly considered to be similar for the design of a scaled-down model (Ratledge & Kristiansen 2006). The state of achieving a higher $k_l a$ value in a reactor compared to another one is not necessarily equivalent to higher OTR in that reactor (Nienow 2015). These two parameters can only have identical profiles if the gas driving force ($C_{gas}^{saturation} - C_{gas}$) is similar in

both cases. Here, C_{gas} and $C_{gas}^{saturation}$ are the dissolved gas concentration and the solubility of the gas under the specified condition, respectively.

Some studies discussed the possibility of using power input as a scale-down parameter (Betts et al. 2006; Hortsch et al. 2010; S. Xu et al. 2017; Hemmerich et al. 2018). The main reason for choosing this parameter is to reach similar flow profiles and mixing conditions while the average $k_l a$ value stays within a specific range (Chalmers 2015). This criterion is mostly selected when the mixing performance is important and the system has to provide an acceptable oxygenation condition for the cells. The energy dissipation rate as a function of the power input per volume and the gas superficial velocity in an aerated reactor (Eq. 3.2) is the other scaling parameter that targets both the mixing performance and the gas transfer coefficient in the reactor (Chalmers 2015).

In another example, reaching a similar cell morphology in the scaled-down model as in the corresponding industrial process is considered to be an important factor. It should be considered that the physical properties of the cell culture environment can have an effect on the morphology of the cells. For instance, the morphology of filamentous fungi changes when applying an excessive shear stress condition (Ratledge & Kristiansen 2006). The level of shear stress is also a key factor in mammalian cell cultures due to their lack of a rigid cell wall (Chapter 3) (Nienow 2014; Nienow 2015). The l tip speed, shear stress and the Kolmogorov scale are commonly selected as scaling parameters for research studies on scaling of fermentation processes (Diaz & Acevedo 1999; Venkat & Chalmers 1996; Nienow 2015).

None of the discussed scale-down criteria focuses on recreating the heterogeneity in the large tank. Microorganisms in large-scale reactors are usually exposed to various environmental gradients, which regulate their metabolic responses and subsequently, the process performance (Brognaux et al. 2014). The production of secondary metabolites, or a reduction of the process yield, are only some common results of operating the bioprocess with a significant gradient. Various strategies have been proposed to create similar heterogeneities in a scaled-down model. Performing a pulse response experiment is one of the suggested approaches for simulating the heterogeneity present at large scale in the lab scale experiment (Wang et al. 2015). Employing oxygen concentration oscillations at small scale is to resemble a cell journey in a big tank in the presence of oxygen gradients. This kind of studies provides valuable information concerning the response of the cell under different environmental conditions. However, the determination of the oscillation strategy in terms of magnitude and frequency of the pulses has always been a challenging task which needs an experienced designer (Mandenius 2016). The introduction of compartment based scale-down designs added a new angle to the traditional One-to-One scale-down strategies. In this compartment based approach, the process condition in the big

tank is simulated in a network of connected reactors (Chalmers 2015; Lemoine et al. 2015; Haringa et al. 2016). The compartment based approach was tested on a wide range of microorganisms from microbial cell cultures such as *E.coli* and *S. cerevisiae* to mammalian cell cultures like CHO cells (Neubauer et al. 2010; Chalmers 2015). The work of Neubauer *et al.* on the application of multiple bioreactors to mimic the large-scale heterogeneity is one of the successful examples of this method (Neubauer et al. 2010). Despite the high flexibility of this approach to create various process conditions, the most challenging issue in the definition of such a system is the difficulty of characterizing the network, which includes the connections and the exchange flows between the reactors. This approach will be discussed in more detail in Chapter 5.

By looking at different scale-down approaches, it is clear that each one has a different focus on a specific target parameter while matching the other parameters is quite ignored. For instance, by choosing the power input as the scaling parameter, the focus is to reach e.g. a similar $k_l a$ value in the scaled-down model. Due to smaller diameters of the impellers in a MBR compared to a bigger tank, operation of the reactors is usually done with excessively high agitation speeds to reach similar gas transfer coefficients as in large scale. However, operating intense agitation conditions causes a high shear stress in the liquid which may not be for the benefit of a sensitive type of cell. Besides the selection of the right scale-down criterion, it is equally important to discuss the process parameters that are not chosen or are not matched with the large-scale process. More specifically, these parameters might play significant roles in the response of a scaled-down model to the changes made in these parameters. In the next sub-chapter, some process parameters that are not usually considered for scaling a process are introduced. These parameters are discussed within the scope of the scale-down limitations.

4.2. Scale characteristics and the challenges of scaling down

In most of the published studies, scaling a process was eventually simplified to matching only one scaling parameter. However, in the case of complex processes, the focus of a design has to be extended in different directions by considering multiple scaling parameters (Bareither et al. 2013). Including more parameters potentially risks the practical implementation of the design. This problem becomes even more significant in the case of using high scaling factors, e.g. from reactors of several cubic meters volume to reactors with a volume of several milliliters. Figure 4.1 shows a qualitative comparison between the difficulties of replicating an industrial process condition in different scales. A big jump across the scales brings inevitable scale-related differences, which excessively complicates matching the process parameters. Moving from an industrial scale towards miniaturized processes is usually constrained to more critical compromises in keeping the process parameters consistent.

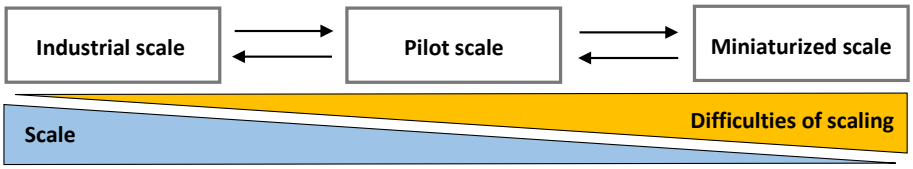

Figure 4.1. Schematic illustration of the difficulty of reproducing a large-scale process condition across different scales.

The most important point is to choose a scale-down approach while being aware of the influence of the upcoming compromises and the trade-offs made in relation to the scale's limitations. The lack of attention to the characteristics of a scale (flexibilities and limitations) can be mentioned as one of the main sources of failure in scaling processes. Some of the scale characteristics are mentioned below:

- **Flow regime**

There is a theory that the common heterogeneity in a large scale tank becomes negligible in a miniaturized reactor (Noorman 2011). This could be a true statement but only within a limited hydrodynamic flow condition. The argument can be compared with the general trend of decreasing the range of achievable Reynolds numbers (Re) with reducing the size of the reactor (Figure 4.3). It should be considered that the drop in the Reynolds number can extend to extreme conditions where the flow approaches a transient or even laminar regime instead of a turbulent motion (Stocks 2013). Figure 4.2 shows an example of the scale limitation in delivering turbulent flow regimes. In the presented case, the minimum required agitation speeds to reach a turbulent flow ($Re > 10^4$) are calculated for three different viscosities (0.001 Pa.s, 0.01 Pa.s and 0.1 Pa.s) and different scales. The assumed bioreactor is a cylindrical tank with the ratio of height/diameter equal to 2 and the ratio of impeller diameter / tank diameter equal to 0.5. The calculations show that a MBR with the same size as an Ambr 250 system has some critical limitations to create a turbulent condition as the similar large-scale reactor within a feasible operating range. This problem becomes more significant with increasing the liquid viscosity. In order to have a turbulent flow in a reactor with a working volume less than a liter, the operation with an agitation speed of more than 10000 rpm might be required for a liquid with a viscosity of 0.01 Pa.s. This agitation condition is usually out of the common operating range.

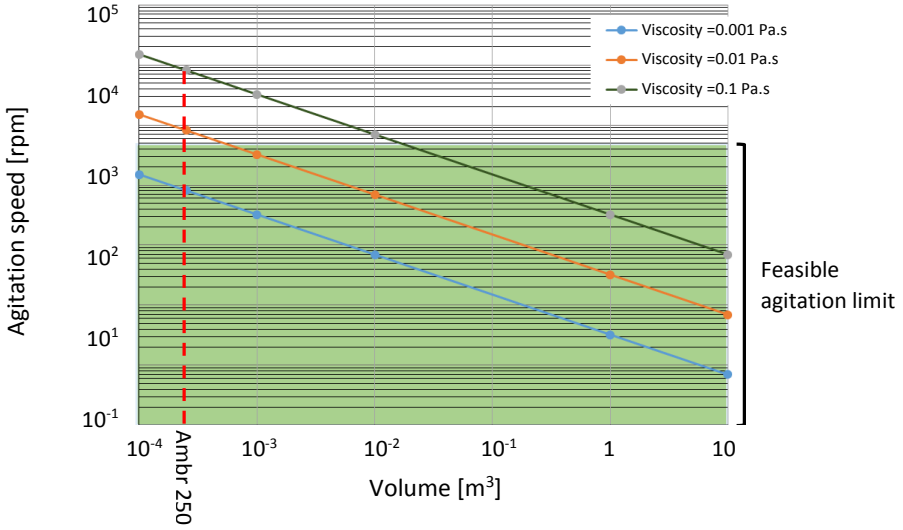

Figure 4.2. Minimum agitation speed to reach turbulence regime ($Re>10^4$) across the scales.

Formation of stagnant zones is the main consequence of disappearing turbulent motions in MBRs (Vallejos et al. 2006). Poincare´ sections are the isolated regions in the liquid which are created when the flow regime changes to transient and laminar flows ($14 < Re < 41$) (Zalc et al. 2002). An unexpected large mixing time is the result of the presence of the stagnant zones in the working volume (Vallejos et al. 2006). Figure 4.3 illustrates the calculated Reynolds numbers for an example at 2000 rpm and different liquid viscosity values in two working volumes of 1L and 100 ml, respectively. The calculated results show the possibility of moving to a transitional regime and creation of Poincare´ zones in MBRs. This non-ideality forces the operator to operate the MBR under extreme agitation speeds in order to create comparable flow regimes to an industrial reactor.

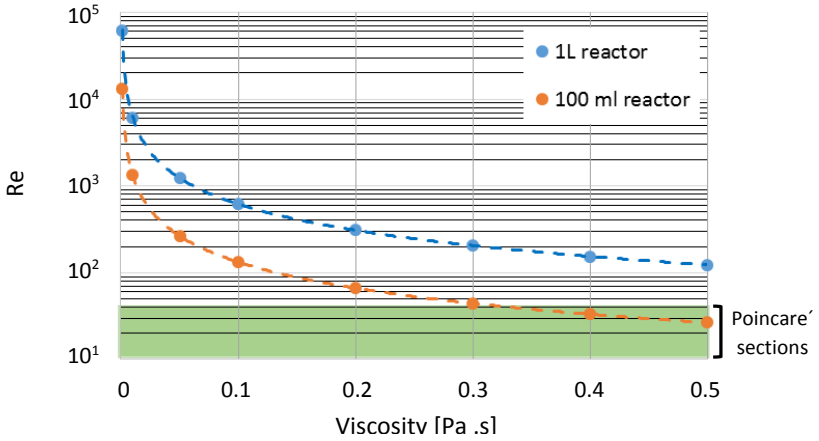

Figure 4.3. The estimated Reynolds number for 2000 rpm agitation speed for a range of liquid viscosities.

The operation at high agitation speeds is a solution to improve the flow turbulence condition in MBRs. However, it should be considered that the operation with very high agitation speeds creates new challenges. For instance, a high agitation speed is usually correlated with an excessive average shear stress, particularly around the impeller blades. Not all cells can tolerate intense shear conditions and they might experience some changes within their structures (Puskeiler et al. 2005; Tajsoleiman et al. 2018). The increase in agitation speed should be done while avoiding the risk of losing the cell's viability or causing any significant change in the cell morphology.

- **Vortices**

Formation of a vortex is a direct consequence of exposing a small liquid volume to an extreme agitation power input (Scargiali et al. 2013). Unfortunately, this phenomenon is not addressed sufficiently in the literature. In small bioreactors where employing high agitation speeds is usual, the risk of a significant vortex formation is considerably higher, particularly for low viscous liquids in unbaffled reactors (Scargiali et al. 2013). The influence of a vortex on the process operating condition was discussed in Chapter 3 within a case study.

By developing the vortex up to the impeller area and rotating the blades at the liquid/headspace interface, a mixture of liquid/gas is created around the impeller in the form of big bubbles. By increasing the gas hold up at the impeller area and developing cavities behind the blades, the impact of the impeller on the liquid phase will decrease dramatically. Moreover, part of the blades has no longer a contribution to mixing due to the decrease in the physical contact area between the blades and the liquid (cavitation). Hence, it is important to keep the rotational speed below the critical agitation setting for achieving the maximum mixing performance.

- **Pressure**

The OTR has always been an important issue for aerobic processes. As mentioned in Chapter 3, the OTR is a function of the $k_l a$ value and the oxygen driving force ($C_{gas}^{saturation} - C_{gas}$). Oxygen saturation is a strong function of the local pressure. In an industrial reactor, the summation of the hydrostatic and the headspace pressures creates a pressurized condition which highly increases the oxygen saturation level in the liquid. This improvement directly influences the OTR value in the big tank (Noorman 2006). It should be considered that the hydrostatic pressure in a MBR approaches zero due to the small working volume. On the other hand, the operation of a high-pressure headspace in polymeric reactors is usually not feasible (Stocks 2013). Therefore, the average oxygen driving force in a MBR is much smaller than in an industrial tank which means that similar $k_l a$ values in both scales anyhow leads to a significantly lower OTR in the smaller reactor. Using high oxygen concentrations in

the inlet gas or employing higher gas flow rates are the applied solutions for improving the OTR values in MBRs (Stocks 2013).

Similar to the challenges of increasing the agitation speed, there are some limitations regarding the gas flow rate. The operation with high gas flow rates in a MBR can increase the gas holdup. High ratios of gas to liquid essentially decrease the effect of the impeller power input on the liquid. In extreme conditions, the Implemented agitation may not even be adequately capable of dispersing the sparged gas in the liquid, and flooding conditions occur (Paul et al. 2004). An example of this condition was discussed in Chapter 3. Hence, the selection of a proper aeration strategy should be done with respect to the mixing performance (agitation), particularly in the case of need for extreme settings.

- **Wall function**

By reducing the scale, the ratio of the wall surface area to the liquid volume increases. Figure 4.4 illustrates this issue as an example. Similar characteristics as shown in Figure 4.2 were used for these calculations. A high surface to volume ratio means that the stationary walls can potentially slow down the turbulent motions. This interaction is in addition to the overall limitation of miniaturized reactors to create turbulent regimes, which highly increases the risk of having a transitional flow in a MBR. The influence of a stationary wall on the flow is not included in the traditional Re equation which shows the necessity of considering a safety margin in the determination of the flow regime based on the calculated Re.

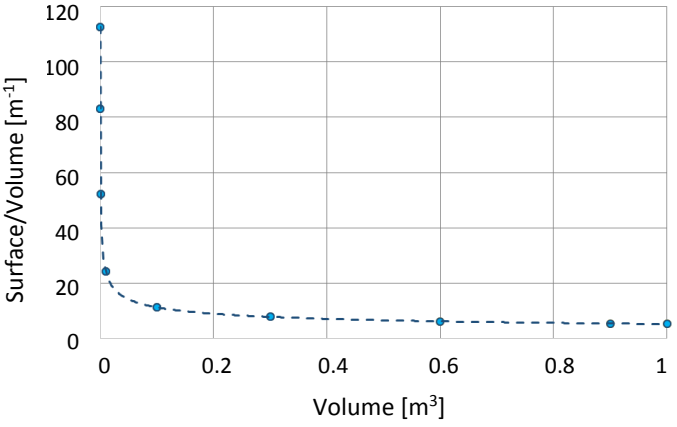

Figure 4.4. The decreasing trend of the wall surface area with increasing the size of the tank in cylindrical reactors with a geometrical ratio of height/diameter equal to two.

Reducing the turbulent motions is not the only effect of having a high surface to volume ratio. In some bioprocesses such as fungal fermentations, wall growth becomes a significant phenomenon.

Increasing the surface ratio therefore potentially enhances the cell wall growth during the process (Hortsch & Weuster-Botz 2010).

- **Governing equations**

As frequently mentioned before, a successful passage across scales with high scaling factors requires a deep understanding of the ongoing phenomena both at small and large scales (Noorman 2011). Mathematical modeling and computational simulations have always been used as helpful tools to extend our knowledge of a process behavior under different operating conditions. However, simulation of the fluid dynamics in a MBR is not exempt from the challenges of working with miniaturized scales.

As discussed before, having a transient flow regime is a likely consequence of using MBRs. The indication of a representative fluid model for this regime of the flow is a complex task concerning the theoretical background and the available numerical tools. From my point of view, the available transient fluid models are not well developed up to the extent that they cannot solve the complexity of a transient regime within an acceptable level of accuracy. Hence, in the work of different research groups it was observed that the authors preferred to use either a turbulent model or an extended version of a turbulent model which eventually cannot be considered as completely true models (Nienow et al. 2013; Larsson et al. 2015).

Moreover, some literature mentions the fact that most of the developed correlations are not generic across the scales (Vallejos et al. 2006; Micheletti & Lye 2006). Since most of the developed equations are applied for large-scale reactors, they should be critically re-evaluated before being used for estimation of the process in other scales. This deviation is mostly caused by the expression of various flow characteristics at different scales.

The above-mentioned points are only some major challenges of using MBRs to scale a range of different processes. The necessity of paying attention to the scale-related flexibilities and limitations should be emphasized, before the design of a scaled-down model is made.

One should always keep in mind that the ultimate goal of a scale-down experiment is in the end to scale back to the industrial size. Moving to ultra-small scales in the range of milliliter and less may not adequately represent industrial process conditions. Thus, the achieved results must be critically evaluated at intermediate scales (e.g. pilot scale) before moving to any larger reactors. Using pilot-scales as a verification model gives the possibility of choosing a broader range of scale-down criteria for better consistency in the process parameters between scales.

Table 4.1. Comparison of state of the art scaling criteria

Possible scaling parameters		
Parameter	**Relevance for process**	**Reference examples**
P/V	Describes power input to liquid volume from mixing and aeration. It is controlled by agitation speed and airflow rate in an aerated stirred tank.	(Hemmerich et al. 2018; Hortsch et al. 2010; Betts et al. 2006; S. Xu et al. 2017)
Gas flow rate per liquid volume	To define similar volumetric gas flow rates to the liquid volume across scales.	(S. Xu et al. 2017)
$k_l a$	To reach similar gas transfer coefficient values between scales. $k_l a$ is a function of the energy dissipation rate and the bubble size.	(Marks 2003; Nienow 2015; Islam et al. 2008; Gill et al. 2008; Kirk & Szita 2013)
Shear rate	It may have an effect on metabolites, morphology or viability of shear sensitive microorganisms.	(Marks 2003)
Superficial gas velocity	Specifies the residence time of rising bubbles and the level of gassing power input.	(S. Xu et al. 2017; Besagni et al. 2017; Subramanian 2017)
Energy dissipation rate	Indicates the turbulence level, the $k_l a$ value and the average bubble size inside the reactor.	(Hortsch et al. 2010)
Tip speed	It is considered to keep a constant ratio between the impeller diameter and the agitation speed across the scales.	(Faure et al. 2001)
OTR	Specifies the gas transfer rate to the liquid phase as a function of $k_l a$ and the oxygen saturation concentration.	(Nienow 2015; Schmideder et al. 2016)
Kolmogorov length	Determines the size of distributed turbulent eddies. It is a key parameter to estimate the influence of the induced turbulence on the suspended cells or microcarriers.	(Venkat & Chalmers 1996; Nienow 2015)

Mixing time	Illustrates the mixing performance to distribute a tracer.	(Nienow 2015)
Other scale dependent parameters that can affect a scale-down model		
Vortex formation	An outcome of intense agitation speeds in low viscous liquid.	(Assirelli et al. 2008)
Evaporation or dilution effects	Becomes significant by increasing the ratio of liquid surface to the liquid volume during a scale down procedure.	(Mears 2018)
Flow regime and the Reynolds number	Describes the fluid dynamics of the flow concerning the turbulence motions.	(Stocks 2013)
DO	Is a function of OTR and the level of oxygen uptake rate by the living microorganism.	(Kirk & Szita 2013)
Off gas CO2	Determines the level of dissolved CO_2 and the performance of CO_2 removal**.**	(Subramanian 2017)

Summary

In the past decade, the application of scale-down models has attracted the attention of biotech industries for more efficient and economical process developments. In this perspective, the potential of miniaturized bioreactors to provide the required operation platform had been proven. Besides all the advantages of using MBRs, the most important task, and simultaneously the most challenging one, is to set the operating conditions which create a representative model of the corresponding large-scale process within the small reactor.

For an efficient scale-down design, it is necessary to be aware of the flexibilities, limitations and bottlenecks of moving across the scales. Meanwhile, it is necessary to investigate the benefits and drawbacks of different scale-down strategies. It should be mentioned that most of the scale-down approaches come along with some critical compromises in choosing the scaling parameters. The result is that one in practice ignores a group of process parameters which might have significant influences on the process responses. Therefore, it is crucially important to be aware of the effect of each parameter on the process behavior before the selection of the target parameters.

In this chapter, the focus and the capabilities of some well-known scale-down approaches were studied. Moreover, a comprehensive study was made about the substantial differences between the ongoing phenomena and fluid dynamic properties across the scales. For instance, the capability of a lab-scale reactor to provide a turbulent regime and a similar pressure condition as an industrial tank was critically evaluated. The possibility of experiencing vortex formation and cell wall growth in MBRs was also discussed. The mentioned points form a collection of important factors, which are responsible for the complexity of scaling bioprocesses. Knowledge about the information summarized in this chapter substantially helps to design better scaled-down models in the future.

Glossary

a	Liquid-gas specific interface area [m^{-1}]
C_{gas}	Gas concentration in the liquid [mol m^{-3}]
$C_{gas}^{saturation}$	Gas saturation concentration in the liquid [mol m^{-3}]
k_l	Liquid mass transfer coefficient [m h^{-1}]
Re	Reynold number
P	Power input [W]
V	Volume [m^3]

References

Assirelli, M. et al., 2008. Macro-and micromixing studies in an unbaffled vessel agitated by a Rushton turbine. *Chemical Engineering Science*, 63, pp.35–46.

Bareither, R. et al., 2013. Automated disposable small scale reactor for high throughput bioprocess development: A proof of concept study. *Biotechnology and Bioengineering*, 110(12), pp.3126–3138.

Besagni, G., Gallazzini, L. & Inzoli, F., 2017. On the scale-up criteria for bubble columns. *Petroleum*.

Betts, J.I., Doig, S.D. & Baganz, F., 2006. Characterization and Application of a Miniature 10 mL Stirred-Tank Bioreactor, Showing Scale-Down Equivalence with a Conventional 7 L Reactor. *Biotechnology Progress*, 22(3), pp.681–688.

Brognaux, A. et al., 2014. Scale-down effect on the extracellular proteome of Escherichia coli: correlation with membrane permeability and modulation according to substrate heterogeneities. *Bioprocess and Biosystems Engineering*, 37(8), pp.1469–1485.

Chalmers, J.J., 2015. Mixing, aeration and cell damage, 30+ years later: what we learned, how it affected the cell culture industry and what we would like to know more about. *Current Opinion in Chemical Engineering*, 10, pp.94–102.

Diaz, A. & Acevedo, F., 1999. Scale-up strategy for bioreactors with Newtonian and non-Newtonian broths. *Bioprocess Engineering*, 21(1), pp.21–23.

Faure, A., York, P. & Rowe, R.C., 2001. Process control and scale-up of pharmaceutical wet granulation processes: a review. *European Journal of Pharmaceutics and Biopharmaceutics*, 52(3), pp.269–277.

Gill, N.K. et al., 2008. Design and characterisation of a miniature stirred bioreactor system for parallel microbial fermentations. *Biochemical Engineering Journal*, 39(1), pp.164–176.

Haringa, C. et al., 2016. Euler-Lagrange computational fluid dynamics for (bio)reactor scale down: An analysis of organism lifelines. *Engineering in Life Sciences*, 16(7), pp.652–663.

Hemmerich, J. et al., 2018. Microbioreactor Systems for Accelerated Bioprocess Development. *Biotechnology Journal*, 13(4), p.1700141.

Hortsch, R., Stratmann, A. & Weuster-Botz, D., 2010. New milliliter-scale stirred tank bioreactors for the cultivation of mycelium forming microorganisms. *Biotechnology and Bioengineering*, 106(3), pp.443–451.

Hortsch, R. & Weuster-Botz, D., 2010. Milliliter-Scale Stirred Tank Reactors for the Cultivation of Microorganisms. *Advances in Applied Microbiology*, 73, pp.61–82.

Islam, R.S. et al., 2008. Scale-up of Escherichia coli growth and recombinant protein expression conditions from microwell to laboratory and pilot scale based on matched kLa. *Biotechnology and Bioengineering*, 99(5), pp.1128–1139.

Kirk, T. V & Szita, N., 2013. Oxygen Transfer Characteristics of Miniaturized Bioreactor Systems. *Biotechnol. Bioeng*, 110, pp.1005–1019.

Łącki, K.M., 2014. High throughput process development in biomanufacturing. *Current Opinion in Chemical Engineering*, 6, pp.25–32.

Larsson, H.K. et al., 2015. Modelling of Mass Transfer Phenomena in Chemical and Biochemical Reactor Systems using Computational Fluid Dynamics.

Lemoine, A. et al., 2015. Response of *Corynebacterium glutamicum* exposed to oscillating cultivation conditions in a two- and a novel three-compartment scale-down bioreactor. *Biotechnology and Bioengineering*, 112(6), pp.1220–1231.

Li, F. et al., 2006. A Systematic Approach for Scale-Down Model Development and Characterization of Commercial Cell Culture Processes. *Biotechnology Progress*, 22(3), pp.696–703.

Mandenius, C.-F., 2016. *Bioreactors : Design, Operation and Novel Applications.*, Wiley.

Marks, D.M., 2003. Equipment design considerations for large scale cell culture. *Cytotechnology*, 42(1), pp.21–33.

Mears, L., 2018. General strategies for control of fermentation processes. *Downloaded from orbit.dtu.dk on*.

Micheletti, M. & Lye, G.J., 2006. Microscale bioprocess optimisation. *Current Opinion in Biotechnology*, 17(6), pp.611–618.

Neubauer, P., Biotechnology, S.J.-C. opinion in & 2010, U., 2010. Scale-down simulators for metabolic analysis of large-scale bioprocesses. *Current Opinion in Biotechnology*, 21(1), pp.114–121.

Nienow, A.W., 2015. Mass Transfer and Mixing Across the Scales in Animal Cell Culture. In Springer International Publishing, pp. 137–167.

Nienow, A.W., 2014. Re "Development of a scale-down model of hydrodynamic stress to study the performance of an industrial CHO cell line under simulated production scale bioreactor conditions" [Sieck, J.B., Cordes, T., Budach, W.E., Rhiel, M.H., Suemeghy, Z., Leist, C., Villiger, T.K., Morbidelli, M., Soos, M., 2013. Journal of Biotechnology 164, 41–49]. *Journal of Biotechnology*, 171, pp.82–84.

Nienow, A.W. et al., 2013. The physical characterisation of a microscale parallel bioreactor platform with an industrial CHO cell line expressing an IgG4. *Biochemical Engineering Journal*, 76, pp.25–36.

Noorman, H., 2011. An industrial perspective on bioreactor scale-down: What we can learn from combined large-scale bioprocess and model fluid studies. *Biotechnology Journal*, 6(8), pp.934–943.

Noorman, H.J., 2006. Mass transfer. In *Basic Biotechnology*. Cambridge: Cambridge University Press, pp. 201–218.

Paul, E.L., Atiemo-Obeng, V.A. & Kresta, S.M., 2004. *Handbook of industrial mixing : science and practice*, Wiley-Interscience.

Puskeiler, R., Kaufmann, K. & Weuster-Botz, D., 2005. Development, parallelization, and automation of a gas-inducing milliliter-scale bioreactor for high-throughput bioprocess design (HTBD). *Biotechnology and Bioengineering*, 89(5), pp.512–523.

Ratledge, C. & Kristiansen, B. (Bjørn), 2006. *Basic biotechnology*, Cambridge University Press.

Scargiali, F. et al., 2013. Power Consumption in Uncovered Unbaffled Stirred Tanks: Influence of the Viscosity and Flow Regime. *Industrial & Engineering Chemistry Research*, 52(42), pp.14998–15005.

Schmideder, A. et al., 2016. High-cell-density cultivation and recombinant protein production with Komagataella pastoris in stirred-tank bioreactors from milliliter to cubic meter scale. *Process Biochemistry*, 51(2), pp.177–184.

Stocks, S.M., 2013. Industrial enzyme production for the food and beverage industries: process scale up and scale down. In *Microbial Production of Food Ingredients, Enzymes and Nutraceuticals*. Elsevier, pp. 144–172.

Subramanian, G., 2017. *Continuous biomanufacturing : Innovative technologies and methods*,

Tajsoleiman, T. et al., 2018. Efficient computational design of a scaffold for cartilage cell Regeneration. *Bioengineering*, 5(2), p.33.

Vallejos, J.R. et al., 2006. Optical analysis of liquid mixing in a minibioreactor. *Biotechnology and Bioengineering*, 93(5), pp.906–911.

Venkat, R. V. & Chalmers, J.J., 1996. Characterization of agitation environments in 250 ml spinner vessel, 3 L, and 20 L reactor vessels used for animal cell microcarrier culture. *Cytotechnology*, 22(1–3), pp.95–102.

Wang, G. et al., 2015. Integration of microbial kinetics and fluid dynamics toward model-driven scale-up of industrial bioprocesses. *Engineering in Life Sciences*, 15(1), pp.20–29.

Xu, P. et al., 2017. Characterization of TAP Ambr 250 disposable bioreactors, as a reliable scale-down model for biologics process development. *Biotechnology Progress*, 33(2), pp.478–489.

Xu, S. et al., 2017. A Practical Approach in Bioreactor Scale-up and Process Transfer Using a Combination of Constant P/V and vvm as the Criterion in Wiley Online Library. *American Institute of Chemical Engineers Biotechnol. Prog*, 33, pp.1146–1159.

Zalc, J.M. et al., 2002. Using CFD to understand chaotic mixing in laminar stirred tanks. *AIChE Journal*, 48(10), pp.2124–2134.

Chapter 5

Systematic scale-down for numerical investigation of heterogeneities

5.1. Compartment based scale-down

The presence of gradients in industrial reactors has been widely studied and the subsequent effects on cell cultures were discussed in detail in several publications (Bylund et al. 1998; Lara et al. 2006; Haringa et al. 2017; Bach 2018). The heterogeneity is essentially the consequence of the applied mixing strategy, and the effects of that strategy can be observed in terms of the distribution of different variables in a reactor, such as oxygen concentration, nutrient distribution or other properties as pH. During a cultivation, the cells experience various environmental zones and changes by moving within a heterogenic environment. Hence, a cell in a large tank experiences a completely different environment than a cell, which has been grown in a homogeneous well-mixed culture such as in MBRs (Neubauer et al. 2010). This difference is one of the main sources of deviations between the cell culture performance obtained in a lab-scale experiment and in an industrial scale reactor.

As discussed in Chapter 4, mimicking the large-scale heterogeneity in lab-scale bioreactors is about creating similar environments for the cells as in the large scale tank. Exposing cells to a diverse environment to simulate the cell's journey in the large scale reactor can be done by using multiple reactors, operating at different conditions. This strategy is commonly named compartment based scale-down design. Two-compartment scale-down models have been used for many years as a scale-down design in which the cells are moving between two stirred tank reactors (STR) or a STR and a plug flow reactor (PFR) (George et al. 1993; Neubauer et al. 2010; Junne et al. 2011; Käß et al. 2014; Lemoine et al. 2015). The application of this method has been established for different purposes such as optimizing feeding strategies or studying the effect of different parameters e.g. pH gradients on the cells (Neubauer et al. 1995; Bylund et al. 2000; Amanullah et al. 2001). In recent years, the use of even

more compartments has been tested for different cell cultures like *Corynebacterium glutamicum* and *Saccharomyces cerevisiae* (Lemoine et al. 2015; Haringa et al. 2017).

Despite the potential of this approach, characterization of the compartments concerning the operating conditions e.g. the working volumes, the connections between compartments and the magnitude of the exchange flows has always been challenging. Different strategies were used to characterize the scale-down model. As an example, Junne *et al.* characterized the compartments based on the analyzed data for different flows and aeration rates and a series of pulse experiments in a *Bacillus subtilis* cultivation (Junne et al. 2011). Lemoine *et al.* used a rather similar principle to scale a *Corynebacterium glutamicum* cultivation in a network of STRs integrated with one or two plug flow reactors (Lemoine et al. 2015). Heins *et al.* used factorial design experimentation to specify the circulation flows between two STRs for studying *Sachharomyces cerevisiae* (Heins et al. 2015).

Most of the presented design strategies benefit from the support of mathematical calculations and detailed analytical work, and a considerable level of user influence was involved in the design (George et al. 1993; Sandoval-Basurto et al. 2005; Heins et al. 2015). There is an essential need in the scientific research on process scaling for more analytical and automated solutions to minimize the requirement for intense (and time-consuming) user involvement, and for general improvement of the designs. The next sections discuss a new analytic approach for the design of more representative scale-down models.

5.2. An automated approach towards a representative scale-down model

To move towards more analytical scale-down designs, Haringa *et al.* proposed an interesting solution based on the cell's trajectories in the full scale tank and monitoring the cell's local metabolic responses to the substrate gradient (Haringa et al. 2016). In their work, they implemented an Eulerian-Lagrangian CFD model to track the lifelines of 175 000 distributed particles in the large-scale reactor. Analyzing the average cell residence time in different zones gave them a valuable overview of the cell journey. This information was used as the basis of a scale-down design. The extracted results suggest fast fluctuations between the reactors within time scales of seconds while the operation of such a design was not practical due to the experimental limitations. Regardless of their interesting results and discussions, it should be considered that such an analysis requires an excessive computational power while the practical feasibility of the results at the present stage is still questionable.

The work of Haringa *et al.* was an inspiration for a new compartment based scale-down design in this project. The proposed method addresses some of the main challenges of Haringa *et al.* concerning the complexity, the computational demands and the practicability of the operating conditions. The new

approach is based on the developed principles for compartment modelling with respect to the assumption of using a network of well-mixed volumes for simulation of the heterogeneity inside the reactor.

In the following sections, first the main principles of the compartment modeling will be described, then a new automated compartmentalization technique will be introduced and finally, the developed compartment based scale-down method will be presented.

5.2.1. CFD based compartment modeling

CFD is an advanced collection of modelling techniques, which provides the possibility of making detailed predictions of the fluid dynamic behavior. However, the complexity of the applied equations can easily result in high computational demands and long calculation times. That is a common outcome of employing high mesh densities, which is often essential for predicting mass, momentum, and energy transfer rates. Thereby, CFD is usually not the recommended option if fast results are needed as in the case of process optimization and designing/tuning on-line controls, or when including complex process phenomena (e.g. population balance modelling) needs to be considered.

Compartment modelling is an alternative approach to reduce the computational demands at the cost of a lower accuracy (Nauha et al. 2018). This trade-off is the result of representing the gradients of the non-ideally mixed volume with a network of homogeneous (well-mixed) sections (compartments) and eventually simplifying the Navier-Stokes equations (Bezzo & Macchietto 2004a).

The accuracy of a compartment model (CM) is highly dependent on the properties of the compartments including the number of compartments, their volumes, the connections in between them, and the intermediate flows between compartments. Characterization of the network of compartments has always been critical. Up to today, manual configuration of the network is the most frequently cited strategy in the literature (Wells & Ray 2005; Le Moullec et al. 2010; Bashiri et al. 2014; Bashiri et al. 2016; Nauha et al. 2018). Vrabel *et al.* used a CM to simulate the mixing behavior in a 30 m^3 aerated reactor with multiple impellers (Vrábel et al. 1999). To describe the mixing performance in a multi-phase system (gas-liquid), they manually specified a set of compartments with constant volumes. Moulec *et al.* applied a similar strategy to set the compartments for the simulation of a gas-liquid reactor for biological wastewater treatment (Le Moullec et al. 2010). For that case study, each compartment was identified by looking at the level of the gas fraction, the velocity profile and the liquid turbulence characteristics. Irizarry used a CM in another type of application, i.e. to study formation of nanoparticles in nonhomogeneous conditions (Irizarry 2012). He introduced a new

compartmental Monte Carlo algorithm integrated with a population balance model to simulate the spatial heterogeneity in a system.

The difficulty of characterizing the compartments to create a representative set of conditions in the compartments that allow mimicking process behavior with a limited number of compartments has been a critical bottleneck of the compartment modelling techniques. The introduction of hybrid CFD based compartment models (CFD/CM) tackled this problem by supporting the compartmentalization step mostly with the required flow information (Bezzo & Macchietto 2004a). Nowadays, the use of CFD/CM has been extended in different areas: Rigopoulos *et al.* solved the complexity of a turbulent mixing model coupled with chemical phenomena by implementing a CFD/CM simulation (Rigopoulos & Jones 2003). With the help of this approach, they could introduce a new reaction engineering framework for multiphase reactors. Yu *et al.* used CFD/CM simulation in the area of high shear granulation processes (Yu et al. 2017). By applying a constant volume Monte Carlo approach on a compartmental population balance model they were able to predict spatial properties of 1.9 L and 4 L granulators. Nauha et al. moved in another direction and combined CFD/CM with population balance models in order to estimate the level of gas hold up in a 100 m^3 stirred tank bioreactor (Nauha et al. 2018). By implementation of a series of user-defined functions in the CFD software ANSYS Fluent 15.1, they were able to calculate the exchange flows between compartments directly from the CFD results and use it as initial values for solving the compartment model. Moreover, gas volume fractions were imported from the CFD results to the CM to initialize the population balance model for estimation of bubble size distributions and the gas hold up.

Despite all the achieved developments in CFD/CM, most of the simulations eventually suffered from the intrinsic weakness of manual compartmentalization. The most critical aspect of using manual compartmentalization is its high level of dependency on a user's experience. Hence, hybrid approaches such as CFD/CM were considered only when other solutions have failed (Bezzo & Macchietto 2004b). In order to minimize a user's influence, i.e. increase objectivity and repeatability of the compartmentalization procedure, Bezzo presented a systematic compartmentalization strategy based on the division of the spatial domain of the studied volume into a limited number of zones (Bezzo 2002). Each specified zone represents one spatial region, which exchanges mass, momentum and energy with some other zones through bidirectional intermediate flows. The exchange flows were extracted from CFD results. Wells *et al.* followed a similar approach by introducing a compartmentalization method based on a successive subdivision of the simulation domain into spatial regions, which shows small variations for the target variables (Wells & Ray 2005). Bezzo *et al.* moved one step further in automating the compartmentalization (Bezzo & Macchietto 2004b). In his approach, a zone is identified by selection of a CFD seed cell and agglomeration of neighboring cells

until the maximum gradient within a zone, with respect to a target variable P, does not exceed the specified tolerance 'ΔP'. Despite the significant potential of the approach, this method showed a substantial weakness when using an unstructured CFD mesh, which is the most applied meshing strategy (Bezzo & Macchietto 2004a). This strategy was applied by Delafosse *et al.* for the description of complex interactions between biological reaction and hydrodynamics in bioreactors (Delafosse et al. 2010). They improved the algorithm of Bezzo *et al.* by implementing different agglomeration techniques such as two different layer-by-layer approaches. The CFD/CM results, based on the designed network of compartments, showed a significant underestimation of the mixing time compared to a manual zoning on the one hand, and CFD simulations on the other hand. In order to minimize the error, they applied an initial manual zoning before implementing the automated strategy to reduce the size of compartments in the tangential direction. The obtained results improved by adding the manual zoning step. However, the results still showed a minimum of 34% error in estimation of the mixing time compared to the CFD results.

Each of the presented methods has its own merits and potentials. Besides that, there is still an essential need to develop more versatile and robust compartmentalization routines to address the main weakness of the existing approaches for the design of more representative networks of compartments. Hence, the development of a new compartmentalization routine was the focus of this work, which will be presented in the next section. In this method, including more than one target variable can be incorporated in the design of compartments. Moreover, this method has no restrictions in terms of the type of mesh and can be applied for structured and unstructured configurations.

5.2.1.1. Automated CFD based compartmentalization

This section presents a new CFD based compartmentalization method with respect to only one or a group of target variables $p \in \{p_1, \dots, p_i, \dots, p_N\}$. The aim is to present the method with the focus on its implementation aspects as an automated platform. Thereby, three main informative matrixes (maps) need to be initially clarified: 1. Compartment-map: which stores the locations, volumes and the corresponding average value of the variable p for each compartment; 2. Interface-map: which saves the relevant interface information between the connected compartments; 3. Flow-map: which stores values of the exchange flows between compartments. The mentioned maps are generated through the following framework. This routine is based on an identification of a 2D map as the first step and subsequent extension of the results to a 3D map, which describes the network of compartments.

- **Initialization:** The compartmentalization routine is initialized by the selection of one or a group of target variables $p \in \{p_1, \dots, p_i, \dots, p_N\}$ and by defining the acceptable homogeneity tolerance range within a compartment $\Delta p \in \{\Delta p_1, \dots, \Delta p_i, \dots, \Delta p_N\}$. p_i is considered as a target candidate if it has a significant influence on the dynamics of the process for instance, velocity, material distribution profile or the gas transfer coefficient.

  An initial CFD simulation has to provide detailed predictions of the target variables within the system volume. The elemental information (coordinate of each CFD element) and the corresponding p values need to be extracted from a CFD result in a reference plane. A reference plane is the closest 2D area to the geometrical symmetry plane. The extracted information forms the basis of the compartmentalization method.

- **Zoning:** This step aims to classify the CFD elements into zones, where the variable p varies within the specified tolerance range Δp. This task involves three sequential steps: a) sorting, b) classification, and c) final configuration.

  a) Based on the values of each target variable p_i, the CFD elements are sorted. Hence, 'N' sorted sets will be obtained based on the existence of 'N' target variables.

  b) Within each sorted set, groups of elements that are within the tolerance range Δp_i are clustered as an individual zone where the value of $(p_{i,max} - p_{i,min})$ is less than the specified Δp_i. The extracted zones are saved by their corresponding elemental coordinates as a zone-map. Thereby, N zone-maps are extracted as a consequence of selecting N variables.

  c) Irregular zone geometries are expected at this level of the routine (Figure 5.1.a). Some geometrical simplifications or adjustments are usually required to ease the 2D/3D translation (see below Compartmentalization for the 3D configuration). In this routine, the rectangular based geometry was selected as the desired configuration for a zone. To achieve this target, the surface of the reference plane is divided into rectangular units (U) with a dimension of ΔX×ΔY (Figure 5.1.a). The Size of a unit is determined based on the geometry of the studied volume, the p gradient, and the target precision that is required. The dominant zone at each unit, which occupies the largest area of that unit, fills that unit. Finally, the shape of the zones is updated (Figure 5.1.b). For the ease of further analysis, the saved elemental information for each zone is replaced by the coordinates of the associated units in the zone-maps.

  We should consider that different parts of e.g. a reactor might have similar profiles. Therefore, an identified zone may cover several discrete areas. To have continuous compartments, it is essential to split the multi-regional zones into several individual areas

(zones). Figure 5.1.b and 5.1.c show an updating procedure, moving from a multi-regional zoning to a mono-regional discretization.

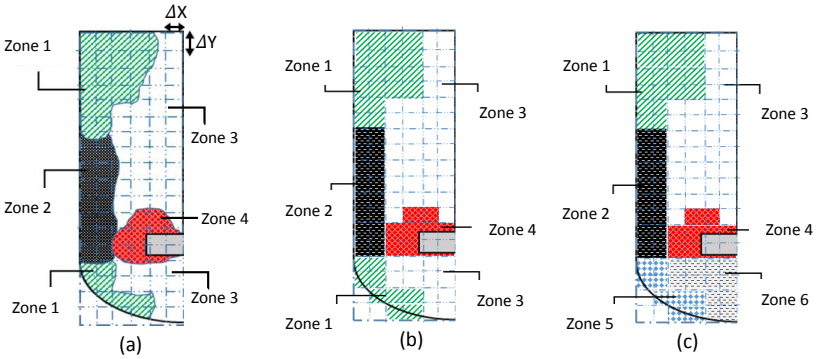

Figure 5.1. Zoning reformation: a) gridding the reference plane and allocation of the initial zones, b) association of the units to the dominant zones, and c) splitting the multi-regional zones into continuous areas.

In practice, the existence of small zones may not be desirable as they increase the computational demands while they might not have a significant impact on the final results. The minimum size of an acceptable zone can be controlled by merging the small zones to a neighbor zone with which it primarily has the longest interface with, or the largest area.

The following box provides an abstract view of the zoning script for one target variable p_i.

Zoning

Input >> elemental coordinates (X,Y) or (X,Z) or (Y,Z) and the local p_i

% Zoning

1. *Sort* >> elements based on p_i
2. *Classify* >> elements based on p_i with interval $=\Delta p_i$
   name as $zone\,(i=1{:}n^{pi}) = \{elements \mid (p_{i\ max} - p_{i,min}) < \Delta p_i\}$

% Zone reformation

Input >> $(\Delta X,\Delta Y)$ or $(\Delta X,\Delta Z)$ or $(\Delta Y,\Delta Z)$

3. *Grid* >> the geometrical working space $\{(X_{min},X_{max}),(Y_{min},Y_{max})\}$ or ⋯
   $\{(X_{min},X_{max}),(Z_{min},Z_{max})\}$ or ⋯
   $\{(Y_{min},Y_{max}),(Z_{min},Z_{max})\}$

   based on $(\Delta X,\Delta Y)$ or $(\Delta X,\Delta Z)$ or $(\Delta Y,\Delta Z)$

   name each *unit as* $U_{j=1:j_{max}}$: $\{X,Y|(X-\Delta X,X+\Delta X),(Y-\Delta Y,Y+\Delta Y)\}$ or ⋯
   $U_{j=1:j_{max}}$: $\{X,Z|(X-\Delta X,X+\Delta X),(Z-\Delta Z,Z+\Delta Z)\}$ or ⋯
   $U_{j=1:j_{max}}$: $\{Y,Z|(Y-\Delta Y,Y+\Delta Y),(Z-\Delta Z,Z+\Delta Z)\}$
4. *for j=1:*j_{max}
   find >> $(zone(i) \mid elements \in zone(i)@U_j \geq \forall\{elements \in zone(\neq i)@U_j\})$
   associates U_j *to* $zone(i)$
   end
5. *for i=1:*i_{max}
   if $zone(i)$ *is not continues*
   Update $zone(i)$ into n continues *zones*
   $n^{pi} = n^{pi} + n$
   end
   end

% Small zone elimination

Input >> $Zone\_tolerance$

6. *for i=1:*n^{pi}
   if $\sum U \in zone(i) < Zone\_tolerance$
   Merge $zone(i)$ to ⋯
   $(zone(\neq i) | has\ the\ longest\ interface\ with\ or\ the\ largest\ neighboring\ zone)$
   end
   end

end

- **Compartmentalization:** A zone-map contains the required information for characterizing a 3D network of compartments. Extraction of 'N' individual zone-maps is the outcome of the last step as an input for characterizing the network of compartments of a specific reactor. The design of the compartments has to cover the overall maps. Hence, a 2D compartment-map is identified based on overlaying the extracted zone-maps. The overlaid zones are obtained by identifying areas, for which the associated units correspond to a similar combination of zones of all maps. For instance, the units belonging to zone 'i' from zone-map I and at the same time zone 'j' from zone-map II create one zone of the overlaid compartment-map (see Figure 5.2 for an example).

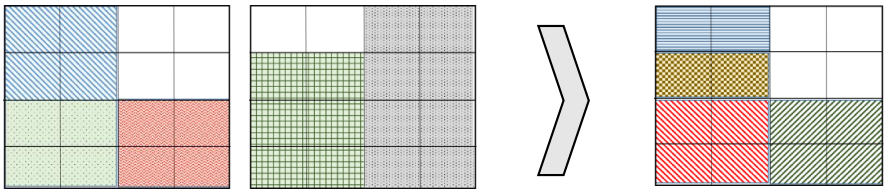

Figure 5.2. Overlaying maps based on the common zones

The 3D compartments can be extracted from the 2D compartment-map and the volumes are calculated accordingly. In a cylindrical coordinate system, the cross-sectional area of each unit can be used to extrude a 3D ring by 360º rotation of the cross-sectional area around the central line. The collective sum of the corresponding rings to a zone builds the final 3D volume. Figure 5.3.c shows the 3D illustration of zone 2 by extrusion of the rings. For other geometries than cylindrical shapes, a hollow shape volume, similar to the geometry, has to be considered instead of the ring for the transition from a 2D map to the 3D compartments. For instance, for cubic based geometries, hollow cubes have to be considered for this transition and hollow spheres are the used 3D units for spherical systems.

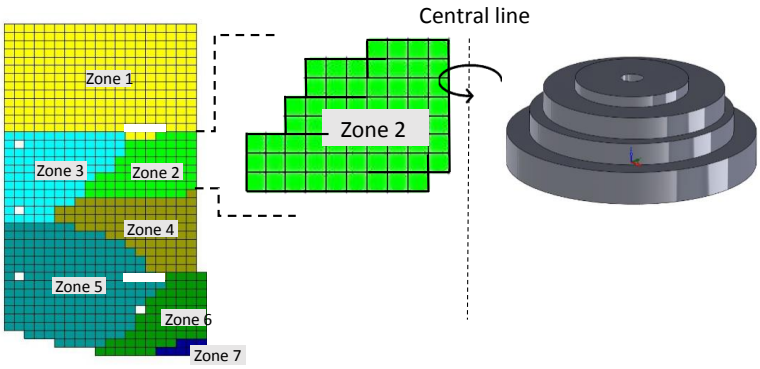

Figure 5.3. Transition from a 2D compartment-map to a 3D network of compartments. a) visualized zoning map, b) a single 2D zone, and c) the corresponding 3D compartment obtained from the 2D zone in b).

The assumption of having a complete ring may result in neglecting the presence of some geometrical features, for example, baffles installed close to the wall of the reactor. It should be considered that this assumption may add some errors in the calculated volumes of the compartments. Since the extracted flows are based on the CFD simulation of the full geometry, the effect of this kind of features is partly included in the identification of compartments. However, for more representative compartmentalization, it is recommended to initially discretize e.g. the tangential cross section of the cylindrical geometry into some sections and then, for each part, an individual compartment-map is extracted based on a new reference plane. Accordingly, the 3D compartments for each section are extracted by partial extrusion of the units. Figure 5.4 shows an example of using multiple reference planes for the extraction of the compartment-maps in a baffled tank. Using multiple reference planes also gives the opportunity of studying systems which do not have an approximately symmetry profile of the target variables.

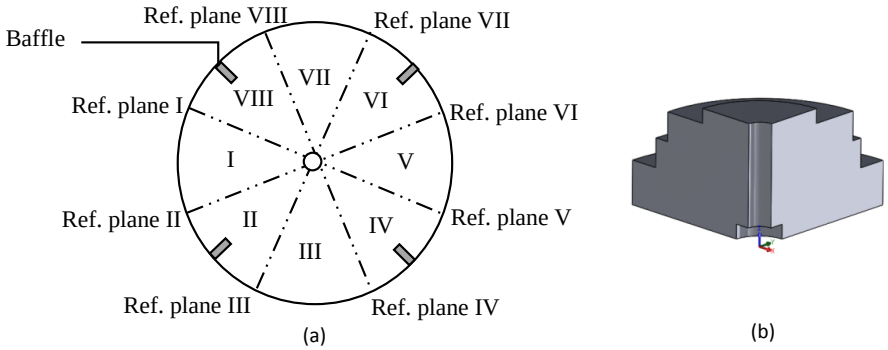

Figure 5.4. a) Application of multiple reference planes for considering the tangential gradients, and b) partial extrusion of a similar zone as zone 2 in Figure 5.3.

- **Connection:** The same 2D/3D terminology is used to specify the connection properties between the compartments. At the 2D level, the zonal interface areas are characterized based on their interface units, located at the zone's boundaries. The coordinates of the interface unit are saved as an interface-map. Figure 5.5 illustrates the saved interface units, marked as dashed areas, in an example interface-map. Relative comparison between the stored coordinates provides the required information concerning the connections and the interface areas.

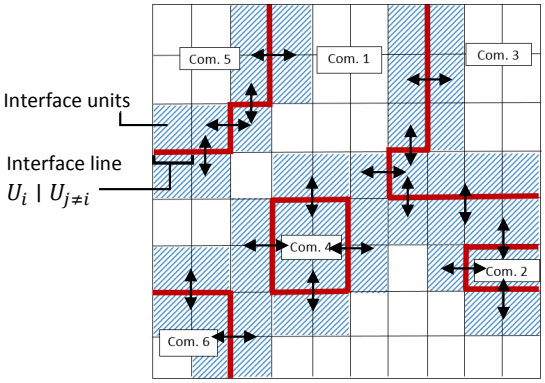

Figure 5.5. Characterization of the compartment network: interface-map.

In order to characterize the network, the interface properties such as the list of connected zones at a 2D level and the compartments in a 3D configuration, the interface areas, and the exchange flows have to be calculated. In the network of zones, the interface properties are quantified based on their connection units $U_i \mid U_{j\neq i}$ and the summation of the perpendicular flow components (axial, radial and circumferential flows in the cylindrical coordinate system) at the interface area. Two units are qualified as a connection if they belong to two individual zones and have a common interface line. A boundary unit can belong to up to three connections. All the

boundary units $\{U_i^1, U_i^2 \dots, U_i^{n_i}\}$ in zone i need to be individually investigated for the possible connections. Two zones or subsequently, two compartments are connected if they have at least one connection.

For each pair of $U_i \mid U_{j\neq i}$, the 3D interface area has to be calculated based on their common interface line. In a cylindrical coordinate system, a vertical interface line represents a cylindrical 2D area while a horizontal line stands for a disc shape 2D area. Accordingly, the perpendicular flow corresponding to the specified $U_i \mid U_{j\neq i}$ connection is extracted from the CFD results (radial flow for the cylindrical interface and axial flow for the disc shape interface). The overall interface area and the exchange flow between two connected compartments i and $j \neq i$ are calculated from the summation of the flows over the extracted areas and the flows over the entire identified $U_i \mid U_{j\neq i}$ connections. The following box shows the scheme of a sequential routine to calculate the interface properties for compartment i.

Calculating the interface properties

Input >> interface-map

for *count_1=1*: n^{p_i}

1. Specify the target unit U_i^{count}
2. Identify $0 \leq k \leq 3$ connections $\sum_k \{U_i^{count} | U_{j\neq i}^{k}\}$,
   if $k > 0$ >> *continue,*
   else >> go to the next iteration

3. *for* *count_2=1:k*
   - Specify the borderline $U_i^{count} | U_{j\neq i}^{k}$ and calculate the interface areas $a_{U_i^{count} | U_j^{count\_2}}$
   - Update >> $A_{ij} = A_{ij} + a_{U_i^{count} | U_j^{count\_2}}$
   - Extract the perpendicular flow $f_{U_i^{count} | U_j^{count\_2}}$
   - Specify the direction of the flow:
     if i to j >> $S_{ij} = 1,\ S_{ji} = 0$
     else >> $S_{ij} = 0,\ S_{ji} = 1$
     end
   - Update the flow $f = \begin{cases} f_{ij} = f_{ij} + \Sigma S_{ij\cdot} \left| f_{U_i^{count} | U_j} \right| \\ f_{ji} = f_{ji} + \Sigma S_{ji\cdot} \left| f_{U_i^{count} | U_j} \right| \end{cases}$

   end

end

It should be considered that the simulation results usually come along with a small quantity of unbalanced materials within the maximum acceptable residual, which for a fully converged simulation is not a significant value. In the extracted results of ANSYS CFX 17.1, the mass balance over a flow component ($\{f_x, f_y, f_z\}$ or $\{f_{radial}, f_{axial}, f_{\text{circumferential}}\}$) is approximately closed at the perpendicular full plane. The specified plane has to start from one side of the geometry to the other end. For example, the input axial flow is equal to the output axial flow at the Plane 1, Figure 5.6.a. However, it was observed that the mass balance over a flow component is not necessarily closed at a portion of the perpendicular plane (Plane 2, Figure 5.6.a) or at the full plane, parallel to the target flow (Plane 3, Figure 5.6.b). This issue is also extended to the three-dimensional space. It was noticed that, for a closed volume inside the geometry (Figure 5.6.c), the mass balance is not always closed but the summation of the balance residuals goes to zero over the full geometry. This means that, despite the unbalanced conditions at parts of the studied volume, the overall mass balance has to be closed for a full converged simulation.

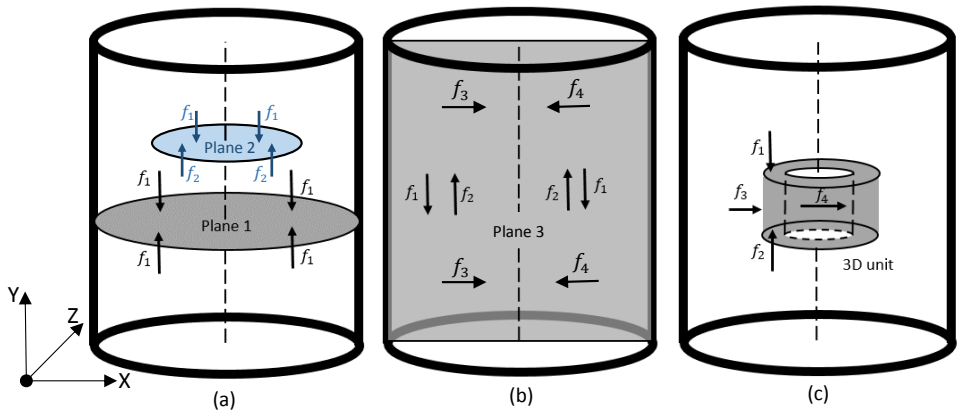

Figure 5.6. Mass balance over the calculated flows at different planes and over a volume

Most of the commercial CFD software systems use an additional step to close the balance over the overall volume while the balance may not be completely closed at smaller volumes within the full geometry. Unfortunately, there is no other work addressing this issue since the final error is mostly negligible. The problem arises when the CFD simulation results are directly used for the design of compartment models where the residuals are illustrated in the extracted flows. Solving the CM equations usually requires a complete balance over each compartment. In order to close the mass balance over each compartment, an additional step has to be considered. The suggested strategy is

based on introducing some additional flows (f') between the connected compartments to compensate for the small residuals between the inlets and outlets of each compartment (Figure 5.7).

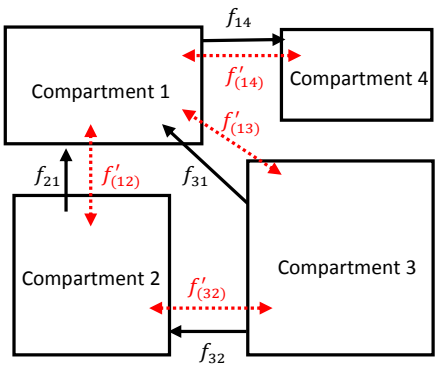

Figure 5.7. Definition of flows and additional flows between compartments

By solving the set of mass balance equations, simultaneously for all the compartments, the additional flows are calculated. For calculation of $n_{f'}$ additional flows over 'n' compartments, we have a maximum $n_e = n - 1$ independent equations and a minimum of $(n - 1)$ unknown additional flows. In the case of more unknowns than the number of independent equations, $(n_{f'} - n_e)$ additional flows are set to zero and the rest are calculated by solving the balance equations. Thereby, the additional flows $f'_{(ij)}$ are prioritized based on the minimum volume of the compartments ($min\{V_i,\ V_j\}$) to the flow rate f_{ij}. Accordingly, $(n_{f'} - n_e)$ additional flowrates, corresponding to the smallest ratios of $\frac{min\{V_i,V_j\}}{f_{ij}}$, are set to zero. Finally, the flows are updated with respect to the calculated additional flows.

In this study, the compartmentalization routine was developed in a MATLAB R2016b environment and the CFD simulations were operated in ANSYS CFX 17.1. The interface is initialized by importing the CFD elemental results. The network of compartments is identified while the exchange flows are directly extracted from the ANSYS CFD-Post 17.1 through the MATLAB interface. Figure 5.8 shows the scheme of the compartmentalization routine.

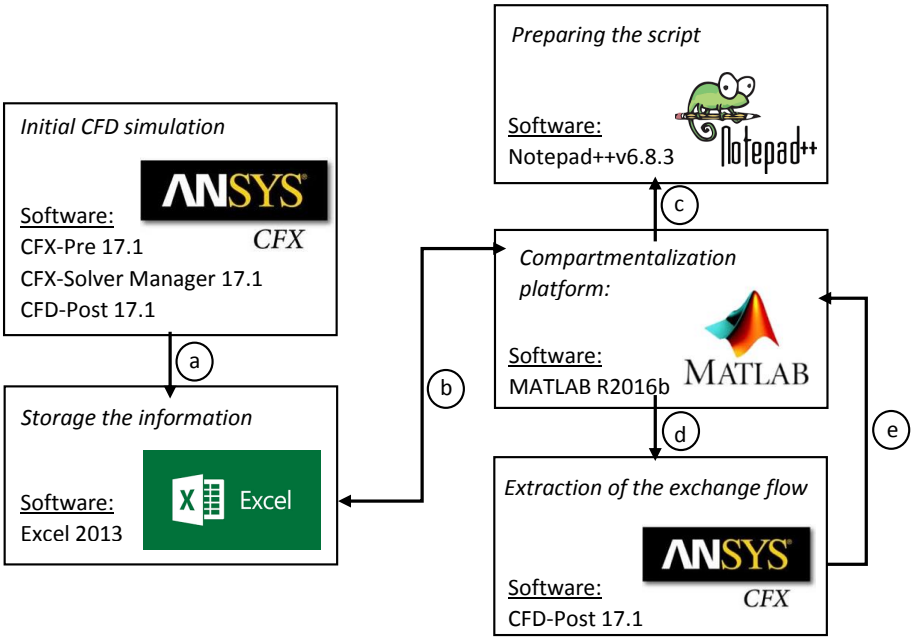

Figure 5.8. Scheme of the compartmentalization platform. a) saving the simulation results and the elemental information, b) saving and calling the compartmental information, c) preparing the scripts for execution of the CFD post, d) execution of the scripts for extraction of the exchange flows in CFD post and, e) collecting the exchange flow information.

Case study: 700 L stirred pilot bioreactor The capability of the developed compartmentalization routine is demonstrated with help of a case study. The target set up is a 700 L stirred tank reactor filled with water, which is equipped with three 6-blade Rushton turbines and four baffles. Figure 5.9.a shows the front view of the studied reactor. The calculated CFD/CM predictions are compared with the extracted CFD results in order to evaluate the developed method.

The CFD simulation was operated with approximately 1.4 million elements. The flow regime within the liquid was simulated by implementing the k-ε turbulence model (Reynolds number >2×10^5). To estimate the mixing time, a tracer pulse was released at the top of the liquid with a steady flow profile. The tracer was screened at six monitor points along the reactor height to estimate the mixing time for different agitation speeds. The calculated mixing time values for 200 rpm (0.45 kW/m^3 power input), 300 rpm (1.51 kW/m^3 power input) and 400 rpm (3.6 kW/m^3 power input) are shown in Figure 5.9. The mixing time results are based on 95% homogeneity.

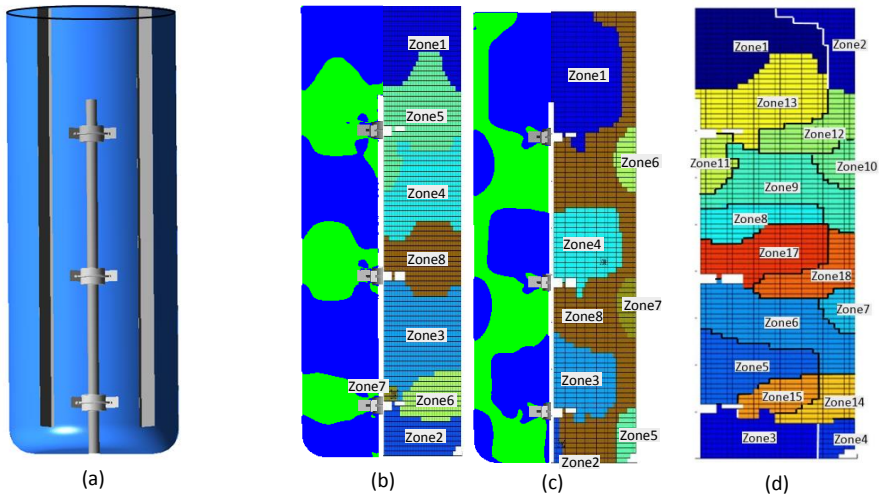

Figure 5.9. Compartmentalization of the 700 L bioreactor at 300rpm. a) geometrical configuration; b) CFD simulation of radial velocity (left) vs. zoning map based on radial velocity (right); c) CFD simulation of axial velocity (left) vs. zoning map based on axial velocity (right); d) final compartment-map based on combined radial and axial velocities (the x-dimension is enlarged for better visualization).

The compartmentalization routine was performed with help of the extracted CFD steady state flow profiles. In this case study, only directions of the axial and radial velocities were considered as the target variables. The zone-maps and the final compartment-map were extracted at half of the XY symmetry plan. Figure 5.9.b and 5.9.c show the identified zones based on radial and axial velocities at 300 rpm corresponding to 1.51 kW/m^3 power input (P/V_{liquid}), respectively, and the overlaid compartment-map is illustrated in Figure 5.9.d. Finally, seventeen individual compartments are characterized.

Figure 5.10 shows the extracted overlaid compartment-maps for 200 rpm and 300 rpm with an equal number of zones and target variables. For the ease of comparison, the extracted map for 200 rpm is mirrored. The comparison between the compartmental maps indicates a direct correlation between the size of compartments located at the impeller zones (top impeller: zones 12, 13; middle impeller: zones 17, 18; bottom impeller: zones 14, 15) and the power input. The size of the identified impeller zones is increasing when increasing the power input. The formation of a weak circulation pattern below the bottom impeller, resulting from a low mixing intensity, was captured by the compartmentalization routine as a distinct compartment (Figure 5.10, zone 10 for 200 rpm). This zone is not recognized anymore as an individual region under higher power input conditions corresponding to 300 rpm. Regardless of the mentioned differences, both maps roughly indicate similar locations for every two comparable zones.

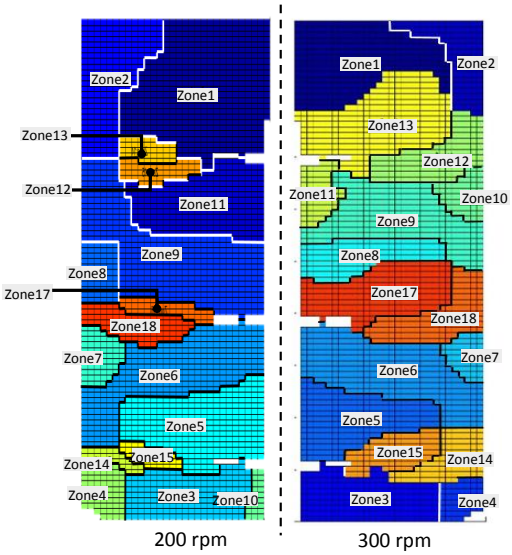

Figure 5.10. Compartmentalization of the 700 L bioreactor for 200 rpm and 300 rpm.

The characterized network of compartments was used as inputs for a CFD/CM simulation to estimate the mixing time τ_{mix}. Figure 5.11 shows the predicted mixing times by the empirical Eq. 5.1 (Nienow 1998), the CFD simulations and the CFD/CMs. The estimated mixing times by Eq. 5.1 show significantly higher values compared to the other two models due to the applied simplifications. By considering the effect of the impeller properties (number of impellers and the design of the blades) on the flow in the CFD simulation, the estimated results become closer to the reality.

$$\tau_{mix} = 3.3 \times \left(\frac{1}{N_{imp}}\right) \times \left(\frac{1}{P_0}\right)^{\frac{1}{3}} \times \left(\frac{D}{H}\right)^{-2.43} \tag{5.1}$$

The comparison between the results shows that the predictions of the CFD/CM model with 17 compartments yield less than 20% deviation from the predictions of the CFD model with 1.4 million elements. This level of precision was achieved by a significantly shorter calculation time and far less computational demands compared to the CFD simulations. For instance, the tracer CFD simulation for the 200 rpm case was performed for approximately 2.5 hours, while the CFD/CM approach took less than two seconds to simulate the tracer experiment by employing similar computational configurations (4 CPU core, Intel(R) Xeon(R) Processor E5-1630 v3, 3.7GHz). This outcome is a considerable result concerning the level of accuracy with respect to the required computational time.

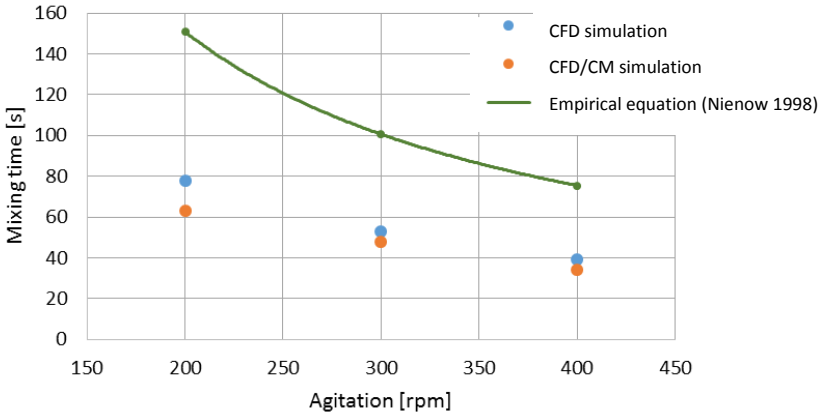

Figure 5.11. Predicted mixing time by the empirical equation (Nienow 1998), CFD simulations and CFD/CM simulations.

Besides this achievement, analyzing the details of the CFD/CM results reveals also valuable information. The simulation results show that by increasing the agitation speed the deviation between the predicted mixing times of the CFD simulations and the CFD/CM decreases. This behavior can be explained by looking at the influence of the circumferential discretization in different agitation conditions. At low power inputs where the turbulent regime is not fully developed, a considerable heterogeneity can be observed within a compartment, which may not be captured by the applied 2D/3D mapping strategy. While, by increasing the power input and strengthening the turbulent motions, the condition within one compartment becomes closer to a well-mixed volume, and therefore, the deviation between the simulation results becomes smaller. Hence, considering the tangential division across the compartments is essential mostly for lower power inputs.

The biggest advantage of using CFD/CM simulations is that they offer the possibility of a fast estimation of the flow related properties such as different concentration profiles and distributions when coupled to kinetic models. This is a considerable advantage particularly for the design of efficient controllers, where fast predictions and operations are needed. However, the main bottleneck of using similar compartmentalization approaches is its inevitable dependency on an initial CFD result to provide the compartmental information. Changing the operational conditions such as agitation or aeration, which directly influence the flows, requires performing new CFD simulations for the initial compartmentalization step. For instance, ‘n’ CFD simulations are required corresponding to ‘n’ agitation conditions for characterizing the compartments in the single-phase stirred reactor. Despite the significant improvement in the calculation demands of CFD/CM simulations, this approach is

critically challenged at its first step of compartmentalization with the computational cost of operating 'n' CFD simulations.

Ideally, a single CFD simulation for one operating condition, e.g. power input, can be used as an input for a range of operating conditions instead of only one specific setting as long as the flow regime has not seen a significant change. In order to investigate this assumption/hypothesis, the identified compartment-map from the 200 rpm CFD result was used as a reference design to predict the mixing conditions for three other agitation speeds. The extracted exchange flows for 200 rpm were updated for other mixing conditions according to Eq. 5.2. The following equation represents the linear correlation between the agitation speed and the average flows between compartments.

$$f_{new} = f_{old} \cdot \left(\frac{\left(\frac{P}{V_{liquid}}\right)_{new}}{\left(\frac{P}{V_{liquid}}\right)_{old}} \right)^{\frac{1}{3}} \tag{5.2}$$

Eq. 5.2 is comparable with the observed trend in changing the mean in the extracted flows, between the compartments, directly from the CFD results versus the agitation speed. The average of the extracted flows directly from the CFD simulations and Eq. 5.2 are shown in Figure 5.12.

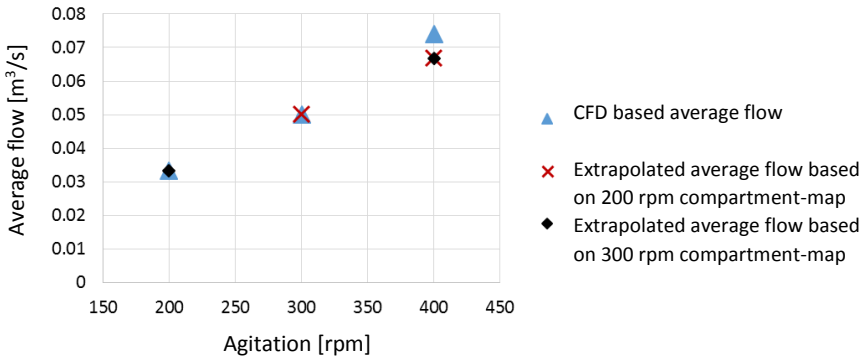

Figure 5.12. Interpolated average exchange flow compare to the extracted flows from the CFD simulations.

Figure 5.13 shows the calculated mixing times obtained from CFD simulations and CFD/CM simulations based on the 200 rpm (0.45 kW/m^3) compartment-map. Due to the assumption of predicting a non-ideal mixed condition with a limited number of well-mixed connected volumes, an underestimation of the CFD results by the CFD/CM simulation result was expected, while the predictions are still comparable. The simulation results show that by increasing the agitation speed, the deviation between the CFD results and the CFD/CM calculations with the extrapolated flows decreases. The

reason for this outcome can be explained by the differences between the actual compartment-map and the extrapolated one. As discussed before, by increasing the power input, the impeller compartments occupy larger volumes. Therefore, relatively larger impeller compartments are expected for higher power inputs compared to the implemented reference configuration (based on 200 rpm CFD simulation). Considering relatively smaller volumes for the most intensive turbulent areas (the impeller impact areas) than the actual ones results in longer mixing times. This outcome is observed as lower deviations between the CFD results and the CFD/CM by partly covering the commonly seen underestimation of the mixing time by the CM. The improvement in the predictions for higher agitation speeds with the CM is the result of combining two sources of error that each push the results in opposite directions, simplification of the gradient into a network of compartments and considering smaller volumes for the impeller impact areas.

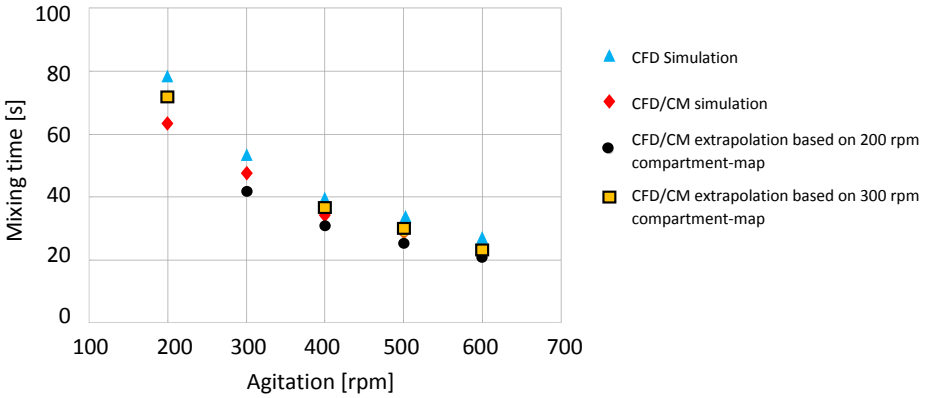

Figure 5.13. Estimation of mixing time for different agitation speeds, using different approaches.

For further investigations, the results were recalculated for CFD/CM simulations based on the 300 rpm compartment-map (Figure 5.13) to estimate the mixing times for 200 rpm, 400 rpm, and 500 rpm. Similarly, the simulation results indicate an underestimation of the mixing time particularly for the lower power input compared to the reference condition (300 rpm). However, the results show better predictions compared to the previous case particularly for mixing speeds higher than 400 rpm where the actual CFD/CM simulation and the interpolation based CFD/CM show almost similar results. By looking at the extracted network of compartments based on 200 rpm, 300 rpm, and 400 rpm CFD results, the growth of the size of impeller compartments from 200 rpm to higher agitation speeds is more prominent (Figure 5.14). However, this outcome is not a persistent trend for an impeller speed of 300 rpm and above. No significant change in the flow profile, and subsequently in the size of compartments, is predicted above 300 rpm. It means that the turbulent flow is well-developed and a

further increase in the power input does not show a substantial influence on the flow pattern. Therefore, the deviation between the applied compartments and the actual one is not significant. Since the compartment-map based on 300 rpm provides a better overview of the higher agitation conditions compared to the 200 rpm compartment-map, the predicted mixing times are even closer to the CFD results.

It should be noted that for the ease of comparison, zone 11 in Figure 5.14.c is missing by merging two zones 11 and 12 in Figure 5.14.c.

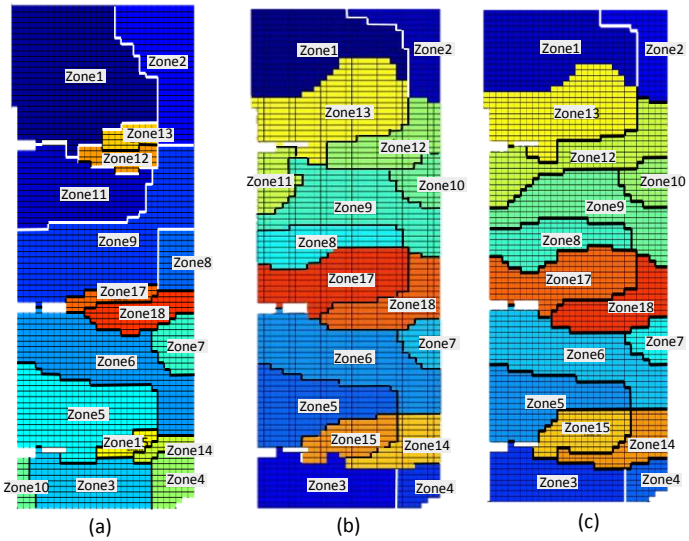

Figure 5.14. Compartment-map based on a) 200 rpm CFD results, b) 300 rpm CFD results, and c) 400 rpm CFD results.

The important point about using such an extrapolation approach is to have a careful look at the effect of changing the operating conditions on the flow regime, the compartments, and the exchange flows. Accordingly, the mentioned correlation (Eq. 5.2) has to be updated for other types of reactors e.g. bubble column, plug flow or packed bed.

5.2.2. The principle of the compartment modelling and the scale-down design

The extracted compartment-map gives an overview about the present heterogeneity of the target variables in the pilot reactor. The main idea is to use this information to simulate the identified gradient in a set of small reactors.

Theoretically, each identified compartment can represent a reactor within a network, which operates with the working volume equal to the calculated one for the corresponding compartment. Each reactor requires the creation of well-mixed conditions during the process. The specified connections between the compartments illustrate the connections between the reactors. Finally, the working liquid is pumped between the reactors according to the calculated exchange flows between the corresponding compartments. This design should be able to deliver a comparable gradient with respect to the target variable as the large-scale reactor with similar total volumes as the large tank. Figure 5.15 illustrates the scheme of the presented concept:

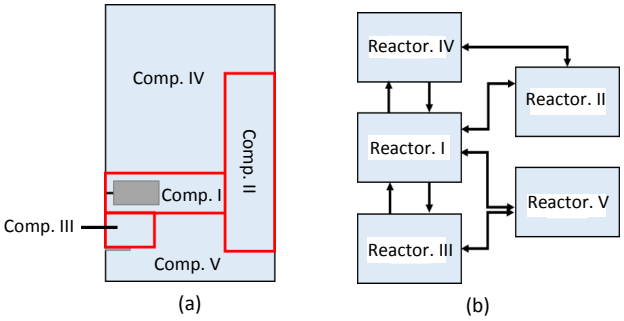

Figure 5.15. Simulation of a) a large-scale tank with b) a network of connected well-mixed reactors.

If one accepts this concept, then the network can be scaled to any other size while the model is still capable of representing similar process conditions as the initial reactor. In order to scale the designed set up, the working volumes $V \in \{V_1, \dots, V_i, \dots, V_n\}$ and the exchange flows $f_{ij}, i\ and\ j = 1{:}n$ should be simultaneously scaled with a similar scaling factor 'c' (Eq.5.3 and Eq.5.4). The validity of this theory is examined by means of a case study in the next part of this chapter.

$$V_{i,scaled} = c.V_i \tag{5.3}$$

$$f_{ij,scaled} = c.f_{ij} \tag{5.4}$$

It should be considered that theoretical designs usually need to be adjusted based on the practical considerations and limitations. For instance, increasing the number of reactors provides the possibility of studying smaller homogeneity tolerances within each reactor and therefore, better prediction of the gradients of the large scale tank can be achieved. However, the operation of a considerable number of connected bioreactors is always challenging due to the limitations of the pumps and the circulation instruments. On the other hand, the maximum and minimum capacities of the reactors have to be considered in choosing the working volumes. Accordingly, the operation of a scaled-down model with high aspect ratios (volume of the largest compartment compared to the volume of the smallest compartment) may not be practical. This usually happens when a strong gradient is identified

in the large scale tank. In such case, merging two or more compartments into one reactor is recommended.

5.2.2.1. Case study I: lactic acid fermentation in a 700 L pilot bioreactor

- **Prediction of the fermentation process in the pilot scale**

The developed scale-down method is demonstrated by an example case study on lactic acid fermentation in the presented 700 L pilot-scale bioreactor. The fermentation process can be simplified into the following reactions.

$$(1 + Y_{Gal}).\,Lactose \rightarrow Biomass + Y_{Gal}.\,Galactose \quad \text{(R1)}$$

$$(1 + Y_{Gal}).\,Lactose \rightarrow Lactic\ acid + Y_{Gal}.\,Galactose \quad \text{(R2)}$$

Spann *et al.* described a first principles kinetic model for lactic acid fermentation which is considered in this study (Spann et al. 2018a; Spann et al. 2018b).

In this case study, the pH value of the cell culture is controlled by a proportional-controller with an adoptive lag-time parameter based on the measurements in compartment 6 (Figure 5.14) to reach the target value pH = 6 (Spann, Roca, et al. 2018). To adjust the pH in the cell culture environment, ammonia is injected in the liquid at the bottom of the reactor (Figure 5.14 compartment 3). The pH profile is measured and estimated for four positions located in compartment 3 (point 1), compartment 4 (point 2), compartment 9 (point 3) and compartment 11 (point 4). Figure 5.16 shows the experimentally estimated pH profile, the CFD simulation and the CFD/CM prediction for 200 rpm agitation speed.

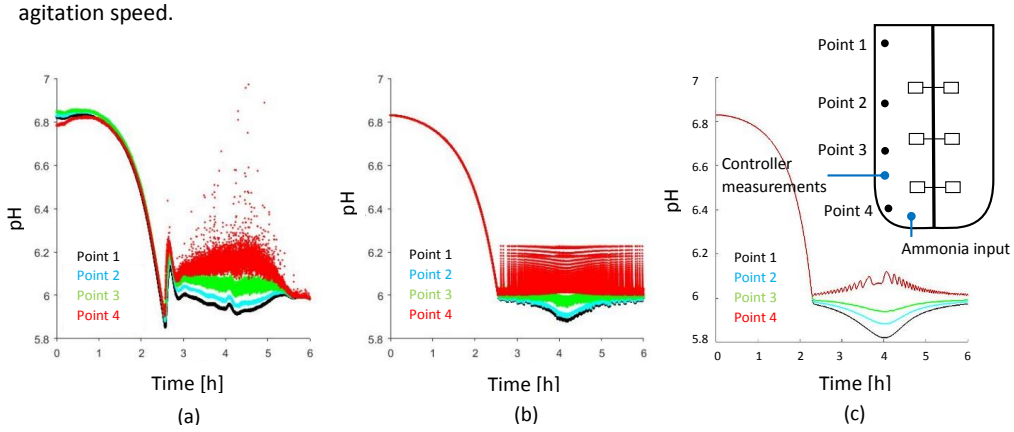

Figure 5.16. pH profile during 6 hours cultivation a) experimental measurements, b) CFD simulation, and c) CFD/CM simulation.

The applied CFD/CM model successfully captured the gradient within the reactor compared to the CFD results. Moreover, the distributions of lactose, biomass, lactic acid, galactose and pH in four of the seventeen compartments are shown in Figure 5.17. The extracted results are considered as the expected profile in the pilot scale, which is used to evaluate the performance of the scale-down designs.

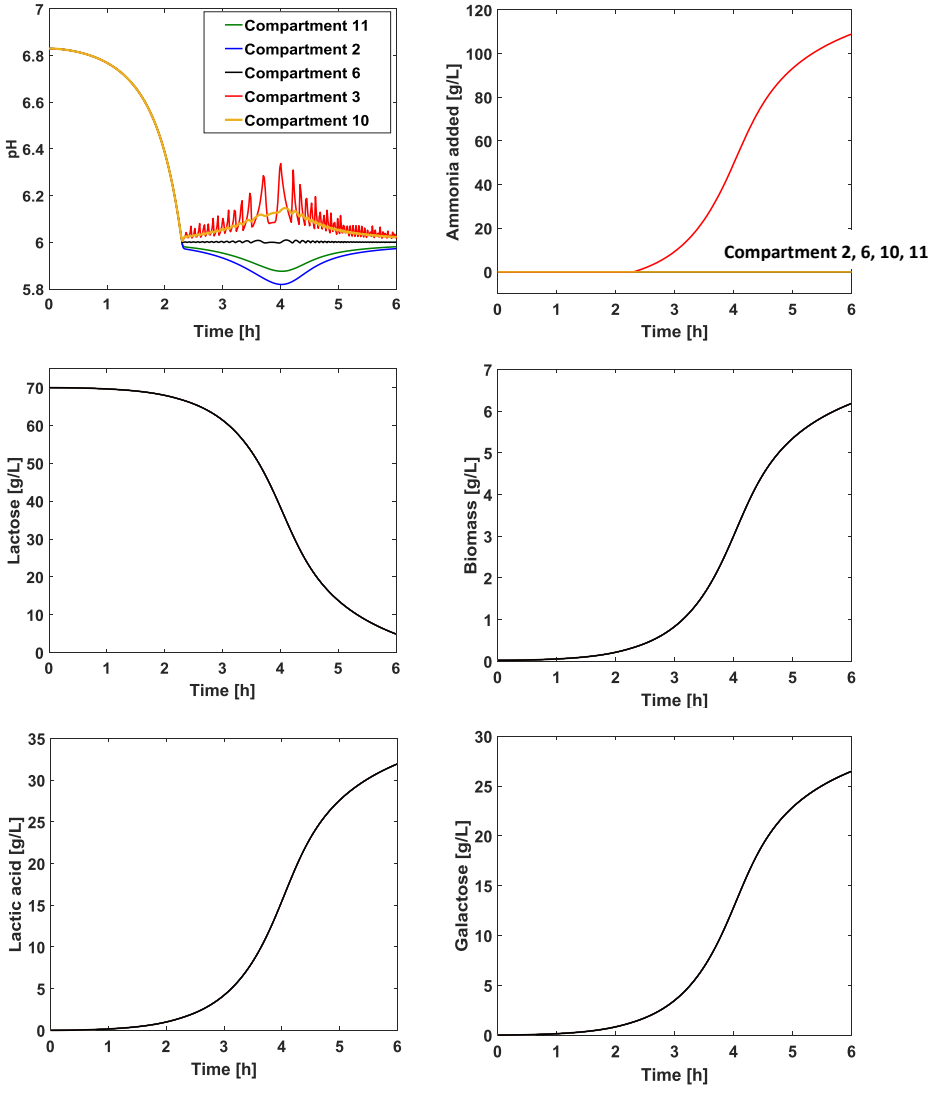

Figure 5.17. CFD/CM simulation of lactic acid fermentation in the 700 L bioreactor with 200 rpm agitation speed. Dynamics of relevant process variables in compartments 2, 3, 6, 10 and 11 are shown.

- **Scale-down study**

The identified compartments are resized with the scaling factors 1/2, 1/20 and 1/50. The effectiveness of the models is evaluated by simulating the designed operating conditions in each of the scale-down designs and comparing the process with the initial scale as follows:

The mixing performance in the pilot scale (700 L) and the smaller scales (350 L, 35 L and 14 L) is compared by implementing a tracer pulse at the compartment 1 for the large tank and the reactor 1 in the scaled models. The estimation of mixing time for all the designed models shows exactly the same mixing time value. In addition, the distribution of the tracer between the reactors shows identical profiles between the scales. Figure 5.18 illustrates the distribution of the tracer in the pilot reactor and in the model that is 50 times smaller (14 L). The results highlight the robustness of the method in maintaining the mixing capacity across the scales.

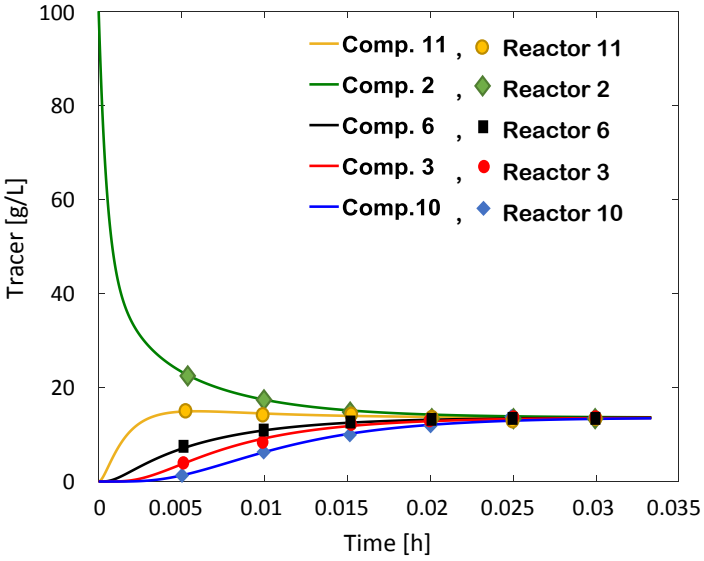

Figure 5.18. Tracer distribution in the network of in total 700L working volume compartments (solid lines) and 14 L working volume reactors (points).

The next step is to compare the distribution of materials and the pH profile during the process. Figure 5.19 shows the estimated pH profiles for the 700 L bioreactor and the 35 L scaled simulated network of bioreactors. The similarity between the estimated profiles in the scaled designs and the pilot reactor indicates the effectiveness of the scale-down strategy to maintain an identical cell culture environment across the scales, concerning the maintenance of a target gradient across scales

.

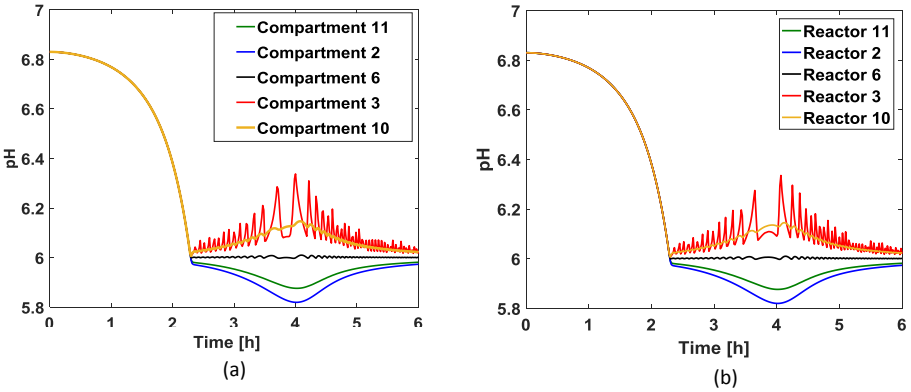

Figure 5.19. Simulation of lactic acid fermentation in a) 700L total volume network of compartments and b) 35 L total volume network of scale-down reactors for 200 rpm agitation speed.

5.2.2.2. Case study II: Saccharomyces cerevisiae in a 100 m³ industrial bioreactor

In this part, the application of other key parameters, such as concentrations, for design of a scale-down model is studied with an example case study of a *Saccharomyces cerevisiae* cell culture in a 100 m^3 industrial bioreactor. The large-scale bioreactor is equipped with 4 Rushton turbines, 4 baffles and a spiral cooling coil at the wall. During the fermentation, the glucose is added from the top and the air sparger is placed below the bottom impeller (Bach 2018).

The fermentation process was simulated in ANSYS CFX 17.1 (Bach 2018). The applied kinetic model for *Saccharomyces cerevisiae* (X) is summarized into a three-regime metabolic reaction scheme as follows (Postma et al. 1989; Verduyn et al. 1990; Weusthuis et al. 1994).

$$C_6H_{12}O_6 + Y_{os}O_2 \Rightarrow Y_{xs,1}X + Y_{COs,1}CO_2 + Y_{H_2Os,1}H_2O \quad \text{Aerobic}$$

$$C_6H_{12}O_6 \Rightarrow Y_{xs,2}X + Y_{COs,2}CO_2 + Y_{ps}C_2H_6O \quad \text{Anaerobic}$$

$$C_6H_{12}O_6 + Y_{Os}O_2 \Rightarrow Y_{xs3}X + Y_{COs,3}CO_2 + Y_{H_2Os,3}H_2O + Y_{ps,3}C_2H_6O \quad \text{Overflow}$$

Y_{os} are the yield coefficients for aerobic and overflow metabolism. Where, $Y_{xs,2}$ and Y_{xs3} are yield coefficients for anaerobic and overflow metabolism, respectively.

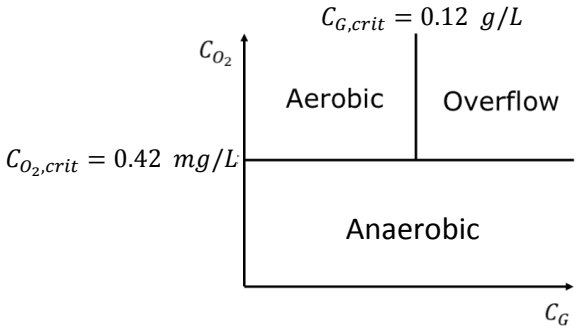

Figure 5.20. Three-regime metabolic model for *Saccharomyces cerevisiae* cell culture.

Each metabolic state is activated in different glucose and oxygen conditions. An oxygen concentration C_{O_2} less than the critical value $C_{O_2,crit}$ always creates an anaerobic condition. While, in the presence of an adequate amount of oxygen, the critical glucose concentration $C_{G,crit}$ defines the limit between the aerobic growth condition and the overflow metabolism. Figure 5.20 shows the scheme of the metabolic shifts.

Each regime is described by a Monod-type kinetic model as Eq. 5.4 (Postma et al. 1989).

$$\mu_G = \frac{\mu_{max} C_G}{K_s + C_G} \tag{5.4}$$

The list of parameters is shown in Table 5.1:

Table 5.1. The applied parameters for simulation of the kinetic model

Parameter	Definition	Value	Reference
K_s	Half saturation concentration of limiting carbon source for aerobic metabolism	0.02 g/L	(Postma et al. 1989)
K_s	Half saturation concentration of limiting carbon source for overflow metabolism	0.07 g/L	(Postma et al. 1989)
K_s	Half saturation concentration of limiting carbon source for anaerobic metabolism	0.1 g/L	(Verduyn et al. 1990)
μ_{max}	Maximum growth rate for aerobic and overflow metabolism	0.49 h^{-1}	(Postma et al. 1989)
μ_{max}	Maximum growth rate for anaerobic metabolism	0.31 h^{-1}	(Verduyn et al. 1990)
$Y_{xs,1}$	Yield coefficient for biomass for aerobic metabolism	0.51 g/g	(Postma et al. 1989)
$Y_{xs,2}$	Yield coefficient for biomass for anaerobic metabolism	0.16 g/g	(Verduyn et al. 1990)
$Y_{xs,3}$	Yield coefficient for biomass for overflow metabolism	0.086 g/g	(Verduyn et al. 1990)
Y_{Os}	Yield coefficient for oxygen for aerobic and overflow metabolism	0.04 g/g	(Weusthuis et al. 1994)

The designed scale-down model is aimed at providing similar oxygen and glucose gradients as the large scale reactor, and as a result to provide an identical journey for the cells through different metabolic shifts as observed for the large scale. Hence, C_{O_2} and C_G are chosen as the scaling parameters with the homogeneity tolerance ranges of [0-$C_{G,crit}$-$C_{G,max}$] and [0-$C_{O_2,crit}$-$C_{O_2,max}$] to resemble the aerobic, anaerobic and the overflow regions as observed in the large reactor.

Two-phase CFD simulations of the cell culture with 80 g/L uniformly distributed biomass were executed for the mentioned feeding conditions. The simulations are summarized in Table 5.2. In this table, 'Yes' means that the cells experience the metabolic shift during their movements in the reactor and 'No' means only one metabolic regime is present in the reactor concerning the glucose or oxygen conditions. For instance, with 23.48 kg/min feed rate the cells experience only aerobic conditions concerning oxygen and overflow metabolism concerning the Glucose concentration.

Table 5.2. Design of simulation experiments

Feed rate	Low (23.48 [kg/min])	Medium (46.96 [kg/min])	High (93.92[kg/min])
Glucose shift	Yes	Yes	Yes
O_2 shift	No	Yes	Yes
Yes/No: if cells experience different metabolic regimes.			

The design of a representative scale-down model for each feeding strategy is discussed in detail:

- **Low feeding rate:** The simulation result (Table 5.2) showed that the cells do not experience any shift concerning the oxygen conditions. However, both aerobic and overflow metabolisms appear in the reactor due to the low mixing performance and therefore the difficulties in distributing the feed. Thereby, the scale-down model is extracted only based on C_G to identify the aerobic and overflow regions in the large scale tank. Figure 5.21 shows the extracted compartment-map and the scheme of the scaled-down design based on C_G for a low feeding rate.

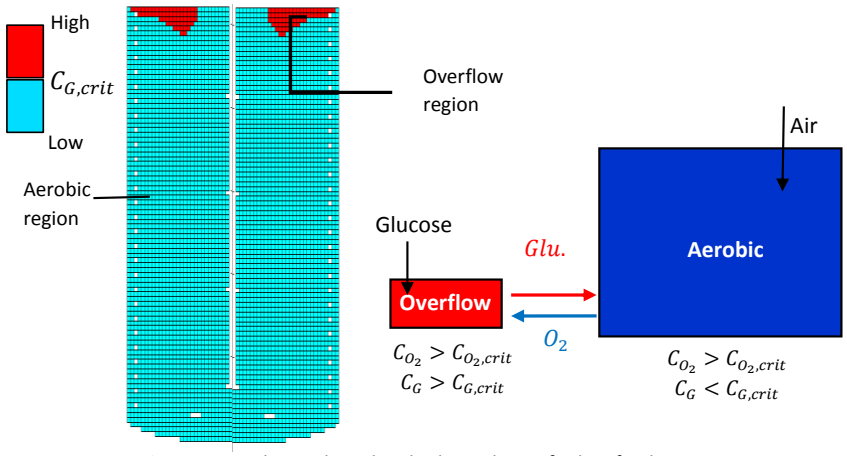

Figure 5.21. Glucose based scale-down design for low feeding rate.

Injection of the feed in the small red reactor in the presence of enough oxygen creates an overflow metabolism in that reactor. By pumping the working volume from the overflow reactor to the larger reactor, the dissolved glucose is diluted which leads to aerobic conditions in the second reactor.

- **Medium feeding rate**: The simulation result showed that the cells experience all the three metabolic regimes in the large scale tank. Hence, both glucose and oxygen profiles were considered for the design of the scale-down model with the medium feeding rate. Figure 5.22 shows the extracted compartment-maps based on glucose, oxygen, and the final one overlapping both variables.

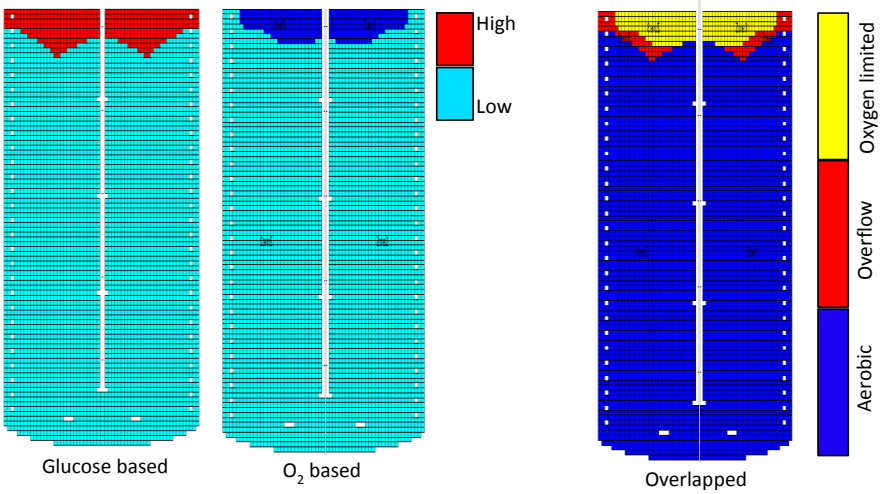

Figure 5.22. Glucose/oxygen based compartment-map for medium feeding rate.

The overlapped compartment-map leads to the following scale-down model (Figure 5.21). This model consists of three reactors with different working volumes. The inlet gas is sparged into the large tank to create an aerobic cell culture while the glucose enters the oxygen-limited reactor. Two countercurrent flows exchange the working volume between the reactors. The flow from the aerobic tank to the overflow reactor and then the anaerobic reactor transports the input oxygen from the aerobic reactor to the other two while the other flow delivers glucose from the anaerobic tank to the overflow tank and then to the aerobic reactor. The main flows between the reactors are shown in Figure 5.23 with the solid line and the dashed line showing the additional low flow rate between the anaerobic and aerobic reactors.

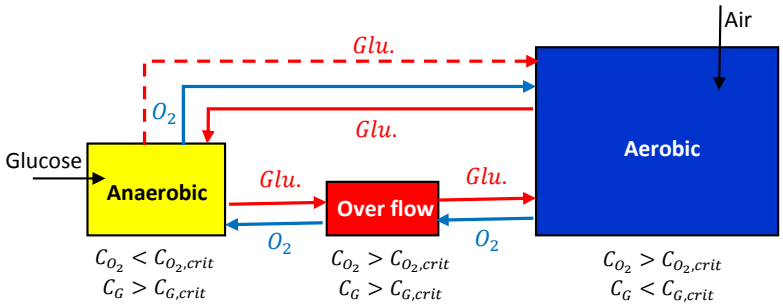

Figure 5.23. Glucose/oxygen based scale-down design for medium feeding rate.

- **High feeding rate:** similar to the previous feeding strategy, the simulation result indicates the presence of all three regimes. Hence, the applied scale-down is based on both glucose and oxygen profiles (Figure 5.24).

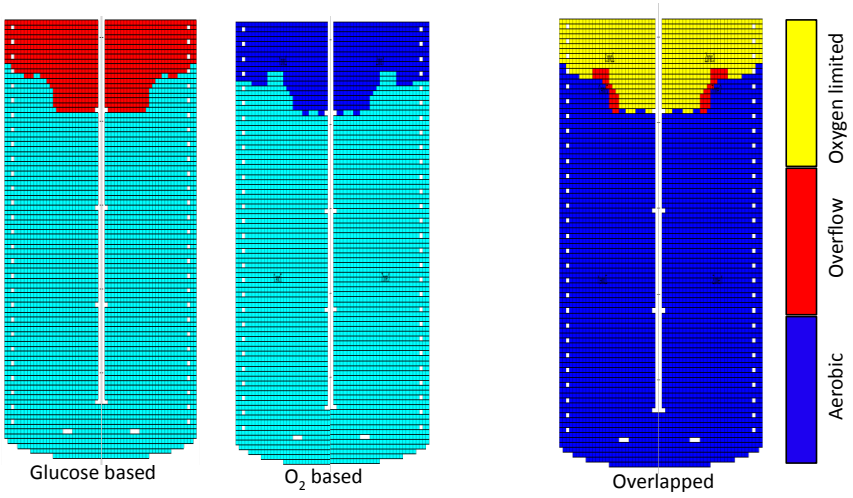

Figure 5.24. Oxygen based compartment-map for a high feeding rate.

By increasing the feed rate and subsequently increasing the oxygen consumption rate at the top part of the reactor, the oxygen-limited region grows and overlaps the main portion of the overflow zone. As a result, the identified region for the overflow metabolism takes less than 1% of the overall volume. With respect to the mentioned discussion on the practical aspects of the design, definition of such an aspect ratio may not be reasonable. Therefore, merging the overflow volume with the aerobic region is suggested. This consideration leads to an oxygen-based design for this feeding rate. Figure 5.25 shows the scheme of the scaled-down design.

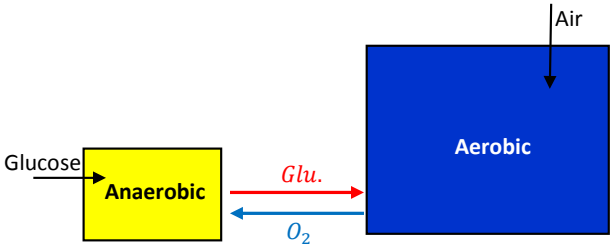

Figure 5.25. Oxygen based scale-down design for high feeding rate.

To summarize, the designed scale-down model varies by changing the operating conditions in the large-scale reactor. In this case study, by increasing the feeding rate, the scale-down strategy changes from a glucose-based approach for low feeding rate to a glucose/oxygen-based design and ultimately to an oxygen-based design for the high feeding rate.

This case study demonstrated the potential of using different target variables, such as nutrient and oxygen concentrations, for the design of a scaled-down model for bioprocesses. The proposed designs need to be validated by the experimental data in the future.

Summary

In this chapter, a scale-down strategy was presented using a novel automated CFD based compartmentalization technique. The developed compartmentalization method is a useful tool to identify and characterize a network of homogeneous regions (compartments) within an investigated volume. The designed routine is based on an initial CFD result and extraction of the elemental information. The elements with similar profiles of the specified variable/variables are identified to characterize the compartmental volumes and the exchange flows between the neighboring compartments are specified. This information is saved as a compartment map. The presented approach is applicable for different types of CFD meshes and has a high flexibility in choosing the number of target variables. The method was critically evaluated by a mixing time case study (700 L stirred tank).

The obtained output of the compartmentalization routine provides the required information for the design of a scaled-down model. The large-scale heterogeneity is simulated in a set of connected miniaturized reactors, where each individual miniaturized reactor and the exchange flows are determined based on the extracted compartment map from the initial scale. Figure 5.26 illustrates the scheme of the scale-down approach. This method was applied in two case studies of a 700 L pilot-scale lactic acid fermentation and a 100 m^3 large-scale fermentation of *Saccharomyces cerevisiae*. The case studies demonstrated the potential of using the compartmentalization routine in the design of more representative scale-down models.

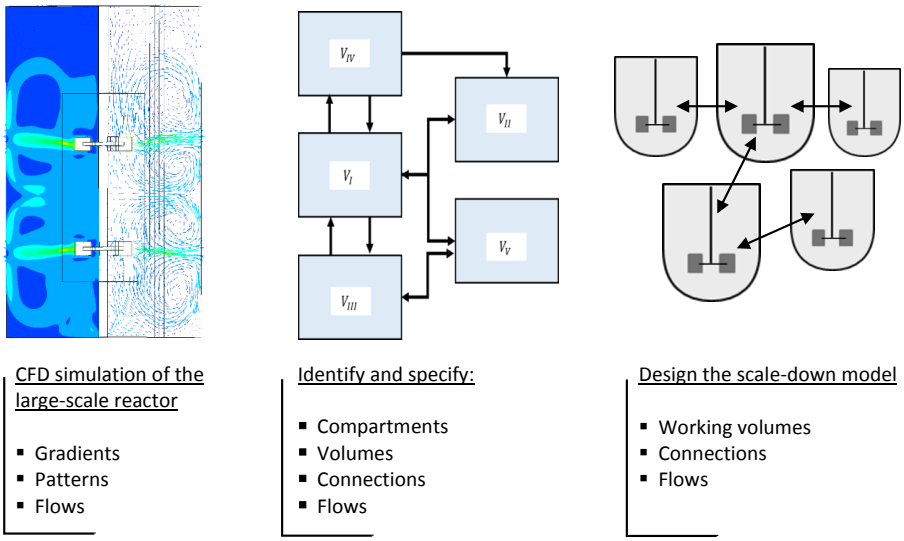

Figure 5.26. Illustration of the compartment based scale-down strategy.

Glossary

C_G	Carbon source concentration [mol L^{-1}]
D	Impeller diameter [m]
f_{ij}	Flow rate from compartment $'i'$ to compartment $'j'$ [m^3 s^{-1}]
$f'_{(ij)}$	Additional flow rate between compartment $'i'$ and $'j'$ [m^3 s^{-1}]
H	Liquid height [m]
K_s	Half saturation concentration of limiting carbon source [g L^{-1}]
N	Number of target variables, number of zone-maps
N_{imp}	Agitation speeds [s^{-1}]
n	Number of zones in a zone-map
$n_{f'}$	Number of additional flows
n_e	Number of independent mass balance equations
P	Power input [W]
p	Target variable []
P_0	Power number
V	Volume [m^3]
Y	Yield coefficient [g g^{-1}]
τ_{mix}	Mixing time [s]
μ_G	Biomass growth rate [h^{-1}]

References

Amanullah, A. et al., 2001. Scale-down model to simulate spatial pH variations in large-scale bioreactors. *Biotechnology and Bioengineering*, 73(5), pp.390–399.

Bach, C., 2018. Modelling of Gradients in Large Scale Bioreactors. *Citation*.

Bashiri, H. et al., 2014. Compartmental modelling of turbulent fluid flow for the scale-up of stirred tanks. *The Canadian Journal of Chemical Engineering*, 92(6), pp.1070–1081.

Bashiri, H., Bertrand, F. & Chaouki, J., 2016. Development of a multiscale model for the design and scale-up of gas/liquid stirred tank reactors. *Chemical Engineering Journal*, 297, pp.277–294.

Bezzo, F., 2002. Design of a general architecture for the integration of process engineering simulation and computational fluid dynamics.

Bezzo, F. & Macchietto, S., 2004a. A general methodology for hybrid multizonal/CFD models. *Computers & Chemical Engineering*, 28(4), pp.513–525.

Bezzo, F. & Macchietto, S., 2004b. A general methodology for hybrid multizonal/CFD models: Part II. Automatic zoning. *Computers & Chemical Engineering*, 28(4), pp.513–525.

Bylund, F. et al., 2000. Influence of scale-up on the quality of recombinant human growth hormone. *Biotechnology and Bioengineering*, 69(2), pp.119–128.

Bylund, F. et al., 1998. Substrate gradient formation in the large-scale bioreactor lowers cell yield and increases by-product formation. *Bioprocess Engineering*, 18(3), p.171.

Delafosse, A. et al., 2010. Development of compartment model based on CFD simulations for description of mixing in bioreactors. *Biotechnol. Agron. Soc. Environ*, 14((S2)), pp.517–522.

George, S., Larsson, G. & Enfors, S.-O., 1993. A scale-down two-compartment reactor with controlled substrate oscillations: Metabolic response of Saccharomyces cerevisiae. *Bioprocess Engineering*, 9(6), pp.249–257.

Haringa, C. et al., 2017. Euler-Lagrange analysis towards representative down-scaling of a 22 m3 aerobic S. cerevisiae fermentation. *Chemical Engineering Science*, 170, pp.653–669.

Haringa, C. et al., 2016. Euler-Lagrange computational fluid dynamics for (bio)reactor scale down: An analysis of organism lifelines. *Engineering in Life Sciences*, 16(7), pp.652–663.

Heins, A.-L. et al., 2015. Experimental and *in silico* investigation of population heterogeneity in continuous *Sachharomyces cerevisiae* scale-down fermentation in a two-compartment setup. *Journal of Chemical Technology & Biotechnology*, 90(2), pp.324–340.

Irizarry, R., 2012. Fast Compartmental Monte Carlo Simulation of Population Balance Models: Application to Nanoparticle Formation in Nonhomogeneous Conditions. *Industrial & Engineering Chemistry Research*, 51(47), pp.15484–15496.

Junne, S. et al., 2011. A two-compartment bioreactor system made of commercial parts for bioprocess scale-down studies: Impact of oscillations on Bacillus subtilis fed-batch cultivations. *Biotechnology Journal*, 6(8), pp.1009–1017.

Käß, F. et al., 2014. Assessment of robustness against dissolved oxygen/substrate oscillations for C. glutamicum DM1933 in two-compartment bioreactor. *Bioprocess and Biosystems Engineering*, 37(6), pp.1151–1162.

Lara, A.R. et al., 2006. Living With Heterogeneities in Bioreactors: Understanding the Effects of

Environmental Gradients on Cells. *Molecular Biotechnology*, 34(3), pp.355–382.

Lemoine, A. et al., 2015. Response of *Corynebacterium glutamicum* exposed to oscillating cultivation conditions in a two- and a novel three-compartment scale-down bioreactor. *Biotechnology and Bioengineering*, 112(6), pp.1220–1231.

Le Moullec, Y. et al., 2010. Comparison of systemic, compartmental and CFD modelling approaches: Application to the simulation of a biological reactor of wastewater treatment. *Chemical Engineering Science*, 65(1), pp.343–350.

Nauha, E.K. et al., 2018. Compartmental modeling of large stirred tank bioreactors with high gas volume fractions. *Chemical Engineering Journal*, 334, pp.2319–2334.

Neubauer, P., Biotechnology, S.J.-C. opinion in & 2010, U., 2010. Scale-down simulators for metabolic analysis of large-scale bioprocesses. *Current Opinion in Biotechnology*, 21(1), pp.114–121.

Neubauer, P., Häggström, L. & Enfors, S.-O., 1995. Influence of substrate oscillations on acetate formation and growth yield in *Escherichia coli* glucose limited fed-batch cultivations. *Biotechnology and Bioengineering*, 47(2), pp.139–146.

Nienow, A.W., 1998. Hydrodynamics of Stirred Bioreactors. *Applied Mechanics Reviews*, 51(1), p.3.

Postma, E., Alexander Scheffers, W. & Van Dijken, J.P., 1989. Kinetics of growth and glucose transport in glucose-limited chemostat cultures ofSaccharomyces cerevisiae CBS 8066. *Yeast*, 5(3), pp.159–165.

Rigopoulos, S. & Jones, A., 2003. A hybrid CFD—reaction engineering framework for multiphase reactor modelling: basic concept and application to bubble column reactors. *Chemical Engineering Science*, 58(14), pp.3077–3089.

Sandoval-Basurto, E.A. et al., 2005. Culture of *Escherichia coli* under dissolved oxygen gradients simulated in a two-compartment scale-down system: Metabolic response and production of recombinant protein. *Biotechnology and Bioengineering*, 89(4), pp.453–463.

Spann, R., Roca, C., et al., 2018a. A probabilistic model-based soft sensor to monitor lactic acid bacteria fermentations. *Biochemical Engineering Journal*, 135, pp.49–60.

Spann, R., Lantz, A.E., et al., 2018b. Model-based process development for a continuous lactic acid bacteria fermentation. *Computer Aided Chemical Engineering*, 43, pp.1601–1606.

Verduyn, C. et al., 1990. Physiology of Saccharomyces Cerevisiae in Anaerobic Glucose-Limited Chemostat Culturesx. *Journal of General Microbiology*, 136(3), pp.395–403.

Vrábel, P. et al., 1999. Compartment Model Approach: Mixing in Large Scale Aerated Reactors with Multiple Impellers. *Chemical Engineering Research and Design*, 77(4), pp.291–302.

Wells, G.J. & Ray, W.H., 2005. Methodology for modeling detailed imperfect mixing effects in complex reactors. *AIChE Journal*, 51(5), pp.1508–1520.

Weusthuis, R.A. et al., 1994. Effects of oxygen limitation on sugar metabolism in yeasts: a continuous-culture study of the Kluyver effect. *Microbiology*, 140(4), pp.703–715.

Yu, X. et al., 2017. A compartmental CFD-PBM model of high shear wet granulation. *AIChE Journal*, 63(2), pp.438–458.

Chapter 6

Conclusions and future perspectives

The application of different model-based methods through systematic routines is useful to extend the power of the traditional approaches for the design and development of more optimum processes. The integration of standard approaches with modelling techniques can be considered in different stages of research and development, from process characterization to the process design and optimization. Various applications of model-based approaches have been studied and reported in detail in the scientific literature (Sahinidis 2004; Daoutidis et al. 2018; Morari & H. Lee 1999; Kazi et al. 2018; Zuluaga-Bedoya et al. 2018). The main concept of all these works is to use the predictive power of mathematical models to generate data in support of the optimized decisions. This kind of decision making can be considered highly relevant for the specific case of selection of a combination of experimental settings which deliver the most information for characterization of a process, or, for choosing the operating conditions in a small reactor which are most appropriate to simulate a full-scale process in the lab.

In this Ph.D. thesis, the focus has been on the application of model-based approaches for process development at the early stage of research and development. The focus of the study was on presenting systematic approaches for the design of informative experiments, and for the operation of experiments in miniaturized bioreactors. Figure 6.1 shows the tree chart of the achieved developments in this thesis. Some considerable developments were delivered in the frame of this study. However, there is always a possibility for further improvements in the future works which some of them are mentioned below.

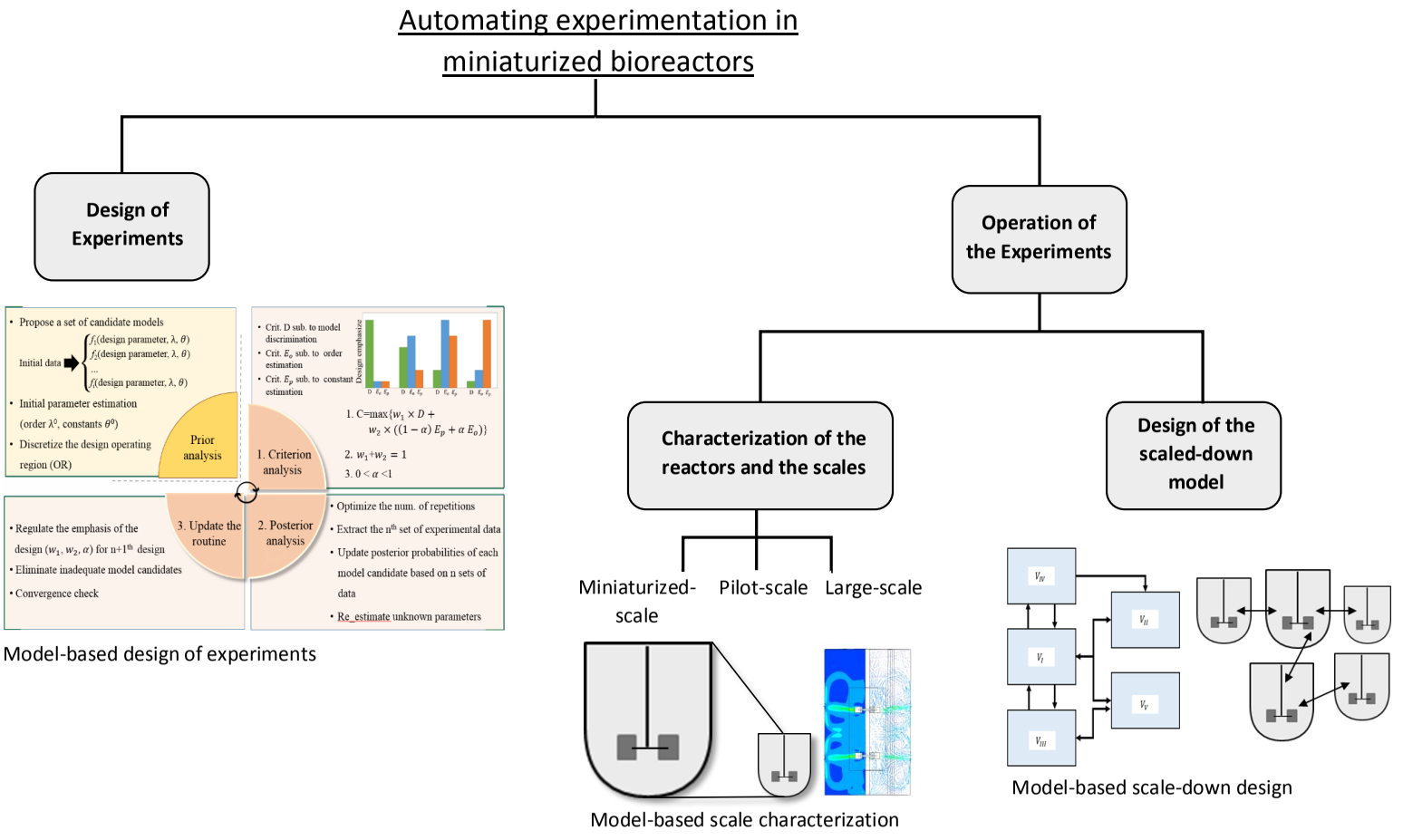

Figure 6.1. Model-based experimental design in miniaturized bioreactors.

In the scope of this work, application of model-based approaches was extended with focus on three main applications:

- **Model-based design of experiments:** A new integrated model-based DoE framework was introduced in chapter 2 with the help of some well-stablished design criteria (Tajsoleiman et al. 2017). The framework can be used for design of the most informative experiments for developing predictive models with an adoptive focus on the definition of the model structure, evaluation of the orders of the equations and estimation of the parameters. The obtained models can then be used for the prediction of the process behavior under different conditions, and for improving the process yield by proposing a set of optimized conditions.

  The presented routine provides an important basis for integration of modelling techniques and DoE approaches to minimize the experimental cost and efforts. Figure 6.2. shows the main focus of this work (the green boxes) in developing an optimized model-based DoE platform and potential improvements (red boxes) in the future works. The platform initiates by proposing a set of candidate model structures based on available information, i.e. information available in the literature or information obtained from past experiences. Integration of different black-box modelling techniques, e.g. surrogate models and hybrid models (Bhosekar & Ierapetritou 2018, Feyo de Azevedo et al. 1997), besides this step can be considered in future works. In the present routine, it was assumed that all the parameters of the candidate models are identifiable. The platform can be improved by including an additional parameter identification step, similar to the one presented by Van Daele *et al.* (Van Daele et al. 2015), to increase the robustness of the platform for different types of models. Finally, for each set of design, the experimental setting is determined based on a presented compound criterion to have targeted experiments according to the specific requirements for developing the model. Over all the mentioned units, considering the addition of an integrated data treatment step, for instance for handling the outliers in the experimental data, can also improve the performance of the routine.

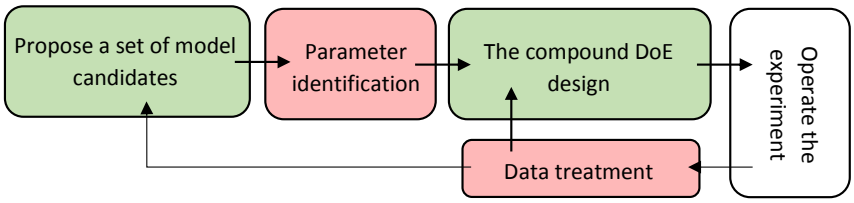

Figure 6.2. The developed (green boxes) and potential units (red boxes) for an optimized M-DoE platform.

The overall platform can also be improved by including additional machine learning algorithms (Lee et al. 2018), which can be applied to automatically extract process related knowledge from the available data. The outcome of applying machine learning should be the design of even better experiments containing the highest level of information.

- **Model-based scale characterization:** In order to run an experiment in a lab-scale setup, it is crucially important to have a detailed knowledge about the capabilities of the system and the specific considerations related to the operation at the chosen scale. The characterization of a process within the specified setups not only helps to have a better experimental study, but can also provide valuable information for improving its physical design or for optimizing the operating conditions (Tajsoleiman et al. 2018). The application of modelling and simulation techniques for characterization of processes in different scales, particularly in MBRs, was considered highly relevant in this study. In chapter 3, different MBRs were studied in detail and the performance of an Ambr®250 system (Sartorius Biotech), as an example of a stirred MBR, was evaluated in microbial and mammalian cell cultures with the help of CFD simulations. The provided results and discussions raised an important point that despite the potentials of using MBR to scale-down a process, the operator should always be aware of the differences of the process environment in MBR compared to the industrial reactor.

  The achieved knowledge resulting from this step provides the essential information for detecting the challenges of operating a process in different scales (lab, pilot and industrial size reactors). Some of the main challenges of scaling down a large-scale process into a MBR were discussed in Chapter 4. A comprehensive understanding of a process, and especially the limitations and flexibilities related to various reactor scales can guarantee a successful scale-down design. There are plenty of works available in the scientific literature which studied different scaling strategies based on one or several scaling parameters such as $k_l a$, OTR, shear stress or power input (Islam et al. 2008; Diaz & Acevedo 1999; Xu et al. 2017; Hortsch et al. 2010). However, there is no generic approach available for the selection of the best scaling parameters for a specific case, and for compensating for the differences in the other parameters between the real-scale reactor and the scaled-down model.

- **Model-based scale-down design:** Starting from a CFD model code, a compartment-based scale-down strategy was presented in this work. The resulting scale-down model (also called compartment model) is able to represent gradients in the large-scale tank by means of a network of a limited number of connected reactors. In order to develop the platform, a new automated compartmentalization method was introduced, which uses the CFD results as an

input to analyze the heterogeneity inside the big tank. Finally, the results are used for the design of the scaled-down setup.

This method was applied to two case studies, i.e. lactic acid bacteria in a 700 L pilot-scale reactor and a *Saccharomyces cerevisiae* fermentation in a 100 m^3 production tank. Further experimental work is required for both cases to experimentally evaluate the performance of the designs. The robustness of the approach has to be tested further for different types of case studies, such as crystallization (Öner et al. 2018), flocculation and polymerization processes.

Each mentioned part can be considered as a piece of a puzzle showcase the applications and potentials of various model-based approaches for an efficient design of experiments. Throughout this study, it was shown that the integration of different modelling and simulation techniques with traditional design approaches can provide a significant opportunity to enhance the quality of the experimental data with more focused, educated and thoughtful experimental designs. This possibility relates to the potentials of modelling to 1. predict the process behavior under various conditions, 2. improve our insights into the challenges of using different setups and the flexibility of the system, and finally 3. pre-evaluate the performance of a process under the specified settings and the scale before real operation of the experiments. Thereby, the main outcome of this work is presenting a systematic approach to use modelling and simulation techniques as complementary tools for optimizing experiments with increasing the level of information of each single trial.

References

Bhosekar, A. & Ierapetritou, M., 2018. Advances in surrogate based modeling, feasibility analysis, and optimization: A review. *Computers & Chemical Engineering*, 108, pp.250–267.

Daoutidis, P. et al., 2018. Integrating operations and control: A perspective and roadmap for future research. *Computers & Chemical Engineering*, 115, pp.179–184.

Diaz, A. & Acevedo, F., 1999. Scale-up strategy for bioreactors with Newtonian and non-Newtonian broths. *Bioprocess Engineering*, 21(1), p.21.

Feyo de Azevedo, S., Dahm, B. & Oliveira, F.R., 1997. Hybrid modelling of biochemical processes: A comparison with the conventional approach. *Computers & Chemical Engineering*, 21, pp.S751–S756.

Hortsch, R., Stratmann, A. & Weuster-Botz, D., 2010. New milliliter-scale stirred tank bioreactors for the cultivation of mycelium forming microorganisms. *Biotechnology and Bioengineering*, 106(3), pp.443–451.

Islam, R.S. et al., 2008. Scale-up of Escherichia coli growth and recombinant protein expression conditions from microwell to laboratory and pilot scale based on matched kLa. *Biotechnology and Bioengineering*, 99(5), pp.1128–1139.

Kazi, M.-K. et al., 2018. A process design approach to manage the uncertainty of industrial flaring during abnormal operations. *Computers & Chemical Engineering*, 117, pp.191–208.

Lee, J.H., Shin, J. & Realff, M.J., 2018. Machine learning: Overview of the recent progresses and implications for the process systems engineering field. *Computers & Chemical Engineering*, 114, pp.111–121.

Morari, M. & H. Lee, J., 1999. Model predictive control: past, present and future. *Computers & Chemical Engineering*, 23(4–5), pp.667–682.

Öner, M. et al., 2018. Scale-up modeling of a pharmaceutical crystallization process. *Computer Aided Chemical Engineering*, 44, pp.181–186.

Sahinidis, N. V., 2004. Optimization under uncertainty: state-of-the-art and opportunities. *Computers & Chemical Engineering*, 28(6–7), pp.971–983.

Tajsoleiman, T. et al., 2017. An efficient experimental design strategy for modelling and characterization of processes. *Computer Aided Chemical Engineering*, 40, pp.2827–2832.

Tajsoleiman, T. et al., 2018. Efficient computational design of a scaffold for cartilage cell Regeneration. *Bioengineering*, 5(2), p.33.

Van Daele, T. et al., 2015. A Numerical procedure for model identifiability analysis applied to enzyme kinetics. *Computer Aided Chemical Engineering*, 37, pp.575–580.

Xu, P. et al., 2017. Characterization of TAP Ambr 250 disposable bioreactors, as a reliable scale-down model for biologics process development. *Biotechnology Progress*, 33(2), pp.478–489.

Zuluaga-Bedoya, C. et al., 2018. A dynamical model of an aeration plant for wastewater treatment using a phenomenological based semi-physical modeling methodology. *Computers & Chemical Engineering*, 117, pp.420–432.

Acknowledgments

Acknowledgments to FujiFilm Diosynth (UK), Novozymes A/S (DK) and Chr. Hansen (DK) for providing the industrial case studies. And also, Robert Spann and Gisela Nadal Rey for providing the mechanistic models and the CFD simulation case studies

List of publications

Articles

Tajsoleiman, Tannaz, Daria Semenova, Ana C. Fernandes, Jakob Kjøbsted Huusom, Krist V. Gernaey, and Ulrich Krühne. 2017. "An Efficient Experimental Design Strategy for Modelling and Characterization of Processes." *Computer Aided Chemical Engineering* 40 (January). Elsevier: 2827–32. doi:10.1016/B978-0-444-63965-3.50473-6.

Tajsoleiman, Tannaz, Mohammad Abdekhodaie, Krist Gernaey, and Ulrich Krühne. 2018. "Efficient Computational Design of a Scaffold for Cartilage Cell Regeneration." *Bioengineering* 5 (2): 33. doi:10.3390/bioengineering5020033.

Tajsoleiman, Tannaz, Mohammad J. Abdekhodaie, Krist V. Gernaey, and Ulrich Krühne. 2016. "Geometry Optimization of a Fibrous Scaffold Based on Mathematical Modelling and CFD Simulation of a Dynamic Cell Culture." In *Proceedings of the*, 1413–18. doi:10.1016/B978-0-444-63428-3.50240-X.

Öner, Merve, Christian Bach, Tannaz Tajsoleiman, Getachew S. Molla, Michael F. Freitag, Stuart M. Stocks, Jens Abildskov, Ulrich Krühne, and Gürkan Sin. 2018. "Scale-up Modeling of a Pharmaceutical Crystallization Process." *Computer Aided Chemical Engineering* 44 (January). Elsevier: 181–86. doi:10.1016/B978-0-444-64241-7.50025-2.

Under review

Tajsoleiman, Tannaz, Robert Spann, Christian Bach, Krist V. Gernaey, Jakob Kjøbsted Huusom and Ulrich Krühne, ''*A CFD based automatic method for compartment model development.'' Computer and chemical engineering.*

Tajsoleiman, Tannaz, Lisa Mears, Ulrich Krühne, Krist V. Gernaey, Sjef Cornelissen, *''An industrial perspective on scale-down challenges using miniaturized bioreactors.'' trend in biotechnology.*

Process and Systems Engineering Centre (PROSYS)
Department of Chemical and Biochemical Engineering
Technical University of Denmark
Søltofts Plads, Building 229
DK - 2800 Kgs. Lyngby
Denmark

Phone: +45 45 25 28 00
Web: www.kt.dtu.dk/forskning/prosys